Development of a Novel Technique for Quantitatively Determining the Products of Electron-Ion Dissociative Recombination

by

Christopher David Molek

(Under the direction of Nigel G. Adams)

Abstract

The chemistry of plasmas is complex, involving many reactive processes such as ion-molecule reactions, ion-ion and electron-ion recombination, and neutral-neutral reactions. Of particular relevance are the plasma processes that take place in interstellar clouds, planetary atmospheres, supernova remnants, cometary comae, etc. The ionization of small neutrals proceeds by multiple gas phase ion-molecule reactions leading to the formation of polyatomic ions which can recombine with electrons, by what is termed dissociative electron-ion recombination (DR). The data presented represents specific examples of ion-molecule chemistry, which leads into studies used to determine the products of DR, both in ground and excited states. Data for ion-molecule chemistry are presented in the reactions of CS_2 with a series of fifteen ions (He^+, He_2^+, Ar^+, N_2^+, N^+, CO^+, CO_2^+, O^+, D^+, CS^+, C^+, S^+, CS_2^+, S_2^+ and D_3^+) for which the rate constants and percentage ion product distributions were determined.

Dissociative electron-ion recombination (DR) is an important ionization loss process and source of reactive radicals in the interstellar medium (ISM) and many other plasmas. Unfortunately, experimental product distributions are difficult to determine with only about 50 reported in the literature. These have been obtained by spectroscopic techniques integrated with flowing afterglows (FA) and by storage rings (SR). The data obtained by SR measurements are more extensive than those of the FA. Some data are available where the two

techniques overlap, however there are very significant discrepancies. To resolve these contradictions, a new technique to quantitatively detect product neutrals has been developed.

This technique is based on the FA and uses an Electron Impact (EI) ionizer to ionize neutral products prior to detection by a quadrupole mass filter/electron multiplier tube. Two experimental methodologies, both using pulsed gas techniques, isolate and quantify the DR products. In one approach, an electron attaching gas is pulsed into the flow to transiently quench DR. N_2H^+ recombination results from this approach give an upper limit of 5% for the NH + N product channel, the remainder being N_2 + H. In the second approach, the reagent gas N_2 is pulsed. Here the absolute percentages of products were monitored versus initial N_2 concentration. Results from this approach give an upper limit of 5% for NH + N production. This establishes that N_2 + H is the dominant channel, being at least 95%, and that there is no significant NH production contrary to a recent storage ring measurement in which yielded 64% NH + N and 36% N_2 + H. Possible reasons for this dramatic difference are discussed. In addition, DR product distribution of the CH_5^+ system will be discussed.

Additionally, excited state products are determined in an emission spectroscopy study of the DR of CS_2^+ and HCS_2^+. From these studies the DR excited state products are obtained by determining the populated electronic and vibrational states. The relative values of the upper level vibrational state populations are determined for both recombining ions, CS_2^+ and HCS_2^+.

INDEX WORDS: Dissociative Recombination, N_2H^+, CH_5^+, Products of Recombination, Ion-Ion Recombination

Development of a Novel Technique for Quantitatively Determining the Products of Electron-Ion Dissociative Recombination

by

Christopher David Molek

B.S., The University of Wisconsin-La Crosse, 2001

A Dissertation Submitted to the Graduate Faculty
of The University of Georgia in Partial Fulfillment
of the
Requirements for the Degree

Doctor of Philosophy

Athens, Georgia

2007

Development of a Novel Technique for Quantitatively Determining the Products of Electron-Ion Dissociative Recombination

by

Christopher David Molek

Approved:

Major Professor: Nigel G. Adams

Committee: Geoffrey D. Smith
I Jonathan Amster

Electronic Version Approved:

Maureen Grasso
Dean of the Graduate School
The University of Georgia
August 2007

Dedication

To my Heavily Father, for without You nothing is possible. To Andy, the best brother one could have. He never gave up on anything in his life and defied the odds. He is an inspiration and hero of mine. He is the one who kept getting back up after falling down.

Acknowledgments

I would like to thank my wife, Karen, for being my best friend and supporting me through it all. My parents for supporting and encouraging me through all of life. Joe Velasquez III for a wonderful friendship and great discussions about science, blacksmithing, woodworking, guns, and many others. Jason McLain for keeping me on my toes in the lab and being a good friend. Greg Grieves for his friendship and great discussions about science and electronics. Dalila Fondren for being a good friend to talk and listen to. Tim Ayers for good times. Raj Ayyampalayam for insightful talks about electronics. My small group for the friendships and support through the last year and a half of craziness! Especially Greg Smith for a great friend and keeping it real at the "Awffle Waffle" on US 441! Many thanks to my committee all of whom have helped me become the scientist I am today, especially to Nigel who has been instrumental in most of my development. He would drop everything to talk to me and help me (like he had nothing else to do), and a great motivator when times seemed bleak. Thanks to Geoff for the helpful discussions about my research, and great feedback on my progress throughout the years. Also, for giving me great words of wisdom on public speaking and presenting my research. Lucia for wonderful and thought provoking discussions about my research. Jon for helping me, even before he was on my committee, with electronics questions and always taking the time to make sure I understood what was going on before I left his office.

Table of Contents

List of Figures

List of Tables

Chapter 1

Introduction and Literature Review

The chemistry of plasmas is complex, involving many reactive processes such as ion-molecule reactions, ion-ion and electron-ion recombination, and neutral-neutral reactions. Of particular relevance are the plasma processes that take place in interstellar clouds, planetary atmospheres, supernova remnants, cometary comae, etc. The ionization of small neutrals proceeds by multiple gas phase ionic reactions (parallel and sequential)[1–4] leading to the formation of polyatomic ions which can recombine with electrons, by what is termed electron-ion recombination (eir). This sequence of events has been long supported by the agreement between chemical models predicting molecular abundances and observed relative abundances.[5–8] The models are based on the enormous amount of data that has been collect in the laboratory on the chemical reactions (both rate constants and product distribution data) discussed above.

The dominant ionization loss process in plasma is the eir, specifically eir is important in many media such as, supernova remnants,[9] cometary comae,[10] planetary atmospheres,[10,11] stellar atmospheres,[12] combustion flames,[13] and laser plasmas.[14] The general equation for eir is

$$ABC^+ + e^- \rightarrow Products \tag{1.1}$$

where the products are dictated by different loss mechanisms, such as radiative recombination, dielectronic recombination, and dissociative recombination (DR).[15] Dissociative

recombination is the dominant ionization loss process in interstellar clouds,[16] planetary ionospheres,[10,11] and supernova remnants.[9] This process can be represented as follows,

$$ABC^+ + e^- \rightarrow A^* + BC^* \tag{1.2}$$

$$\rightarrow AB^* + C^* \tag{1.3}$$

$$\rightarrow A^* + B^* + C^* \tag{1.4}$$

where the * indicates possible excitation (kinetic, electronic, vibrational, or rotational). The neutrals that are produced are often radicals and can react further in ion-molecule reactions or neutral-neutral reactions. In addition to eir processes there are ion-ion recombination processes taking place. This is similar to eir except that the negative charge carrier is a bulky atom or molecule instead of an electron, which can reduce the rate constant nearly an order of magnitude lower than DR.[17] Negative ions are formed if an electron attaching gas is present. The attachment can proceed by either a binary dissociative electron attachment or a ternary electron attachment, which is three body stabilized.[18] These processes are shown below.

$$CCl_4 + e^- \rightarrow Cl^- + CCl_3 \tag{1.5}$$

and

$$O_2 + e^- + M \rightarrow O_2^- + M \tag{1.6}$$

The loss of the negative ions then proceeds by positive ion - negative ion recombination, often termed mutual neutralization or ion-ion recombination (iir), which can proceed by a binary or ternary process, represented below.

$$AB^+ + CD^- \rightarrow AB^* + CD^* \tag{1.7}$$

$$\rightarrow ABC^* + D \tag{1.8}$$

$$AB^+ + CD^- + M/e^- \rightarrow Neutral\ Products^* \tag{1.9}$$

The * indicates the possibility of internal excitation. Note that only internal excitation is a possibility. Since the long range charge transfer mechanism will only excite the internal energy states of the reacting species. However, if an intimate interaction occurs the energy of the iir process can be deposited in the kinetic energy of the products as well. It should be noted that the iir process has a lower amount energy produced than the DR process. This energy difference between DR and iir is caused by the e^- being bound to the molecule (CD), whereas it is free in the DR process. The energy is exactly the electron affinity (EA) of the neutral (CD).

$$CD^- \rightarrow CD + e^- \tag{1.10}$$

There has been little experimental data on the rates constants and products for iir due to the complexities involved with these experiments. There has only been about 50 rate constants measured, whereas well over 15,000 rate constants for ion-molecule reactions have been measured[19] and over 100 for DR, of which $\sim$50 have product distributions.[17]

The study of ion-molecule reactions and DR (both rates and products) processes particularly those that happen in the interstellar medium and planetary ionospheres have been the a major focus in research laboratories for many years. In recent years, the main technique associated with ion-molecule research has been the Selected Ion Flow Tube (SIFT).[20] Using this technique the rate constants and product distributions for many ion-molecule reactions have been measured (>4,500) and collected in the most recent compilation by Anicich.[19] In addition, some temperature dependence studies for ion-molecule reactions have been undertaken.[21]

There are several techniques for determining the rate constant of a reaction(e.g. Stationary Afterglow, Flowing Afterglow, and Storage Ring) and rate constants as a function of temperature. The study of the products of DR are more scarce in the literature. The two main techniques used to determine the product distribution, are Flowing Afterglows (FA) and Storage Rings (SR). Initially, FA measurements were used to identify products via vuv absorption spectroscopy and Laser Induced Fluorescence (LIF) measurements.[22–25] In these

experiments, LIF was used for the detection of radical species (e.g. OH). For the OH radical, a laser wavelength (∼281 nm) was use to excite $\mathrm{OH}\big(\mathrm{A}^2\Sigma(v'=1) \leftarrow \mathrm{X}^2\Pi(v''=0)\big)$ transition and the non-resonance transition was observed from $\mathrm{OH}\big(\mathrm{A}^2\Sigma(v'=1) \rightarrow \mathrm{X}^2\Pi(v''=1)\big)$. The intensity of fluorescence (I_f) was related to the number density of OH in the ground state (i.e. $\left[\mathrm{OH}\left(\mathrm{X}^2\Pi(v''=0)\right)\right]$ by the calibration reaction,

$$H + NO_2 \rightarrow OH(^2\Pi(v''=0)) + NO \tag{1.11}$$

thus if the concentrations, [H] and [NO_2], are known then $\left[\mathrm{OH}\left(\mathrm{X}^2\Pi(v''=0)\right)\right]$ is also known and a calibration constant (c) can be determined such that,

$$I_f = c\left[OH\left(X^2\Pi(v''=0)\right)\right] \tag{1.12}$$

Experimentally, [NO_2] is a measured gas introduced into the flow tube, but [H] is more difficult to establish. This is done using a vuv absorption experiment, in which the column density of [H] is measured across the flow tube using the H-atom resonant line, L_α = 121.57 nm.[22] Using the [H] radial profile, the absolute [H] can be determined see Adams et al. for details.[22] The difficulty associated with this experiment is its need for multiple quantitative spectroscopic techniques, which differ in wavelength, for the different products. Thus to obtain a full distribution is an arduous task.

The Storage Ring (SR) has its own set of difficulties as well. To get a distribution requires a detailed and involved analysis, as well as corrections for collisions with background gases. Briefly, the experiments occur in a large ring, circumference of 51.6 meters, at a pressure of 1 x 10^{-11} Torr in which the injected ions circulate. The ions are injected into the ring from an ion source such that up to 10^7 ions can be stored. The ions are guided by a series of bending and focusing magnets for several seconds so that they have time to vibrationally relax via radiative emission, when such transitions are allowed. The ion kinetic energy is typically equal to 96 MeV divided by the mass of the ion (e. g. H^+ will have 96 MeV whereas O_2^+ will have 3 MeV). This beam is then merged with a renewed cold e^- beam (electron cooler) of the same velocity at over 100,000 times a second such that the Coulomb interaction between

the ions and electrons will transversely and longitudinally cool the ion beam. During this cooling process some of the ions are lost due to electron-ion recombination. When the cooling process has sufficiently cooled the ion beam, the electron beam velocity is adjusted a little so that electron-ion recombination will take place at the required center-of-mass energy. The neutrals generated will leave the ring unaffected by the magnets. They are detected by hitting the face of an ion-implanted silicon detector, where the pulse height from the detector is proportional to the energy of the impacting neutrals. Since the detector can not distinguish between an impact from ABC or a simultaneous impact of A + B + C, a grid is placed in front of the detector. The grid has a certain transmittance and each neutral has a certain probability of passage through the grid. The products of recombination are then calculated from the probabilities of each neutral passing the grid and comparison to the intensity versus energy distribution obtained over the course of an experiment.[26] It can been seen that there is a large amount of analysis that goes into determining the products as well as experimental difficulties. Difficulties that arise from the neutral products colliding with background gases which cause fragmentation of the larger molecular products, thus creating a bias in the product distribution toward more fragmentation. Another limitation of the SR is that the ability to distinguish between products 1 amu apart diminishes for heavier products (e.g. C_nH_m, where $n \geq 2$).

Where data are available, there are significant discrepancies between the FA and SR results, namely for H_2O^+, H_3O^+, and N_2H^+. The difficulties associated with these experiments have lead to the development of a new technique to quantitatively determine the products of DR. This is the main topic of this dissertation. The new technique utilizes the chemical versatility of the FA and employs electron impact ionization and subsequent detection by quadrupole mass spectrometry to monitor the neutral recombination products. Neutrals, both background gas and products of recombination, from the flow tube are sampled. The signal from products of recombination is distinguished by pulsing an electron attaching gas into the FA, which quenches DR. The difference between the attaching gas out

versus in results in signal from the DR products. This mass spectrometric method allows the technique to readily mass resolve DR products at higher masses. Masses which are separated by 1 amu such as those involved in heavy hydrocarbon chemistry that is critically important in Titan's atmosphere.[27,28]

In a brief overview of this dissertation, it begins with a discussion of the ion-molecule reactions of CS_2 with a series of fifteen ions (He^+, He_2^+, Ar^+, N_2^+, N^+, CO^+, CO_2^+, O^+, D^+, CS^+, C^+, S^+, CS_2^+, S_2^+ and D_3^+) in which the rate constants and percentage ion product distributions were determined. These studies lead into DR studies of product excitation by monitoring spectroscopic emissions originating from CS_2^+ and HCS_2^+ plasmas. From these spectra the DR excited state products can be obtained by determining in which electronic and vibrational states the energy is being deposited. The final chapters discuss the development of the new technique and this is illustrated by the DR of N_2H^+ and CH_5^+. This is followed by a conclusions and suggested future directions.

1.1 References

[1] Dalgarno, A.; Black, J. H. *Rept. Prog. Phys.* **1976**, *39*, 573–612.

[2] Herbst, E.; Klemperer, W. In *Physics of Electronic and Atomic Collisions*; Risley, J. S., Geballe, R., Eds.; Univ. of Washington Press, 1976; page 62.

[3] Watson, W. D. *Rev. Mod. Phys.* **1976**, *48*, 513–552.

[4] Smith, D.; Adams, N. G. *Int. Revs. Phys. Chem.* **1981**, *1*, 271–307.

[5] Hartquist, T. W.; Black, J. H.; Dalgarno, A. *Mon. Not. Roy. Ast. Soc.* **1978**, *184*, 643–646.

[6] Prasad, S. S.; Huntress, W. T. *Ap. J.* **1980**, *239*, 151–165.

[7] Herbst, E. *Ap. J. Supp. Ser.* **1983**, *53*, 41–53.

[8] Millar, T. J. In *Molecular Astrophysics*; Diercksen, G. H. F. e. a., Ed.; Reidel, 1985.

[9] Dalgarno, A. In *Dissociative Recombination: Theory, Experiment and Applications IV*; Larsson, M., Mitchell, J. B. A., Schneider, I. E., Eds.; World Scientific: Singapore, 2000; pages 1–12.

[10] Cravens, T. E. In *Dissociative Recombination of Molecular Ions with Electrons*; Guberman, S. L., Ed.; Kluwer: New York, 2003; pages 385–400.

[11] Fox, J. L. In *Dissociative Recombination: Theory, Experiment and Applications*; Rowe, B. R., Mitchell, J. B. A., Canosa, A., Eds.; Plenum: New York, 1993; pages 219–42.

[12] Millar, T. J. In *Rate Coefficients in Astrochemistry*; Millar, T. J., Williams, D. A., Eds., Rate Coefficients in Astrochemistry; Kluwer: Dordrecht, 1988.

[13] Goodings, J. M.; Karellas, N. S.; Hasanali, C. S. *Int. J. Mass Spectrom. Ion Proc.* **1989**, *89*, 205–226.

[14] Biondi, M. A. In *Recombination.*; Bekefi, G., Ed.; Wiley: New York, 1976; page 125.

[15] Adams, N. G.; Babcock, L. M.; McLain, J. L. In *Encyclopedia of Mass Spectrometry: Theory and Ion Chemistry, Vol.1*; Armentrout, P., Ed., Vol. 1; Elsevier: Amsterdam, 2003; pages 542–555.

[16] Herbst, E. *Adv. Gas Phase Ion Chem.* **1998**, *3*, 1–47.

[17] Adams, N. G.; Babcock, L. M.; Molek, C. D. In *Encyclopedia of Mass Spectrometry: Theory and Ion Chemistry, Vol.1*; Armentrout, P., Ed., Vol. 1; Elsevier: Amsterdam, 2003; pages 555–561.

[18] Adams, N. G. In *Atomic, Molecular and Optical Physics Handbook*; Drake, G. W. F., Ed.; AIP Press: New York, 1996; page 441.

[19] Anicich, V. *An Index of the Literature for Bimolecular Gas Phase Cation-Molecule Reaction Kinetics: JPL Publication 03-19;* Jet Propulsion Laboratory: Pasadena, 2003.

[20] Adams, N. G.; Smith, D. *Int. J. Mass Spectrom. Ion Phys.* **1976**, *21*, 349–59.

[21] Rowe, B. R.; Dupeyrat, G.; Marquette, J. B.; Smith, D.; Adams, N. G.; Ferguson, E. E. *J.Chem.Phys.* **1984**, *80*, 241–245.

[22] Adams, N. G.; Herd, C. R.; Smith, D. *J. Chem. Phys.* **1989**, *91*, 963–973.

[23] Rowe, B. R.; Queffelec, J. L. In *Dissociative Recombination: Theory, Experiment and Applications*; Mitchell, J. B. A., Guberman, S. L., Eds.; World Scientific: Singapore, 1989; pages 151–61.

[24] Herd, C. R.; Adams, N. G.; Smith, D. *Ap. J.* **1990**, *349*, 388–392.

[25] Adams, N. G.; Herd, C. R.; Geoghegan, M.; Smith, D.; Canosa, A.; Gomet, J. C.; Rowe, B. R.; Queffelec, J. L.; Morlais, M. *J. Chem. Phys.* **1991**, *94*, 4852–4857.

[26] Larsson, M. In *The Encyclopedia of Mass Spectrometry: Theory and Ion Chemistry*; Armentrout, P. B., Ed., Vol. 1; Elsevier, 2003; pages 195–199.

[27] Waite, J. H.; Nieman, H.; Yelle, R. V.; Kasprzak, W. T.; Cravens, T. E.; Luhmann, J. G.; McNutt, R. L.; Ip, W.-H.; Gell, D.; de la Haye, V.; Muller-Wordag, I.; Magee, B.; Borggren, N.; Ledvina, S.; Fletcher, G.; Walter, E.; Miller, R.; Scherer, S.; Thorpe, R.; Xu, J.; Block, B.; Arnett, K. *Science* **2005**, *308*, 982–986.

[28] Cravens, T. E.; Robertson, I. P.; Waite, J. H.; Yelle, R. V.; Kasprzak, W. T.; Keller, C. N.; Ledvina, S. A.; Nieman, H. B.; Luhmann, J. G.; McNutt, R. L.; Ip, W.-H.; de la Haye, V.; Mueller-Wodarg, I.; Wahlund, J.-E.; Anicich, V.; Vuitton, V. *Geophys. Res. Letts.* **2006**, *33*, L07105.

Chapter 2

Experimental Values of Rate Constants and Ion Product Distributions for Reactions of a Series of Ions with CS_2[1]

[1]Molek, C. D.; McLain, J. L.; Adams, N. G.; Babcock, L. M.; Gibbs, L. L. *Int. J. Mass Spec.*, 235:199-205, 2004. Reprinted here with permission of publisher.

2.1 Introduction

Part of the rationale for this study was the significance of sulfur containing compounds in interstellar clouds (isc)[1,2] and comets.[3] To date, in the isc, 14 sulfur containing species have been detected (SO, NS, CS, H_2S, SO_2, OCS, C_2S, H_2CS, SiS, HNCS, C_3S, CH_3SH, SO^+, and HCS^+). However, this poses a problem since these only comprise <4 % of the cosmic abundance[1,2,4] and therefore a considerable abundance of other sulfur containing species must be present. In a search for a solution to this problem, the reactions of S^+,[5] S_2^+,[6,7] SO^+[8] and CS^+[9] have previously been studied with a series of observed and likely interstellar molecules. These studies provided an insight into the problem suggesting that HS_2 and the protonated ion HS_2H^+, may be significant repositories of sulfur.[10] Not included in these studies were reactions with CS_2. CS_2 has not been detected in isc because its symmetry renders it unobservable in the infrared and the microwave, but the analogue, OCS has been detected. CO_2 is similarly undetected, although its protonated form HCO_2^+ has been seen;[1,2,4] thus, CS_2 is undoubtedly present. In order to provide a more complete database of reactions of sulfur containing species, we have studied the reactions of CS_2 with a series of fifteen ions (He^+, He_2^+, Ar^+, N_2^+, N^+, CO^+, CO_2^+, O^+, D^+, CS^+, C^+, S^+, CS_2^+, S_2^+ and D_3^+) and have determined the rate constants and percentage ion product distributions.

2.2 Experimental

These studies were conducted using a Selected Ion Flow Tube (SIFT) apparatus, which has been described previously[11] and this detailed discussion will not be repeated here. Fourteen of the fifteen ions (He_2^+ was generated by three body association of injected He^+) were generated by dissociative and non-dissociative ionization in an electron impact ion source, variously containing He(He^+, He_2^+) , Ar(Ar^+), D_2 (D^+, D_3^+ by the reaction $D_2^+ + D_2$), N_2 (N_2^+, N^+), CS_2 (CS_2^+, CS^+, C^+, S^+, S_2^+ by the reaction $S^+ + CS_2$) and CO_2 (CO_2^+, CO^+, C^+, O^+) and injected into the flow tube after mass selection in a quadrupole mass filter. Thence

the ions were carried along the flow tube to a downstream mass spectrometer/ion counting detection system by a He carrier gas (at a throughput of 16 slm and a He pressure of 0.5 Torr). To study the reactions, controlled and accurately measured flows of CS_2 were added to the He carrier with reaction distances of 29.8, 59.6, and 83.6 cm depending on the rate of the reaction. The rate constants and percentage product ion distributions were determined in the usual way.[12,13] The rate constants are accurate to ±20% and the percentage product ion distributions to ±5 in the quoted percentage. The CS_2 had a purity of 99.9% and was further purified by freeze-pump-thaw cycles. Source gases were used without further purification. All measurements were made at room temperature (297K).

2.3 Results

Rate constants were determined from semi-logarithmic ion count decays versus CS_2 flow that were linear from more than one order of magnitude up to three orders of magnitude. No evidence was seen for internal excitation in the reactant ions in terms of non-linearity of the semi-logarithmic plots or the detection of endothermic channels. An example for the reaction of N_2^+ with CS_2 is given in Figure 2.1. Data for determining product distributions were taken using small flows of CS_2 so that they could be accurately determined. Kinetic information obtained in this study is given in Table 2.1.

Of these data obtained, only five (Ar^+, N_2^+, CO_2^+, CS_2^+, and D_3^+) of the fifteen reactions with CS_2 have been studied previously and these earlier data are also included in the table (note literature data for CS^+ is for an excited ion reaction with CS_2[21] and therefore was not included in the table). For Ar^+, both the rate constants and product distributions are in agreement to within error with the previous study,[22] but this study also indicates a slightly higher percentage of CS_2^+. For N_2^+, the rate constant is in agreement with that previously obtained in the same study as the Ar^+ measurement. However, although the same product ions are detected and with the same ion being dominant, the difference between the product percentages is outside the limits of experimental error. There is presently no explanation

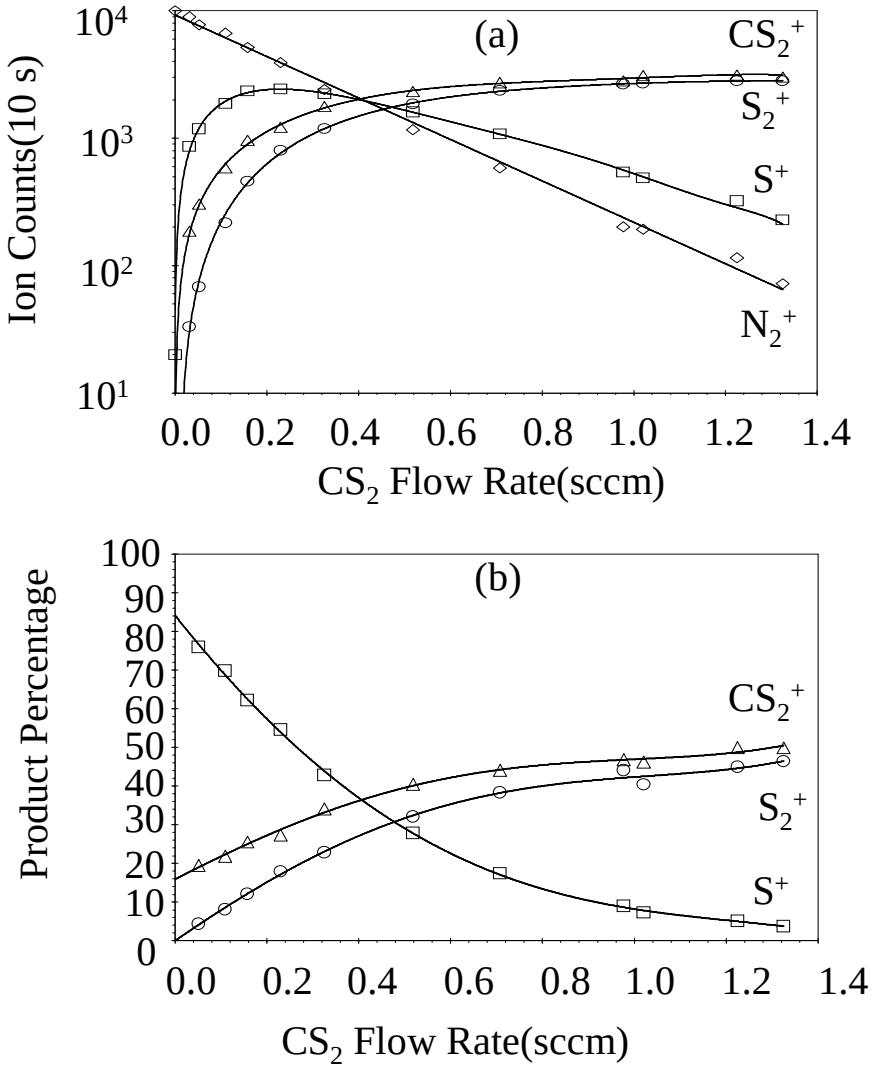

Figure 2.1: (a) Variations of N_2^+ counts and product ion counts, and (b) percentage of the ion products, with CS_2 flow. In (a) the decay of N_2^+ show excellent linearity over 2 orders of magnitude decrease in counts. In (b) extrapolation to zero flow, using polynomial fits, gives the percent product ion distribution (shown in Table 2.1, together with those for the other CS_2 reactions). S^+ and CS_2^+ are primary products with the S^+ reacting further to give additional CS_2^+ and the secondary product S_2^+.

Table 2.1: Rate constants and percentage product ion distributions for the reactions of CS_2 with the ions indicated. For comparison, equivalent data from the literature[14–16] are given for the analogous reactions of CO_2 and OCS with these ions. Also included are the theoretical rate constants determined using variational transition state theory[17] with polarizabilities and dipole moments taken from the literature.[18] The number in parentheses beside each ion is the recombination energy in eV. The ionization energies for CS_2, OCS and CO_2 are 10.073, 11.18 and 13.777 eV respectively.[18]

Reactant ion	Product	CS_2					OCS^a			$CO_2{}^a$		
		Percentage		k_{Exp}(cm^3/s)		k_{Theor}(cm^3/s)[b]	Product	Percentage	k_{Exp}(cm^3/s)	Product	Percentage	k_{Exp}(cm^3/s)
		Present	Literature	Present	Literature							
He^+(24.587)	S^+	58	–	2.07(-9)	–	3.56(-9)	–	–	–	C^+	2	1.0(-9)
	CS^+	31	–							O^+	14	
	C^+	11	–							CO^+	78	
										CO_2^+	5	
He_2^+(22.223)	S^+	75	–	–	–	2.58(-9)	–	–	–	–	–	–
	C^+	25										
	CS^+	small										
Ar^+(15.759)	S^+	≥ 93	88	3.70(-10)	3.5(-10)	1.36(-9)	S^+		1.3(-9)			
	CS_2^+	≤ 7	12		2.6(-10)		OCS^+			CO_2^+	100	4.8(-10)
N_2^+(15.581)	S^+	84	60	1.42(-9)	1.2(-9)	1.54(-9)	S^+	80	1.36(-9)		–	
	CS_2^+	16	40				OCS^+	20		CO_2^+	100	8.0(-10)
N^+(14.534)	S^+	12	–	1.55(-9)	–	2.02(-9)	S^+	22	1.4(-9)			
	CS^+	8	–				CS^+	5		CO^+	18	1.12(-9)
	CS_2^+	80	–				OCS^+	73		CO_2^+	82	
CO^+(14.014)	S^+	71	–	1.56(-9)	–	1.54(-9)	S^+	10	1.41(-9)	CO_2^+	100	1.10(-9)
	CS_2^+	29	–				OCS^+	90				
CO_2^+(13.777)	CS_2^+	100	100	1.39(-9)	9.9(-10)	1.32(-9)	OCS^+	100	9.60(-10)	–	–	
					1.3(-9)							
O^+(13.618)	CS^+	40	–	1.56(-9)	–	1.91(-9)	S^+	3	6.70(-10)	O_2^+	100	1.10(-9)
	CS_2^+	60	–				OCS^+	97				
D^+(13.603)	S^+	65	–	3.44(-9)	–	4.98(-9)	–	–	–	CO_2^+	100	3.5(-9)
	DS^+	24	–									
	CS^+	11	–									
CS^+(11.33)	CS_2^+	100	–	1.30(-9)	–	1.32(-9)	CS_2^+	100[c]	7.7(-10)			
C^+(11.26)	CS^+	91	–	1.81(-9)	–	2.16(-9)	CS^+	80	2.0(-9)	CO^+	90	1.1(-9)
	CS_2^+	9	–				OCS^+	20		CO_2^+	10	
S^+(10.36)	S_2^+	52	–	1.39(-9)	–	1.46(-9)	S_2^+	100	9.1(-10)			<5 (-13)
	CS_2^+	48	–									
CS_2^+(10.073)	$CS_2^+ \bullet CS_2$	100	–	3.33(-11)[d]	–	1.13(-9)	–	–	–	–	–	
S_2^+(9.356)	N/A[e]	–	–	1.0(-11)	–	1.18(-9)	–	–	–	–	–	–
D_3^+	DCS_2^+	100	100	3.07(-9)	3.1(-9)	2.95(-9)	HCO^+	<10	1.9(-9)	DCO_2^+	100	1.74(-9)
							$HCOS^+$	>90				

[a]Experimental literature values.[14–16]

[b]Theoretical capture value calculated using the model of Su and Chesnavich.[17]

[c]Taken from Dzidic et al.[19](Note typographical error in the Anicich compilation[20]).

[d]Effective binary k at $p_{He} = 0.493$ Torr and is equivalent to a ternary k of 2.4 x 10^{-27}cm^{6}s^{-1} with a He third body; literature values of 1.8 and 5.8 x 10^{-27}cm^{3}s^{-1} are available with O_2 and CO_2 third bodies.[14]

[e]Product distribution could not be determined for this slow reaction.

for this difference; it could, however, be due to differing corrections for mass discrimination. For the CO_2^+ and D_3^+ reactions, the same single charge transfer (c.t.) and proton transfer (p.t.) products, respectively, were detected and with the same rate constants as in previous studies.[23,24] For the CS_2^+ reaction, the literature values of 1.8 and 5.8 x 10^{-27}cm^6 s^{-1}, with O_2 and CO_2 third bodies respectively, are consistent with the current value of 2.4 x 10^{-27}cm^6 s^{-1} with He as third body.[14–16] The overall evidence indicates that the present measuring techniques are well calibrated.

2.4 Discussion

As can be seen from Table 2.1, within these data there is a general trend of c.t. and dissociative c.t. products. Note that long-range c.t. is not an option in all cases since as the recombination energy of the reactant ion decreases, the long-range dissociation mechanism without complex formation becomes endothermic. The D_3^+ and CS_2^+ reactions are exceptions to this trend, with proton transfer and association being the only channels respectively. The D_3^+ reaction proceeds at the collisional rate as is common for this mechanism [25], with the CS_2^+ association being relatively slow. CS_2^+ is a common c.t. product, although it is not observed for the highest recombination energy species (He^+ and He_2^+), where dissociative c.t. channels are exothermic. Note that the products could not be identified in the slow reaction of S_2^+ (no direct c.t. processes are energetically possible in this case), which proceeds at about 1% of the collisional rate. All other reactions proceed at, or close to, the collisional rate. Also, there is no consistent trend of increasing CS_2^+ product percentage with decreasing recombination energy, and the other products indicate that the mechanism could be a mixture of direct/long range c.t. and complex formation.

2.4.1 He^+/He_2^+

He^+ and He_2^+ reactions proceed by exothermic dissociative c.t. giving the same product channels (S^+, C^+ and CS^+). The CS^+ product channel for the He_2^+ reaction is surprisingly

much smaller than for the He^+ reaction, given the difference in recombination energy between the two reactants is only 228 kJ/mol (2.36 eV).

$$He^+ + CS_2 \rightarrow S^+ + CS + He + 932kJ/mol \quad 58\% \quad (2.1)$$

$$\rightarrow CS^+ + S + He + 839kJ/mol \quad 31\% \quad (2.2)$$

$$\left.\begin{array}{l} \rightarrow C^+ + 2S + He + 132kJ/mol \quad (2.3) \\ \rightarrow C^+ + S_2 + He + 558kJ/mol \quad (2.4) \end{array}\right\} \quad 11\%$$

$$He_2^+ + CS_2 \rightarrow S^+ + CS + 2He + 708kJ/mol \quad \sim 75\% \quad (2.5)$$

$$\rightarrow CS^+ + S + 2He + 614kJ/mol \quad < 1\% \quad (2.6)$$

$$\rightarrow C^+ + S_2 + 2He + 333kJ/mol \quad \sim 25\% \quad (2.7)$$

S_2^+ production, although exothermic in both cases, is not observed, probably because of the steric hindrance due to the two S atoms being at opposite ends of the reactant CS_2. Indeed, in the whole series of reactions, even where complex formation is required, S_2^+ is only observed as a product for the S^+ and CS^+ reactions where there is an additional source of S.

2.4.2 Ar^+/N_2^+

For Ar^+ and N_2^+, a comparison is interesting since the recombination energies are very similar (differing by only 17.4 kJ/mol (0.18 eV), with that of N_2^+ being the smaller). In these cases the product distributions are similar with S^+ being the dominant product and CS_2^+ production being small.

$$Ar^+ + CS_2 \rightarrow S^+ + Ar + CS + 80kJ/mol \quad \geq 93\% \quad (2.8)$$

$$\rightarrow CS_2^+ + Ar + 549kJ/mol \quad \leq 7\% \quad (2.9)$$

$$N_2^+ + CS_2 \rightarrow S^+ + N_2 + CS + 63kJ/mol \quad 84\% \quad (2.10)$$

$$\rightarrow CS_2^+ + N_2 + 531kJ/mol \quad 16\% \quad (2.11)$$

Bond formation in the product neutrals producing ArCS is not possible for Ar^+, but in the N_2^+ case this is a possibility yielding N_2CS. The major products in these distributions are associated with the less energetic pathway; the explanation can be found by looking at the potential energy surface for several electronic states of CS_2^+.[25] In the non-dissociative c.t. pathway there is enough energy to excite CS_2^+ to the $B^2\Sigma_u^+$ electronic state, which intersects with the dissociative curve crossing yielding $S^+ + CS$.

2.4.3 D^+/O^+

D^+ and O^+ also have similar recombination energies, but in these cases, the products are very different with non-dissociative c.t. being dominant for the exothermic O^+ reaction and nonexistent for D^+ even though it is similarly exothermic.

$$O^+ + CS_2 \rightarrow CS^+ + SO + 302kJ/mol \qquad 40\% \qquad (2.12)$$

$$\rightarrow CS_2^+ + O + 342kJ/mol \qquad 60\% \qquad (2.13)$$

and

$$D^+ + CS_2 \rightarrow S^+ + (DCS) + N/A \qquad 65\% \qquad (2.14)$$

$$\rightarrow DS^+ + CS + N/A \qquad 24\% \qquad (2.15)$$

$$\rightarrow CS^+ + DS + 139kJ/mol \qquad 11\% \qquad (2.16)$$

$$\rightarrow CS_2^+ + D + 341kJ/mol \qquad 0\% \qquad (2.17)$$

Note that in the D^+ reaction the DS^+ channel dominates over CS^+ as would be expected if multiple charge transfers occur as the products separate, since DS has a smaller ionization energy than CS by 87 kJ/mol (0.9 eV) and would be energetically favored (N/A indicates that insufficient literature data were available to calculate the reaction energetics). If this is so, it is surprising that SO^+ is not produced in the O^+ reaction since the ionization energy of SO is 100 kJ/mol (1.04 eV) less than that of CS. Even though no SO^+ is produced, the $CS^+ + SO$ channel (2.12) is of similar magnitude to the sum of channels (2.15) and (2.16) consistent with a similar overall mechanism.

2.4.4 C^+/CS^+

C^+ and CS^+ also have similar recombination energies, however, here the reaction products appear very different, with CS_2^+ being small for the C^+ reaction and the only channel for the CS^+ reaction.

$$C^+ + CS_2 \rightarrow CS^+ + CS + 266kJ/mol \quad 91\% \quad (2.18)$$

$$\rightarrow CS_2^+ + C + 115kJ/mol \quad 9\% \quad (2.19)$$

$$CS^+ + CS_2 \rightarrow CS_2^+ + CS + 121kJ/mol \quad 100\% \quad (2.20)$$

For the C^+ reaction, an S atom abstraction would yield the observed and dominant CS^+ product. However, the CS^+ reaction only proceeds by the non-dissociative c.t. channel. This channel has similar energy to the non-dissociative channel in the C^+ reaction, but the observed dominant CS^+ product channel is energetically favored by 151 kJ/mol (1.57 eV).

2.4.5 N^+/CO^+

Although N^+ and CO^+ have relatively similar recombination energies (differing by only 50 kJ/mol (0.52 eV)), the product distributions for their CS_2 reactions are quite different.

$$N^+ + CS_2 \rightarrow S^+ + (NCS) + N/A \quad 12\% \quad (2.21)$$

$$\rightarrow CS^+ + NS + 355kJ/mol \quad 8\% \quad (2.22)$$

$$\rightarrow CS_2^+ + N + 430kJ/mol \quad 80\% \quad (2.23)$$

$$CO^+ + CS_2 \rightarrow S^+ + (C_2OS) + N/A \quad 71\% \quad (2.24)$$

$$\rightarrow CS_2^+ + CO + 380kJ/mol \quad 29\% \quad (2.25)$$

In both cases S^+ and CS_2^+ are products, but the percentages are approximately reversed. The channel producing S^+ and N + CS is endothermic and thus the reaction requires complex formation with bonding in the neutral products, yielding NCS. In the reaction of N^+ with

OCS, the analogous product channel S^+ + NCO was observed. Additionally, in the CO^+ reaction with CS_2, the channel producing S^+ and CO + CS is an endothermic process thus the reaction must yield C_2OS.

2.4.6 CO_2^+/S^+

The CO_2^+ reaction proceeds by the non-dissociative c.t. only (the only case studied where this occurs). The S^+ reaction has a dissociative c.t. channel and a non-dissociative channel. The dissociative channel leads to S_2^+ production, which may be due to the S-atom abstraction.

$$CO_2^+ + CS_2 \rightarrow CS_2^+ + CO_2 + 357kJ/mol \qquad 100\% \qquad (2.26)$$

$$S^+ + CS_2 \rightarrow S_2^+ + CS + 82kJ/mol \qquad 52\% \qquad (2.27)$$

$$\rightarrow CS_2^+ + S + 28kJ/mol \qquad 48\% \qquad (2.28)$$

This S_2^+ product is only observed in one other reaction in the series studied, that of CS^+, where the mechanism again does not require the formation of the S_2^+ from the two S atoms at opposite ends of the CS_2 molecule. That S_2^+ is not produced in any of the other reactions indicates that the coalescence of the 2 S atoms from CS_2 is sterically hindered and is not efficient. The S atoms in the S_2^+ product are then from both reactants indicating intermediate complex formation.

2.4.7 Comparison with Literature Data for the O Containing Analogs OCS and CO_2

In the Ar^+ reactions with CS_2 and OCS, S^+ and non-dissociative c.t. are both products, although the quantitative product distribution for OCS was not determined (see Table 2.1 for these and other literature data on the reactions with OCS and CO_2). CO_2^+ was the only product in the CO_2 reaction, since in this reaction, dissociation yielding O^+ is not energetically favorable. For N_2^+, the comparable channels with CS_2 and OCS have similar

contributions to the product distribution, however CO_2^+ is the only product in the CO_2 reaction.

For the N^+ and CO^+ reactions, the rate constants are all close to collisional. For N^+, in all cases non-dissociative c.t. is dominant at ∼80%, the remaining channel in the CO_2 reaction being the strongly bonded CO^+. The analogous CS^+ channel is observed in the CS_2 and OCS reactions. Additionally an S^+ channel is observed, which is possible in the OCS case by formation of NCO product neutral and therefore presumably possible with formation of NCS product neutral in the CS_2 reaction. Surprisingly the CO^+ channel is not seen in the OCS reaction. This may be partly due to sulfur having a lower ionization energy than CO. In comparison with N^+, in the CO^+ reaction with CS_2 there is a decrease in the non-dissociative c.t. as the recombination energy of the reactant ion decreases and with an increase in S^+ product channel. Comparing the $CO^+ + CS_2$ reaction to the analogous CO^+ reactions with OCS and CO_2, it is noticed that the OCS and CO_2 reactions have the non-dissociative c.t. channel as the dominant channel. The reason why this channel is not the dominant channel in the CO^+ reaction with CS_2 could not be explained and needs to be further investigated.

For the O^+, CO_2^+ and D^+ reactant ions, all the reactions are rapid (but with the OCS reaction being somewhat slower) except in the CO_2^+ reaction with CO_2 where only the undetectable resonant c.t. is possible. The D^+ reaction with OCS has not been studied. In the other CO_2^+ reactions, non-dissociative c.t. is the only product. For the O^+ reactions with CS_2 and OCS non-dissociative c.t. is observed along with dissociative channels. Additionally, only the dissociative channel is observed in the O^+ reaction with CO_2. Note that CO^+ is not a product, which may be due to O_2 having a lower ionization energy. The combination of a small difference in recombination energy between CO_2^+ and O^+ and dissociative product channels only existing in the O^+ reactions may imply that formation of an intermediate complex occurs in the O^+ case.

The D^+ reaction with CO_2 is very different giving only non-dissociative c.t. Here for O_2^+ to be a product would require the more weakly bonded CD to be produced, and also the 2 O

atoms to bond from opposite ends of the O=C=O. It was noted earlier that in reactions with CS_2, the S_2^+ product channel is only seen if the reactant ion contains a S atom, presumably for the same reason.

The C^+ and CS^+ reactions are all rapid (the reaction of CS^+ with CO_2 has not been studied). Although the recombination energies of the ions are getting smaller, non-dissociative c.t. is not becoming more prevalent except for the CS^+ reaction with CS_2, where it is the only channel. The same CS_2^+ product ion is similarly observed in the CS^+ reaction with OCS, indicating a S-atom abstraction reaction (note that the product ion was incorrectly reported in a recent compilation[20]). In the reaction of C^+ with CS_2 the dominant dissociative channel is energetically favored over the non-dissociative c.t. channel by 151 kJ/mol (1.57 eV). A dominant dissociative channel is similarly seen in the reactions of C^+ with OCS and CO_2. The C^+ reaction with OCS forms the CS^+ product ion and neutral CO, presumably because CS has a lower ionization energy than CO. Similarly the C^+ reaction with CO_2 produces CO^+ as the dominant product ion.

In the S^+ reactions, the S_2^+ product channel for CS_2 and OCS presumably take place by a S-atom abstraction. No equivalent O-atom abstraction occurs for the CO_2 reaction even though the strongly bonded CO would be produced. The S^+ reaction with OCS produces 100% S_2^+ in contrast to the S^+ reaction with CS_2 where the large channel is due to the non-dissociative charge transfer. The S_2^+ channel produced in the OCS reaction is energetically exothermic by 217 kJ/mol (2.25 eV) and the analogous channel in the CS_2 reaction is exothermic by 82 kJ/mol (0.85 eV), which is only 55 kJ/mol (0.57 eV) larger than the competitive non-dissociative c.t. product channel. No literature data are available for the CS_2^+ reaction. Literature data are also not available for the S_2^+ reaction.

The D_3^+ reactions proceed almost exclusively by proton transfer as might be expected. Only in the case of the OCS reaction is there another channel with the likely neutral product being D_2S. This would imply that the proton attacks the electronegative O-atom and would then lead to the isomer COD^+ rather than DCO^+ and this needs to be investigated.

2.5 Conclusions

Of the fifteen reactions studied, a majority of the reactions proceed by a non-dissociative charge transfer. There was no clear trend by which this channel became more prevalent with a decreasing recombination potential of the reactant ion. However, there is an expected consistency between the product distribution abundances and the energetics. The comparison between the CS_2 reactions and previously studied OCS and CO_2 reactions is consistent with similar mechanisms taking place between the reactant ion and neutrals as dictated by the energetics.

In the CS_2 reactions, the major products, S^+, S_2^+, C^+, CS^+, and CS_2^+ are all significant in chemical models of the interstellar medium. S^+ and S_2^+ are involved in further ion-molecule reactions, which have been discussed by Decker et al.[5–7] The reaction products C^+ and CS^+ react with H_2 to give CH^+ and HCS^+,[20] respectively, both of which have been detected in isc.[1,2] Also, CS_2^+ reacts with atomic H to produce HCS^+ and this reaction could play an important role in diffuse clouds where atomic H is prevalent. Additionally, photofragmentation of CS_2^+ could occur leading to smaller ion fragments, which could react with H_2 producing observed isc species such as CH^+ and HCS^+. In dense clouds, where atomic H is much less prevalent than H_2, CS_2^+ can be a long lived species allowing dissociative electron-ion recombination to occur, as has been studied recently (Plasil et al., 2004, in preparation). In addition, CS_2^+ could react with abundant CO, which has not been investigated in the laboratory. CS_2 reactions may play an important role in contributing to the observed sulfur containing molecules in the isc and therefore the unobservable CS_2 may partly contribute to the difference in the cosmic abundance of sulfur and the abundance of observed sulfur species.

2.6 References

[1] McCarthy, M. C.; Thaddeus, P. *Chem. Soc. Revs.* **2001**, *30*, 177–185.

[2] Thaddeus, P.; McCarthy, M. C. *Spectrochimica Acta* **2001**, *A57*, 757–774.

[3] Crovisier, J.; Encrenaz, T. *Comet Science;* Cambridge University Press: Cambridge, 2000.

[4] Adams, N. G.; Babcock, L. M.; Ray, N. S. In *Atomic Processes in Plasmas*; Schultz, D. R., Meyer, F. W., Ownby, F., Eds.; AIP: Melville, NY, 2002; pages 182–193.

[5] Decker, B. K.; Babcock, L. M.; Adams, N. G. *J. Phys. Chem.* **2000**, *104*, 801–810.

[6] Decker, B. K.; Adams, N. G. *Int. J. Mass Spectrom. Ion Proc.* **1997**, *165/6*, 257–269.

[7] Decker, B. K.; Adams, N. G.; Babcock, L. M. *Int. J. Mass Spectrom.* **1999**, *185/186/187*, 727–743.

[8] Decker, B. K.; Adams, N. G.; Babcock, L. M. *Int. J. Mass Spectrom.* **2000**, *195/196*, 185–201.

[9] Decker, B. K.; Adams, N. G.; Babcock, L. M. *Int. J. Mass Spectrom.* **2001**, *208*, 99–112.

[10] Adams, N. G.; Decker, B. K.; Babcock, L. M. In *1999 Centennial Meeting of the American Physical Society*, Vol. 44, page 450, Atlanta, GA, 1999.

[11] Adams, N. G.; Smith, A. D.; Wiley-Interscience: New York, 1988; page 165.

[12] Adams, N. G.; Smith, D. *Int. J. Mass Spectrom. Ion Phys.* **1976**, *21*, 349–59.

[13] Adams, N. G.; Smith, D. *J. Phys. B.* **1976**, *9*, 1439–51.

[14] Ikezoe, Y.; Matsuoka, S.; Takebe, M.; Viggiano, A. A. *Gas Phase Ion-Molecule Reaction Rate Constants through 1986;* Ion Reaction Research Group of the Mass Spectroscopy Society of Japan: Tokyo, 1987.

[15] Anicich, V. *J. Phys. Chem. Ref. Data* **1993**, *22*(6), 1469–1569.

[16] Anicich, V. *Ap. J.* **1993**, *84*(2), 215–315.

[17] Su, T.; Chesnavich, W. J. *J. Chem. Phys.* **1982**, *76*(10), 5183–5185.

[18] Linstrom, P. J., Mallard, W. G., Eds. *NIST Chemistry WebBook;* National Institute of Standards and Technology, March 2003.

[19] Dzidic, I.; Good, A.; Kebarle, P. *Can. J. Chem.* **1970**, *48*, 664–673.

[20] Anicich, V. *An Index of the Literature for Bimolecular Gas Phase Cation-Molecule Reaction Kinetics: JPL Publication 03-19;* Jet Propulsion Laboratory: Pasadena, 2003.

[21] Henglein, A. *Z. Naturforschg.* **1962**, *17a*, 37–43.

[22] Shul, R. J.; Upschulte, B. L.; Passarella, R.; Keesee, R. G.; Castlemann Jr., A. W. *J Phys. Chem.* **1987**, *91*(10), 2556–2562.

[23] Su, T.; Bowers, M. *Int J. Mass Spectrom. Ion Phys.* **1975**, *17*, 309–319.

[24] Rakshit, A. B.; Warneck, P. *J. Chem. Soc: Farad. Trans II* **1980**, *76*(9), 1084–1092.

[25] Tosh, R.; Shukla, A.; Futrell, J. *J Phys. Chem.* **1995**, *99*(42), 15488–15496.

Chapter 3

Experimental Determination of Energy Disposal in the Dissociative Electron Recombinations of CS_2^+ and HCS_2^{+1}

[1]Molek, C. D.; Plasil, R.; McLain, J. L.; Adams, N. G.; Babcock, L. M. *J. Phys. Chem. A.*, Submitted. Reprinted here with permission of publisher.

3.1 Introduction

Dissociative electron-ion recombination(DR) is an important ionization loss process in many plasmas varying from the interstellar medium (ism) to those used as gas lasers.[1–8] In studies of this process, a considerable amount of effort has been devoted to determining the recombination rate coefficients, including a few as a function of temperature,[9–12] and more recently, effort has been directed to determining the neutral product (ground electronic state) distributions.[13–44] Since this is an energetic process, often the products can be in electronically excited states. Information on the states populated, and vibrational excitation in these states, suggests reaction mechanisms and puts constraints on theory. For example the recombinations of N_2H^+ and N_2D^+ result in the population of the $N_2(B\ ^3\Pi\ _g)$ state which undergoes a radiative transition to the $A^3\Sigma_u^+$ state.[45] Observation of these emissions, together with the known Franck-Condon factors for the transition, led to a determination of the vibrational population distribution of the B state populated in the recombinations. Comparison of the ratio of the population distributions produced with N_2H^+ and N_2D^+ has shown that the relative population of $v' = 6$ for N_2H^+ is enhanced by a factor of $\sim$1.6 over the population for N_2D^+ at 300 K, increasing dramatically to 6 at 100 K.[11,46] The energy level for $v' = 6$ is closely resonant with the vibrational ground state ($v = 0$) of the recombining N_2H^+ ion and this accidental resonance strongly suggests a mechanism involving quantum tunneling through a barrier between the bound ionic potential surface and the repulsive dissociative curve to the products $N_2(B\ ^3\Pi_g)$ and H. Such a scenario was suggested by Bates as a general possibility prior to this work.[47–49] Recently, potential energy curves(A and W) for the products N_2 + H have been calculated for the N_2H^+/e^- system.[50] Unfortunately, the N_2 B state crossing, $N_2(^3\Pi_g)$, was not calculated and therefore detailed information is still needed to determine the likelihood of the suggested tunneling mechanism. In addition, Rosati et al.[51] quantitatively assigned the total emission intensity from the measured $N_2(B\rightarrow A)$ with a yield 19%$\pm$8% originating from the $N_2(B,\ v' \geq 1)$.

There is also some indication of a tunneling mechanism in the case of the CO(a) state produced in the recombinations HCO^+/DCO^+.[46] However, it was not possible to determine the relative population of the resonant level (because of spectral line overlap) although there is some indication of an enhancement as this level is approached. Theoretical calculations are available for this system, although there is disagreement as to where the ion potential surface (represented as a curve) is crossed by the repulsive curve to ground state products.[52,53] No detailed information is available for dissociation to the CO(a) state, however, calculations with approximate potentials,[54] have given reasonable agreement with the experimental vibrational distribution.

An example of the applied significance of these recombinations is the observation of CO (a $\rightarrow$ X) Cameron band emissions from the Red Rectangle of the interstellar medium.[55] These show a CO (a) state vibrational population distribution very similar to that observed in the laboratory from the HCO^+ recombination. Yan et al.[56] have analyzed this situation in detail and concluded that this recombination is indeed the source of the interstellar emissions, the first time an individual chemical reaction has been observed outside the solar system. This lends strong independent support of the widely accepted view that interstellar chemistry is driven significantly by ionic reactions. This conclusion was previously based on the general agreement between model calculations and observed neutral abundances.

In addition, the observed sulfur content in the ism only contributes about 4% of the calculated cosmic abundance of sulfur.[57–59] How much CS_2 is contributing to the total cosmic abundance of sulfur is unknown, but recombination studies of CS_2^+ and HCS_2^+ could give insight into the existence of the molecule and possibly its contribution to the ism. Like CO_2, CS_2 is also symmetrical, thus rendering it unobservable in the microwave and infrared regions available in the ISM, but recent work has proved the presence of CS_2 in comets by identification of UV emission lines.[60] In addition, CS and S have been observed in the ism[58] and cometary comae.[61] These are both products of the DR of CS_2^+, which may point to the existence of CS_2 in the ism.

In order to try to establish general trends in the DR process and also to gain knowledge about charge transfer mechanisms of ion-neutral reactions (i.e. long range versus an intimate encounter) we have continued to investigate recombination emissions with studies of the CS_2^+ recombination analogue of CO_2^+ studied previously[62–64] and HCS_2^+, which is moving the studies to more complex protonated ions. This additionally enables the effect of the proton on recombination to be assessed.

3.2 Experimental

The studies were performed using a flowing afterglow, the basic features of which have been described in detail previously,[65,66] and this detail will not be repeated here. Briefly, He is passed through a microwave discharge ionization source, and the plasma and remaining He proceeds along the flow tube to a downstream mass spectrometer under the action of a Roots pump. At a series of positions along the tube, measured flows of various reactant gases can be added and the chemical reactions monitored by the mass spectrometer/ion detection system. Ionization density can be determined as a function of distance along the flow tube using an axially movable Langmuir probe.[67,68] At a position downstream in the flow, photon emissions from the afterglow plasma can be observed by focusing those emissions onto the entrance slit of an optical monochromator (Action Research Corporation Model AM-506), spectrally dispersed and detected by a cooled photomultiplier (Products for Research housing with an EMI 9816QB photomultiplier) followed by photon counting, by a Gated Photon Counter(Stanford Research Systems Model SRS 200). A reactant gas inlet port is situated just downstream of the monochromator viewing region and is a single tube facing upstream so that the emissions can be produced in a very localized region; a He flush is added to this flow to optimize the chemistry in the emitting region. A port is located further upstream in the flow tube through which known flows of reactant gases can be pulsed to produce slugs of reactive gases in the flow; this is used in some of the spectroscopic experiments to distinguish emissions from specific reactions.[69,70] In this mode, two photon counters are

used one of which collect counts when the pulsed gas is absent and the other when it is present. Counting on each point in the scan is done until a pre-determined signal-to-noise ratio is achieved, such that each point with signal is just as statistically accurate as the next.[69,70] All of the other ports are ring ports facing upstream so that the gas is uniformly dispersed in a small axial distance. The details of the spectroscopic techniques have recently been published.[70] In these studies Ar, H_2 and CS_2 were variously added to the He flow as discussed in Section 3.2.1. All the measurements were conducted at room temperature, although the apparatus has the capability to operate between 80 and 600K. Reactant gases were used as supplied by the manufacturer (National Welders Supply Co.) and, in all cases, were further purified by passing through molecular sieve traps at low temperature (80K for He (99.995%) and H_2 (99.999% purity) and 200K for Ar (99.999% purity)). CS_2 (99.9% purity) was freeze-pump-thawed several times before use.

3.2.1 Plasma Kinetics and Spectral Emissions

He^+ and helium metastable atoms, He^m, were produced in the discharge and studies were conducted at about 2 Torr to ensure that most of the He^+ was destroyed a short distance downstream by the association reaction

$$He^+ + He + He \longrightarrow He_2^+ + He \qquad k = 1 \times 10^{-31} cm^6 s^{-1} \tag{3.1}$$

Note that, k, is the reaction coefficient and is termolecular for equation 3.1 and bimolecular for the rest of the chemical equations. Ar was added further downstream to destroy He_2^+ and He^m by

$$He_2^+ + Ar \longrightarrow Ar^+ + 2He \qquad k = 2.0 \times 10^{-10} cm^3 s^{-1} \tag{3.2}$$

$$He^m + Ar \longrightarrow Ar^+ + e + He \qquad k = 7 \times 10^{-11} cm^3 s^{-1(71)} \tag{3.3}$$

creating an Ar^+/e plasma, with only a small presence of He^+, approximately 0.2% of the total ion density at the addition point of CS_2. This vapor was added to produce the recombining

ion CS_2^+.

$$Ar^+ + CS_2 \longrightarrow S^+ + CS + Ar \qquad 93\% \quad k = 3.7 \times 10^{-10} cm^3 s^{-1(72)} \tag{3.4}$$

$$\longrightarrow CS_2^+ + Ar \qquad 7\% \tag{3.5}$$

Note also that S^+ reacts further by

$$S^+ + CS_2 \longrightarrow S_2^+ + CS \qquad 52\% \quad k = 1.4 \times 10^{-9} cm^3 s^{-1(72)} \tag{3.6}$$

$$\longrightarrow CS_2^+ + S \qquad 48\% \tag{3.7}$$

as measured in our laboratories.[72] Note, rate coefficients (k) and the percentage product distributions were obtained from literature compilations,[73] unless otherwise indicated by a reference after the rate constant. S_2^+ and CS_2^+ then only react slowly with CS_2 by association and are available to recombine with electrons. Ground state S_2^+ can only recombine to give S atoms and, with the energy available (4.95 eV). It is only energetically possible to produce low-lying, non-radiating states of S. The accessible states ($^1S_0$, $^1D_2$, $^3P_{0,1,2}$) are all in the ground electronic state ($3s^2 3p^4$) of S.

The HCS_2^+ recombining ion was produced by adding H_2 to the flow tube downstream of the Ar but prior to the CS_2, whence the reaction sequence is

$$Ar^+ + H_2 \longrightarrow ArH^+ + H \qquad k = 8.9 \times 10^{-10} cm^3 s^{-1} \tag{3.8}$$

$$ArH^+ + H_2 \longrightarrow H_3^+ + Ar \qquad k = 6.3 \times 10^{-10} cm^3 s^{-1} \tag{3.9}$$

$$H_3^+ + CS_2 \longrightarrow HCS_2^+ + H_2 \qquad k = 6.8 \times 10^{-9} cm^3 s^{-1(72)} \tag{3.10}$$

A small percentage of H_2^+ (2%) is also generated in reaction 3.8, but this is rapidly converted to H_3^+ by reaction with H_2.[73] For CS_2^+ and HCS_2^+ recombination, the following channels are energetically possible,

$$CS_2^+ + e \longrightarrow S + CS + 5.51\ eV \tag{3.11}$$

$$\longrightarrow C + S_2 + 2.57\ eV \tag{3.12}$$

and

$$HCS_2^+ + e \longrightarrow H + CS_2 + 6.53\ eV \tag{3.13}$$

$$\longrightarrow SH + CS + 7.35\ eV \tag{3.14}$$

$$\longrightarrow CH + S_2 + 2.51\ eV \tag{3.15}$$

$$\longrightarrow S + HCS + 4.02\ eV \tag{3.16}$$

$$\longrightarrow C + HS_2{+}?\ eV \tag{3.17}$$

but are not necessarily all significant. Energetics refer to ground state products and have been calculated using data from NIST compilations.[74] The reaction sequences producing these ions have been modeled kinetically as a function of distance along the flow tube for the neutral concentrations used in these studies and the ion concentrations are plotted as a function of distance in Figure 3.1.

In the CS_2^+ formation case, CS_2^+ is the dominant ion by a factor of 1.33 over S_2^+. In any case, as noted earlier, ground state S_2^+ recombination can only yield S atoms in non-radiative states. The next most abundant ion, Ar^+, is nearly two orders of magnitude smaller in this region, and has a slow recombination rate. Thus it is not competitive. In the HCS_2^+ case, prior to the introduction of CS_2 there is some remaining He^+, an order of magnitude lower than H_3^+, which can react with CS_2.

$$He^+ + CS_2 \longrightarrow S^+ + CS + He \qquad 58\% \quad k = 2.0 \times 10^{-9} cm^3 s^{-1} \tag{3.18}$$

$$\longrightarrow CS^+ + S + He \qquad 31\% \tag{3.19}$$

$$\longrightarrow C^+ + S_2 + He \qquad 11\% \tag{3.20}$$

The S^+ and CS^+ products react rapidly, 1.4 x 10^{-9}cm^{3}s^{-1} and 1.3 x 10^{-9}cm^{3}s^{-1} respectively, with CS_2 generating S_2^+ (52%) and CS_2^+ (48%) from S^+ reaction and 100% CS_2^+ from the CS^+ reaction.[72] Even with this generation of CS_2^+, its number density is still more than 30 times less than HCS_2^+, the ion of interest, thus interfering emissions are relatively insignificant. The small product channel C^+ (3.20) reacts with CS_2 to produce CS^+ and C^+, 91% and

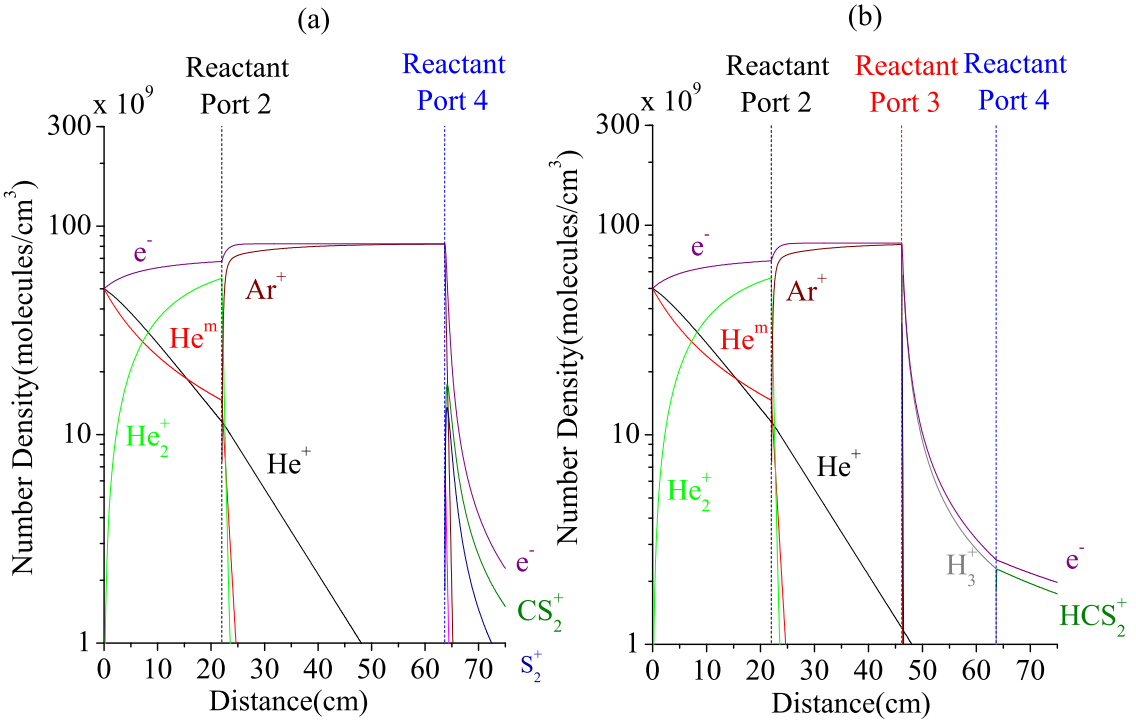

Figure 3.1: Kinetic modeling of the ion concentrations as a function of position along the flow tube for typical conditions under which the spectral studies were made. Distance 0 cm on the x-axis indicates the position of the plasma source (i.e. microwave discharge)(a) For an $He/Ar/CS_2$ plasma and (b) for an $He/Ar/H_2/CS_2$ plasma. Typical neutral concentrations were [Ar] = 4.5 x 10^{13} molecules cm^{-3} (added at port 2), [H_2] = 1.0 x 10^{14} molecules cm^{-3} (added at port 3) and [CS_2] 9.0 x 10^{13} moleucules cm^{-3} (added at port 4) with a He pressure of 2 Torr. Note that spectroscopic emissions are observed in the vicinity of the CS_2 addition point. Details of the ion concentration variations are discussed in the text.

9% respectively, yet the ion concentrations are insignificant compared to the magnitude of HCS_2^+. Thus it can be seen from the modeling that HCS_2^+ is by far the dominant ion.

3.3 Results and Discussion

Spectral scans of the from the CS_2^+/e and HCS_2^+/e plasmas were acquired over the wavelength range 180 to 800 nm and the wavelength regions where there were significant emissions are shown in Figures 3.2 and 3.3.

The identified emission features are the CS($A^1\Pi \rightarrow X^1\Sigma^+$), S($^5S_2^0 \rightarrow ^3P_2$), S($^5S_2^0 \rightarrow ^3P_1$), CS($a^3\Pi \rightarrow X^1\Sigma^+$), CS($B^1\Sigma^+ \rightarrow A^1\Pi$), CS^+($B^2\Sigma^+ \rightarrow A^2\Pi_i$), and CS_2^+ ($\tilde{A}^2\Pi_u \rightarrow X^2\Pi_g$). Obviously the ion emissions can only originate from ion-molecule reactions whereas the neutral emissions can originate from these or from DR. The origins of the neutral emissions were determined in several ways. For example, for the CS($A \rightarrow X$) emissions, the spectrum over the wavelength range 240-290 nm was obtained, Figure 3.4.

To distinguish emissions from processes involving electrons, a ~1% mixture of SF_6 in He was pulsed into the flow tube, just upstream of reactant port 3, whilst accumulating the counts at each wavelength when the SF_6 was absent and present. When SF_6 is present, the electrons are rapidly attached to form mainly SF_6^- with a small amount of SF_5^-[75,76] and DR is quenched, thus quenching the emissions from that source. Therefore, subtraction of the counts when electrons are absent from those when electrons are present, gives a spectrum due only to processes involving electrons, which in this case is limited to the DR process. An example of the type of spectrum obtained is given in Figure 3.4.

The details of this technique have been published recently.[70] Note that when electrons are absent, negative ions are present and thus ion-ion recombination can occur. Any emissions from this process would have appeared as negative counts, which were not observed. This process is not expected to be very significant, since the recombination rate constants are typically an order of magnitude smaller than DR rate constants.[77] Also, less energy is available by the electron detachment energy of the negative ion, giving less chance for electronic

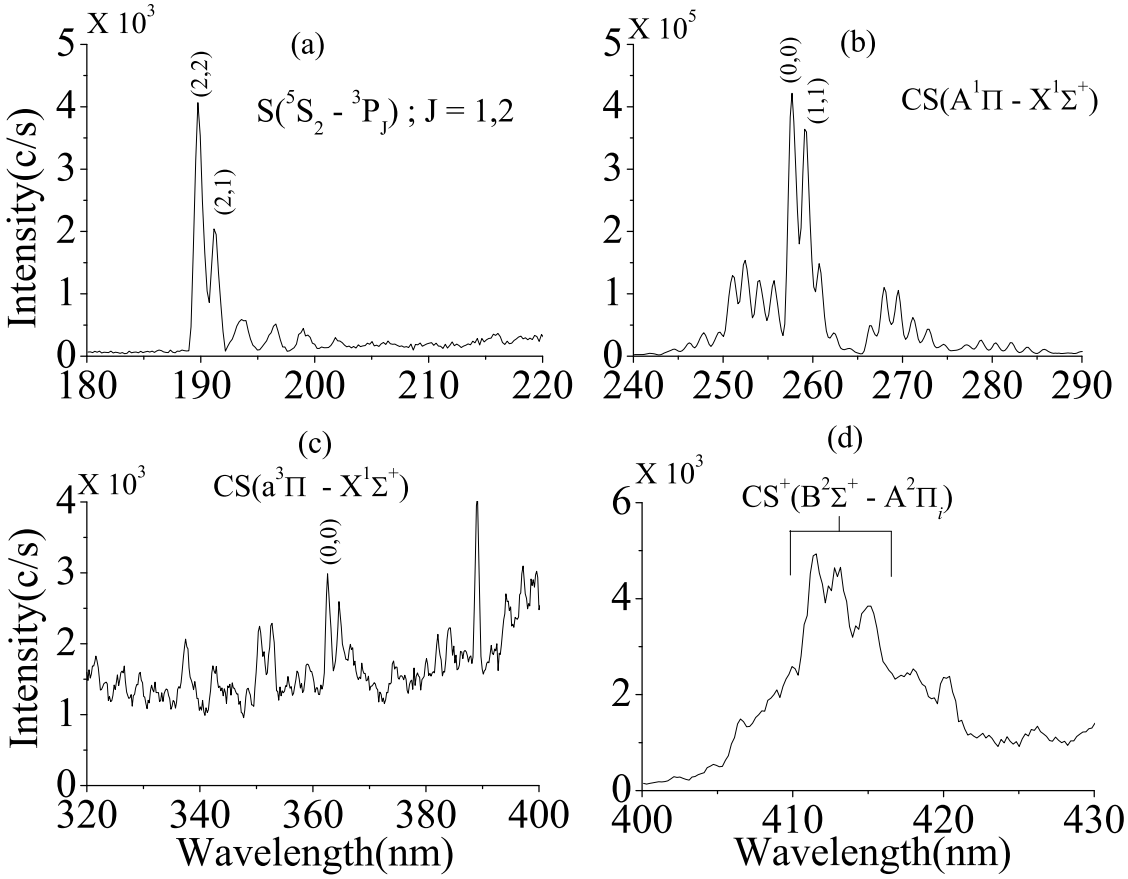

Figure 3.2: Spectral scans in the range of 180 to 800 nm for the CS_2^+ recombining plasma. The major emission features are indicated. These have been rescaled and plotted in four different graphs, labeled (a), (b), (c), and (d) corresponding to each feature on main scan.

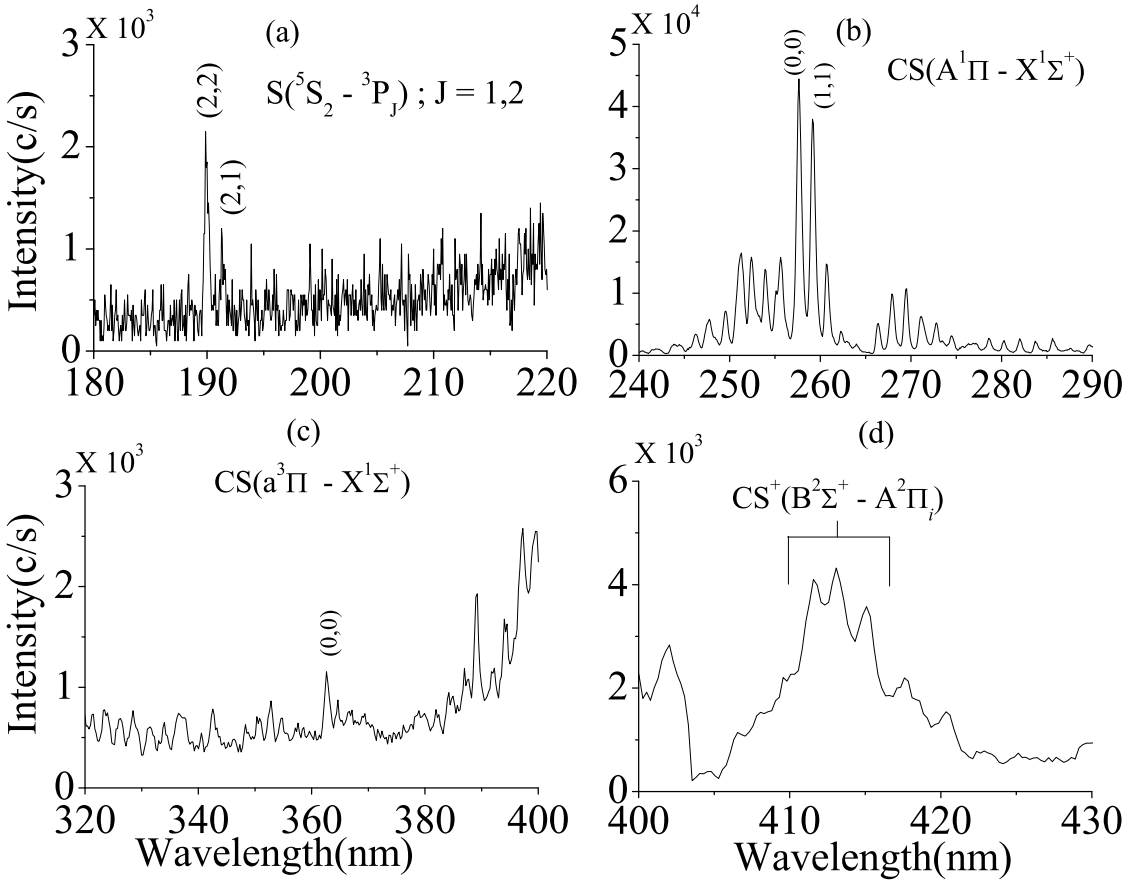

Figure 3.3: Spectral scans in the range of 180 to 800 nm for the HCS_2^+ recombining plasma is shown at the bottom of the figure. Illustrated are the major emission features. These have been rescaled and plotted in four different graphs, labeled (a), (b), (c), and (d) corresponding to each feature on main scan.

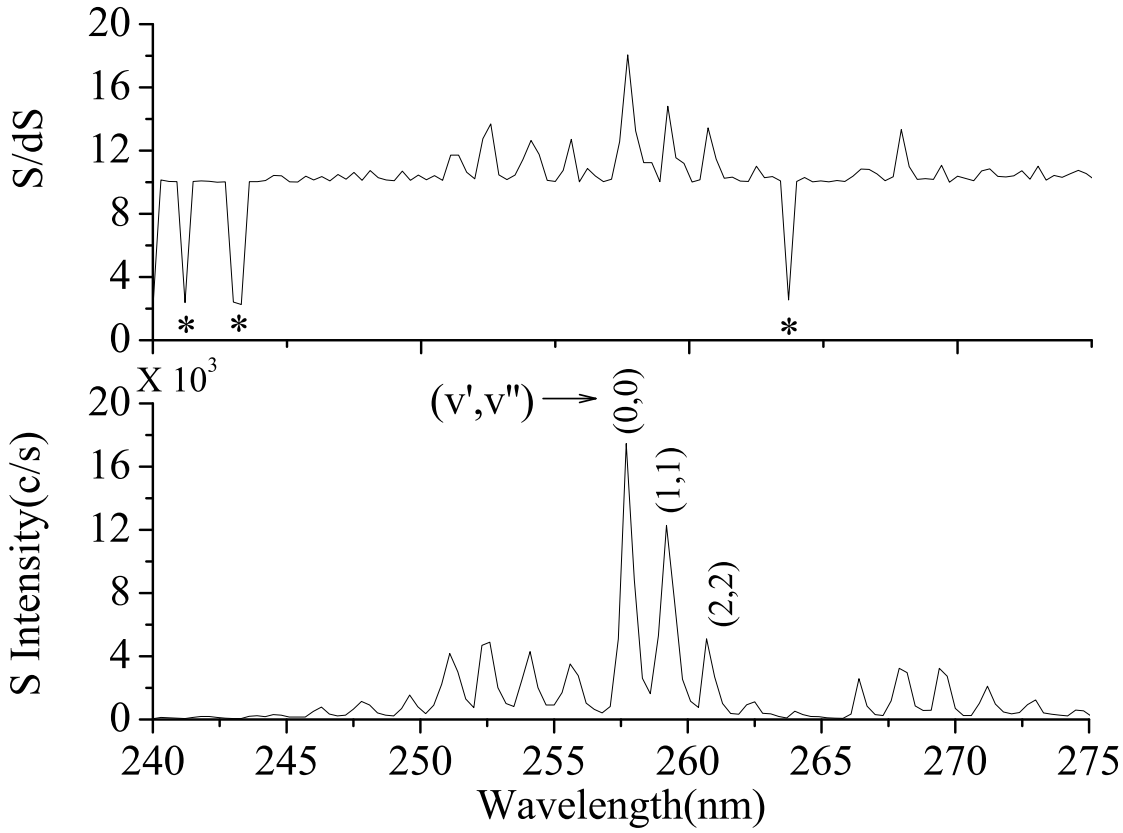

Figure 3.4: Shown are vibrationally resolved CS(A-X) emissions, generated following electron recombination of CS_2^+. These emissions were obtained by pulsing SF_6 into the Ar^+/e plasma upstream of the CS_2 addition point to attach electrons forming negative ions and quenching DR emissions. Details of this technique are in a recent publication.[70] The difference, S, between SF_6 out and SF_6 pulsed in is integrated until a predetermined S/δS is achieved and is normalized to c/s, where δS is the statistical error associated with counting.[70] These emissions, S, are the only ones evident in this wavelength range and some of the vibrational states (v',v'') are indicated. S/δS is also shown, which represents the constant signal to noise ratio in the spectrum achieved by appropriately changing the count period. In this case, photon counts have been accumulated at each wavelength until a S/δS ratio of at least 10 was achieved. Note, * indicates where the predetermined S/δS could not be achieved in a reasonable time because of absence of signal, thus the count was terminated.

excitation. The ion-ion recombination process is generally considered to proceed by electron transfer at long range and so would only produce the neutralized ions. However, there has been no evidence of such emissions in the region of the CS(A $\rightarrow$ X) transitions. With the amount of SF_6 added to cause rapid attachment, there would have been no significant effect on the ion chemistry, since rapid attachment coefficients are typically 2 orders of magnitude larger than for ion-molecule reactions.

To further confirm that the CS(A $\rightarrow$ X) emissions were only from DR, the discharge cavity was moved to change the upstream ionization density and thus the electron density, [e], in the flow tube. The density just upstream of the CS_2 addition point was determined using the axially movable Langmuir probe operating in the orbital limited region[68] and the spectrum was determined at each density with a separate determination of the intensity of a series of the spectral peaks including one resulting from each v' populated. For a recombination source of the emissions, intensity is proportional to [+][e] or $[e]^2$ for a recombining ion density which is a constant fraction of [e]. The relationship between intensity and electron density is developed below.

$$\frac{d[e]}{dt} = -\alpha[e][+] = -\frac{d[Product]}{dt}, for\ quasineutral\ plasma\ [e] = [+] \tag{3.21}$$

$$\frac{d[Product]}{dt} \propto Intensity \tag{3.22}$$

$$Intensity \propto [e]^2 \tag{3.23}$$

Figure 3.5 shows a log–log plot of intensity versus [e] for a series of vibronic transitions which is linear with a slope of 2 indicating a recombination source for the CS(A $\rightarrow$ X). Here the only possible source is reaction 3.11. In contrast to this, the dependence of the CS_2^+ emissions on electron density for various vibronic transitions are also shown in Figure 3.5. These have a slope close to one as expected for an ion-molecule reaction source ($Ar^+ + CS_2$), such as reaction 3.5. Note, that emissions from ion-molecule reactions are independent from

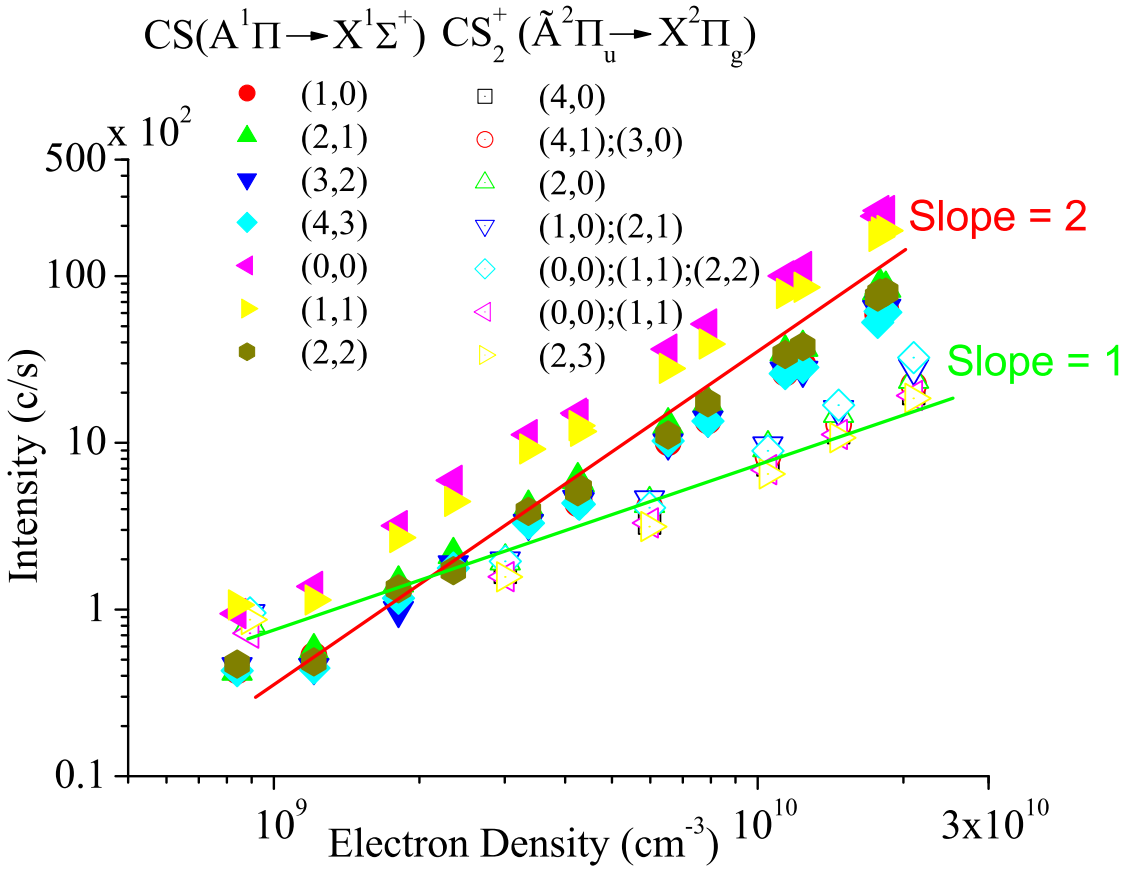

Figure 3.5: Intensity change due to a variation in the electron density for a series of (v',v'') transitions. The slope of the data on a log-log plot indicates the type of reaction, ion-molecule or DR, that is producing the emissions. A slope of 2 is indicative of the DR process, yielding CS(A-X) transitions. A slope of 1 is due to ion-molecule reactions, seen in the CS_2^+(Ã-X) transitions (see Section 3.3 for further explanation).

the pulse valve operation. Therefore, these emissions get subtracted out from the signal (S = A - B) collect for emissions from DR products, thus are not a source of interference.

Emissions from the DR process give rise to two main electronic transitions which arise from the dominant energy channels, 3.11 and 3.14. The additional energy beyond the energy needed for electronic excitation to CS(A) and CS(a) states can go into kinetic and internal energy of the molecule. Assuming all energy goes into internal energy, the vibrational level $v' = 5$ (CS_2^+/e) and $v' = 24$ (HCS_2^+/e) of the CS(A) state can be energetically accessed. For CS(a), $v' = 17$ (CS_2^+/e) and $v' = 37$ (HCS_2^+/e) are energetically accessible. The observed vibrational levels have been identified for CS(A $\rightarrow$ X) and CS(a $\rightarrow$ X) in spectra of the CS_2^+/e and HCS_2^+/e plasmas, Figures 3.6 and 3.7.

These observed vibrational levels are all energetically accessible for both CS(A) and CS(a) states with the exception of $v' = 6$ (CS(A) state) from the CS_2^+/e plasma. This emission is relatively weak, 2% of the main (0,0) transition, but may be due to residual internal energy in CS_2^+. The residual internal energy could be quenched by the addition of excess CS_2. The extra CS_2 would react with the internally excited CS_2^+ (CS_2^+*) in a charge transfer reaction that would leave the excess energy in the neutralized CS_2, see below:

$$CS_2^{+*} + CS_2 \rightarrow CS_2^* + CS_2^+ \tag{3.24}$$

Evidence for the above reaction could be obtained by monitoring the intensity of transitions, produced by DR, with the addition of excess CS_2. If internal excitation existed, then the intensities for the scanned transitions would change because of quenching the internal excitation and an effective reduction of the intensities would be observed. This effect is not seen in figure 3.8, where the CS(A $\rightarrow$ X) transitions are monitored at a CS_2 number density as used in the experimental data presented and at a number density of CS_2 that is four times larger for both CS_2^+/e and HCS_2^+/e plasmas. It can be seen that there is no change in any of the transitions indicating the absence of internal excitation. Note that in the CS_2^+ plasma the change is so small that the two spectra are on top of one another. The identified vibrational transitions along with available Franck-Condon factors (FCF) for the electronic transitions

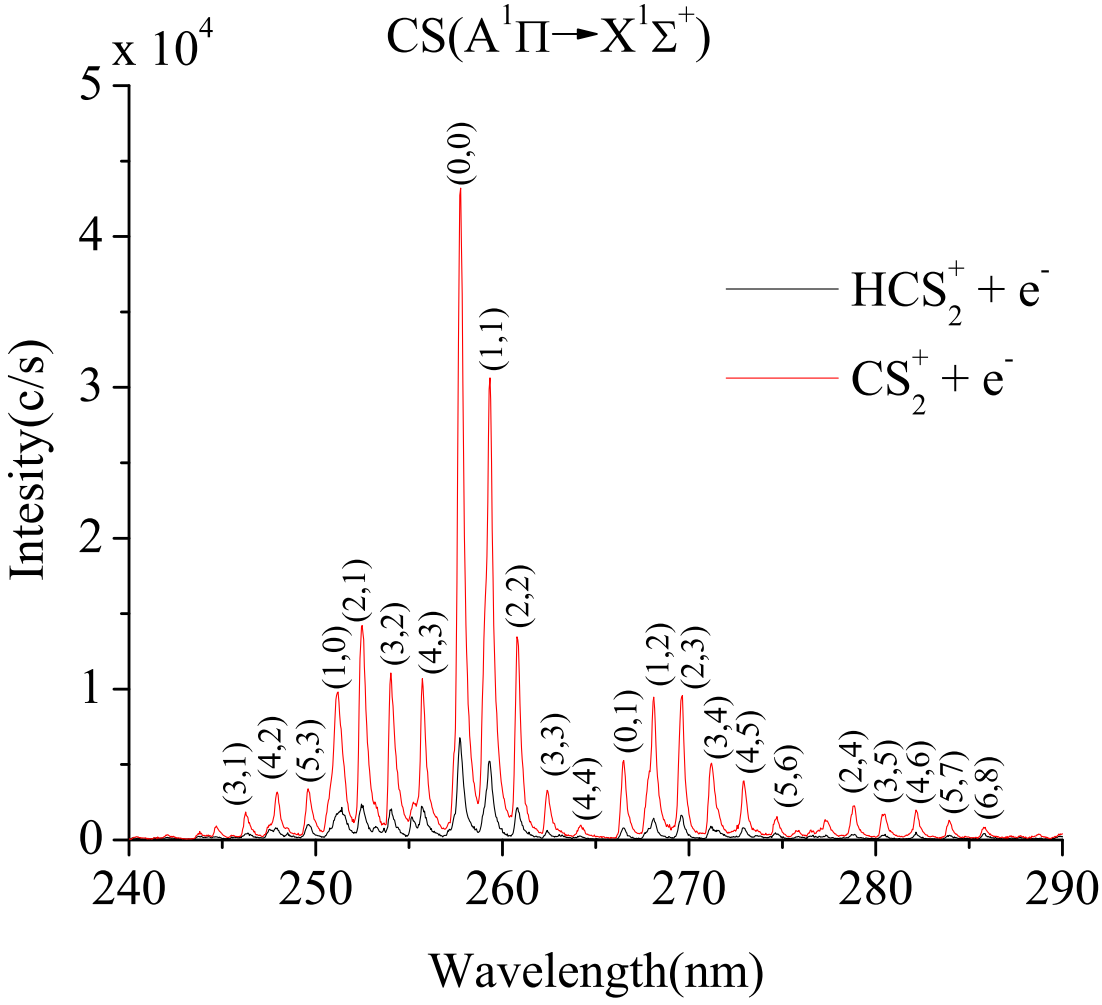

Figure 3.6: Major vibronic (v', v'') emission features from the CS($A^1\Pi \rightarrow X^1\Sigma^+$) transition in a CS_2^+ recombining plasma(red) and a HCS_2^+ recombining plasma(black).

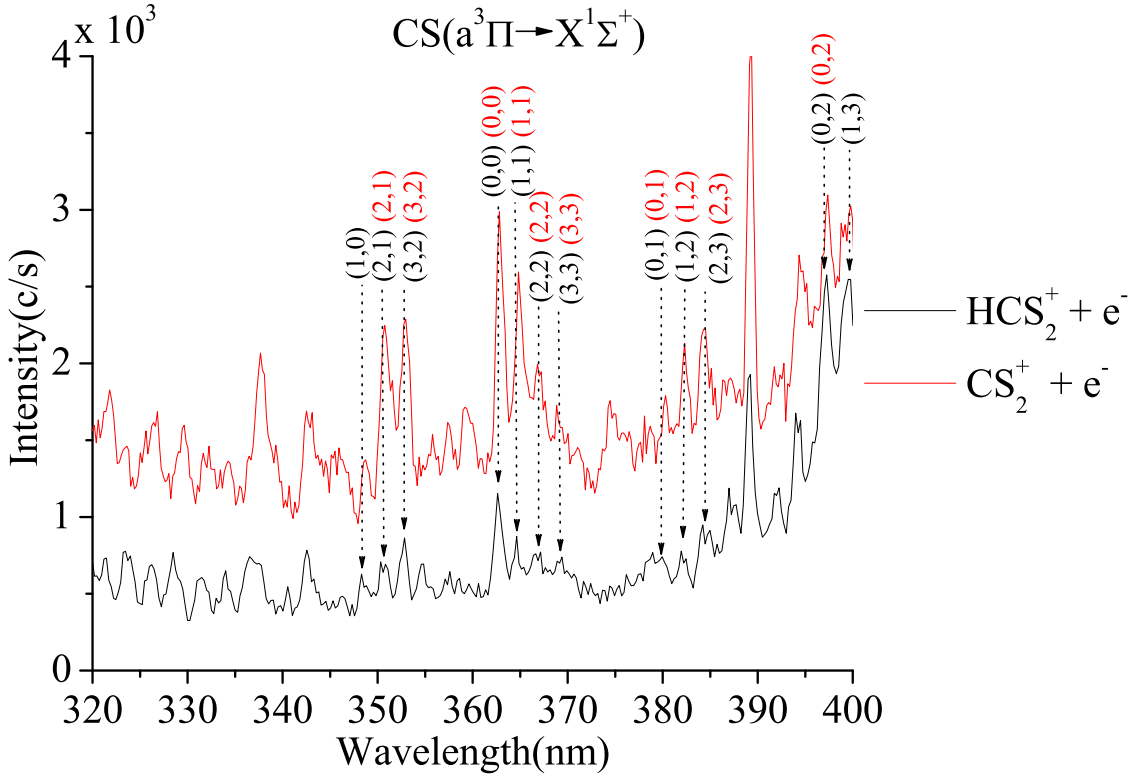

Figure 3.7: Major vibronic (v', v'') emission features from the CS($a^3\Pi \rightarrow X^1\Sigma^+$) transition in a CS_2^+ recombining plasma(red) and a HCS_2^+ recombining plasma(black). These features arise from a spin forbidden transition resulting in lower intensity features than those from the CS($A^1\Pi \rightarrow X^1\Sigma^+$) transition, Figure 3.6.

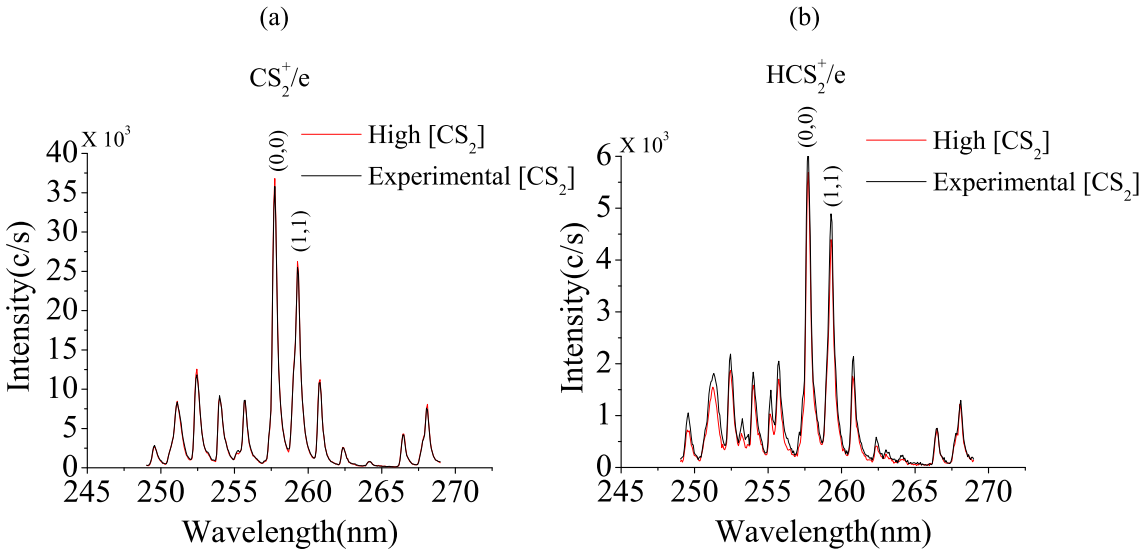

Figure 3.8: The spectra of CS_2^+/e recombining plasma (a) and HCS_2^+/e recombining plasma (b) taken in the region of the CS($A^1\Pi \rightarrow X^1\Sigma^+$) transition, at both a high number density (red) of CS_2 and the lower number density used in experiments (black). There is no change in intensity of the transitions between the number density used in the experiments and a number density that is four times larger. This is evidence supporting the absence of additional excitation in the recombining ion (see the text discussion referring to equation 3.24 for a detailed explanation.

were used to calculate the relative vibrational distribution,

$$I_{v'v''} \propto \nu^3 N_{v'} FCF \tag{3.25}$$

where ν is the frequency of the transition and $N_{v'}$ is the population of vibrational level v'. These relative distributions are shown in Table 3.1 below. For the CS(A) state there

Table 3.1: The relative vibrational distributions for CS($A^1\Pi \rightarrow X^1\Sigma^+$) and CS($a^3\Pi \rightarrow X^1\Sigma^+$) transitions originating from DR. The electronic transitions are presented for both recombining plasmas, CS_2^+/e^- and HCS_2^+/e^-. All vibrational levels are normalized to the $v' = 0$ level.

	Relative Distribution CS($A^1\Pi \rightarrow X^1\Sigma^+$)			Relative Distribution CS($a^3\Pi \rightarrow X^1\Sigma^+$)	
v'	CS_2^+	HCS_2^+	v'	CS_2^+	HCS_2^+
0	1.000	1.000	0	1.000	1.000
1	1.075	1.262	1	1.200	0.900
2	0.800	0.952	2	1.400	0.900
3	0.500	0.643			
4	0.500	0.762			

is an increase in relative population from the $v' = 0$ to $v' = 1$ for both recombining ions. This population inversion has been observed before in previous studies where the CS($A^1\Pi \rightarrow X^1\Sigma^+$) is produced by dissociative excitation of CS_2, by electron impact[78] and by the reaction, $Ar(^3P_2)$ + CS_2.[79] It is noticed that in the HCS_2^+ recombination that the $v' = 1$ has a greater population inversion, which maybe due to the higher energy associated with this recombination. Also interesting to note is the increase in relative population going from the $v' = 3$ to $v' = 4$ (HCS_2^+), which is not observed in the CS_2^+ case. This change was not observed by Zubek et al.[78] or Xu et al.[79] The reason for this behavior is unknown to the authors . The distribution for the CS(a) state only goes to $v' = 2$ due to the lack of availability of FCF for other transitions. It is noticed that there is a population inversion that increases with increasing v' in the CS_2^+ plasma, yet this is not observed in the HCS_2^+ plasma. It is interesting that there is not a population inversion in the HCS_2^+ case.

The S I emissions at wavelengths of 190.04 and 191.47 nm, are equivalent to a transition energy of 6.52 eV. Neither the CS_2^+ nor HCS_2^+ DR (equations 3.11 and 3.16) have sufficient energy to produce the sulfur transitions observed. The other possible cause may be an ion-molecule reaction, yet the log–log plot of intensity versus [e] has a slope of 2, which corresponds to the DR process. Note this plot is not shown to avoid repetition due to the similarities to the plot of the CS($A \rightarrow X$) transitions in Figure 3.5. Since there is no evidence for excitation in the CS_2^+ recombining ion (Figure 3.8), the other possibility is excitation in S_2^+, which can recombine to produce the emissions observed. There would be no spectral interference from this source with the recombining ions of interest since the all radiative emissions from S atoms are at shorter wavelengths than emissions of interest (i.e. CS($A \rightarrow X$) and CS($a \rightarrow X$)).

Another transition that was identified as an ion-molecule transition was the $CS^+(B^2\Sigma^+ \rightarrow A^2\Pi_i)$ in the region of 405-415 nm. The $CS^+(B^2\Sigma^+ \rightarrow A^2\Pi_i)$ vibronic transition intensities were observed to vary proportionally to the electron density on a log–log scale, similar to the CS_2^+ transitions, as expected from ion-molecule reactions. Vibronic transitions (0,0), (1,1) and (2,2) for this transition have been observed in previous work by Yencha et al.[80] In addition, the CS($B^1\Sigma^+ \rightarrow A^1\Pi$) transition has been identified in the region of 390-420 nm as well using previous work by Yencha et al.[80] Both of these transitions have been identified as coming from the $He^+ + CS_2$ reaction by Yencha et al. The comparison between the results from this study and the results from Yencha et al. study agree that the $CS^+(B^2\Sigma^+ \rightarrow A^2\Pi_i)$ transitions are originating from ion-molecule reactions and not from DR.

3.4 Conclusions

It has been shown that dominant emissions from the CS($A^1\Pi \rightarrow X^1\Sigma^+$) occur in both the CS_2^+/e and HCS_2^+/e plasmas. From these emissions relative vibrational state distributions have been assign up to the $v' = 4$ level. The increase in the population inversion for $v' = 1$ in the HCS_2^+/e plasma compared to the CS_2^+/e plasma, is consistent with the higher energy

associated with the HCS_2^+ electron attachment. Also consistent with the higher recombination energy are the $v' \geq 2$ levels for the HCS_2^+/e plasma are all greater in relative population than for the CS_2^+ case There is evidence for the vibrational transition from the $v' = 6$ in CS_2^+/e plasma, yet this is only one quantum number (0.12 eV) above the highest energetically accessible $v' = 5$ level. Comparing spectral intensities at two CS_2 number densities, one at experimental concentration and one higher, gives no indication of internal excitation in the recombining ion, Figure 3.8. In addition this vibrational level, $v' = 6$, is only 2% of the main transition, not a strong indication of internal excitation.

The issue of cascading must be addressed, for the case of the HCS_2^+/e plasma there is enough energy to populate the singlet CS(A′, $v' \leq 7$) and the triplet CS(a′ $^3\Sigma^+$, $v' \leq 46$), CS(d $^3\Delta_i^n$, $v' \leq 26$) and CS($e^3\Sigma^-$, $v' \leq 22$) states. Starting with the CS(A′) state, considering the possible contribution to the singlet CS(A) state transitions from (v',0), were looked at and no significant peaks were observed. The next contributions considered were transitions from the triplet states, CS(a′), CS(d) and CS(e)), to the CS(a). These fall in the range from 400–800 nm for the (v', 0) transitions. From 580–800 nm there are no features corresponding to any of these transitions, but from 400–580 nm it is difficult to tell due to overlapping transitions, from ion-molecule reactions. In the case of the CS_2^+ plasma there is less energy available from the DR, thus the CS(A′) state is not accessible and the only accessible v' levels in the triplet states are CS(a′ $^3\Sigma^+$, $v' \leq 18$), CS(d $^3\Delta_i^n$, $v' \leq 12$) and CS($e^3\Sigma^-$, $v' \leq 8$). None of the (v', 0) transitions were observed, yet this maybe be due to unfavorable Franck-Condon factors and to the authors knowledge these are not available in the literature. Thus there are not any conclusive findings to say that these higher energy triplet states are contributing to the CS(a) state vibrational population.

In summary, it was concluded that the emissions at 190.04 nm and 191.47 nm were S I transitions. These transitions are associated with DR, which is possibly from excited state S_2^+ ion generated in $S^+ + CS_2$ reaction. Next, the CS ($a \rightarrow X$) is the only spin forbidden transition seen, yet this shows that slower emitting transitions are observed and that detection of other

slow radiative decays could be obtained, yet none were observed. It should be noted that both the CS(a $\rightarrow$ X) and CS(A $\rightarrow$ X) transitions have been identified as originating from the DR, whereas the $CS_2^+(\tilde{A} \rightarrow X)$ transition has been shown to arise from ion-molecule reactions. Other transitions originating from ion-molecule reactions are the $CS^+(B^2\Sigma^+ \rightarrow A^2\Pi_i)$ and $CS(B^1\Sigma^+ \rightarrow A^1\Pi)$, presumably from the He^+ reaction with CS_2 as seen in the literature.[80]

There is evidence of CS_2 in cometary comae.[60] It is not unreasonable to assume that the protonated form, HCS_2^+, exists also. Evidence for smaller fragments of these molecules have also been seen, making the study of the recombination of these two molecules important in determining the contribution to interstellar molecules, both neutrals and ions. This information will guide the theory of these two recombination processes and possible give insight into determining the potential energy surfaces for these recombinations.

3.5 References

[1] Herbst, E. *Adv. Gas Phase Ion Chem.* **1998**, *3*, 1–47.

[2] Cravens, T. E. In *Dissociative Recombination of Molecular Ions with Electrons*; Guberman, S. L., Ed.; Kluwer: New York, 2003; pages 385–400.

[3] Fox, J. L. In *Dissociative Recombination Theory, Experiment and Applications II*; Rowe, B. R., Mitchell, J. B. A., Canosa, A., Eds.; Plenum: New York, 1993; page 219.

[4] Millar, T. J., Ed. *Chemistry in Expanding Circumstellar Envelopes.*, Rate Coefficients in Astrochemistry; Kluwer: Dordrecht, 1988.

[5] Dalgarno, A. In *Dissociative Recombination: Theory, Experiment and Applications IV*; Larsson, M., Mitchell, J. B. A., Schneider, I. E., Eds.; World Scientific: Singapore, 2000; pages 1–12.

[6] Goodings, J. M.; Karellas, N. S.; Hasanali, C. S. *Int. J. Mass Spectrom. Ion Proc.* **1989**, *89*, 205–226.

[7] Post, D. E. In *Physics of Ion-Ion and Ion-Electron Collisions*; Brouillard, F., McGowan, J. W., Eds.; Plenum Press: New York, 1983; pages 37–99.

[8] Biondi, M. A. In *Recombination.*; Bekefi, G., Ed.; Wiley: New York, 1976; page 125.

[9] McLain, J. L.; Poterya, V.; Jackson, D. M.; Adams, N. G.; Babcock, L. M. *J. Phys. Chem. A* **2005**, *109*, 5119–5123.

[10] McLain, J. L.; Poterya, V.; Molek, C. D.; Babcock, L. M.; Adams, N. G. *J. Phys. Chem. A* **2004**, *108*, 6704–6708.

[11] Poterya, V.; McLain, J. L.; Adams, N. G.; Babcock, L. M. *J. Chem. Phys. A* **2005**, *109*, 7181–7186.

[12] Adams, N. G.; Smith, D. In *Rate Coefficients in Astrochemistry*; Millar, T. J., Williams, D. A., Eds.; Kluwer: Dordrecht, 1988; pages 173–92.

[13] Heber, O.; Andersen, L. H.; Seiersen, K.; Bluhme, H.; Svendsen, A.; Maunoury, L. In Wolf, A., Ed., *Sixth International Conference on Dissociative Recombination: Theory, Experiments and Applications, Mosbach, Germany*. Inst. Phys. J.Phys. Conf. Ser., 2004.

[14] Thomas, R. D.; Ehlerding, A.; Geppert, W.; Hellberg, F.; Larsson, M.; Zhaunerchyk, V.; Bahati, E.; Bannister, M. E.; Vane, C. R.; Petrignani, A.; van der Zande, W. J.; Andersson, P.; Petteersson, J. C. In Wolf, A., L. L. S. P., Ed., *Sixth International Conference on Dissociative Recombination: Theory, Experiment and Applications, Mosbach, Germany*. Inst. Phys.Conf. Ser., 2004.

[15] Mitchell, J. B. A.; Rebrion-Rowe, C.; Le Garrec, J. L.; Angelova, G.; Bluhme, H.; Seiersen, K.; Andersen, L. H. *Int. J. Mass Spectrom.* **2003**, *227*, 273–9.

[16] Kalhori, S.; Viggiano, A. A.; Arnold, S. T.; Rosen, S.; Semaniak, J.; Derkatch, A. M.; af Ugglas, M.; Larsson, M. *Astron. Astrophys.* **2002**, *391*, 1159–1165.

[17] Andersen, L. H.; Heber, O.; Kella, D.; Pedersen, H. B.; Vejby-Christensen, L.; Zajfman, D. *Phys. Rev. Letts.* **1996**, *77*, 4891–4.

[18] Rosen, S.; Derkatch, A. M.; Semaniak, J.; Neau, A.; Al-Khalili, A.; Le Padellec, A.; Vikor, W. S. L.; Thomas, R.; Danared, H.; af Ugglas, M.; Larsson, M. *Farad. Discuss.* **2000**, *115*, 295–302.

[19] Petrignani, A.; Hellberg, F.; Thomas, R. D.; Larsson, M.; Cosby, P. C.; van der Zande, W. J. In *Dissociative Recombination, Theory, Experiments and Applications*; Wolf, A., Lammich, L., Schmelcher, P., Eds., Vol. 4; Inst. Phys: J. Phys. Conf Series 4: London, 2005; pages 182–186.

[20] Rowe, B. R.; Queffelec, J. L. In *Dissociative Recombination: Theory, Experiment and Applications*; Mitchell, J. B. A., Guberman, S. L., Eds.; World Scientific: Singapore, 1989; pages 151–61.

[21] Queffelec, J. L.; Rowe, B. R.; Vallee, F.; Gomet, J. C.; Morlais, M. *J. Chem. Phys.* **1989**, *91*, 5335–42.

[22] Adams, N. G.; Herd, C. R.; Geoghegan, M.; Smith, D.; Canosa, A.; Gomet, J. C.; Rowe, B. R.; Queffelec, J. L.; Morlais, M. *J. Chem. Phys.* **1991**, *94*, 4852–4857.

[23] Queffelec, J. L.; Rowe, B. R.; Morlais, M.; Gomet, J. C.; Vallee, F. *Planet. Space Sci.* **1985**, *33*, 263–270.

[24] Vallee, F.; Gomet, J. C.; Rowe, B. R.; Queffelec, J. L.; Morlais, M. In *Astrochemistry*; Varda, M. S., Tarafdar, S., Eds.; Kluwer: Dordrecht, 1987; pages 29–30.

[25] Rowe, B. R.; Vallee, F.; Queffelec, J. L.; Gomet, J. C.; Morlais, M. *J. Chem. Phys.* **1988**, *88*, 845–850.

[26] Vejby-Christensen, L.; Andersen, L. H.; Heber, O.; Kella, D.; Pedersen, H. B.; Schmidt, H. T.; Zajfman, D. *Ap. J.* **1997**, *483*, 531–540.

[27] Jensen, M. J.; Bilodeau, R. C.; Heber, O.; Pedersen, H. B.; Safvan, C. P.; Urbain, X.; Zaijman, D.; Andersen, L. H. *Phys Rev. A* **1999**, *60*, 2970–6.

[28] Vikor, W. S. L.; Al-Khalili, A.; Danared, H.; Djuric, N.; Dunn, G. H.; Larson, A.; Le Padellec, A.; Rosen, S.; af Ugglas, M. *Astron. Astrophys.* **1999**, *344*, 1027–33.

[29] Larson, A.; Le Padellec, A.; Semaniak, J.; Stromholm, C.; Larsson, M.; Rosen, S.; Peverall, R.; Danared, H.; Djuric, N.; Dunn, G. H.; Datz, S. *Ap. J.* **1998**, *505*, 459–65.

[30] Derkatch, A. M.; Al-Khalili, A.; Vikor, W. S. L.; Neau, A.; Shi, W.; af Ugglas, M.; Larsson, M. *J. Phys. B* **1999**, *32*, 3391–8.

[31] Semaniak, J.; Minaev, B. F.; Derkatch, A. M.; Hellberg, F.; Neau, A.; Rosen, S.; Thomas, R.; Larsson, M.; Danared, H.; Paal, A.; af Ugglas, M. *Ap. J. Suppl.* **2001**, *135*, 275–83.

[32] Williams, T. L.; Adams, N. G.; Babcock, L. M.; Herd, C. R.; Geoghegan, M. *Mon. Not. Roy. Astr. Soc.* **1996**, *282*, 413–420.

[33] Neau, A.; Khalili, A. A.; Rosen, S.; Le Padellec, A.; Derkatch, A. M.; Vikor, W. S. L.; Semaniak, J.; Thomas, R.; Nagard, M. B.; Anderson, K.; Danared, H.; af Ugglas, M. *J. Chem. Phys.* **2000**, *113*, 1762–1770.

[34] Jensen, M. J.; Bilodeau, R. C.; Safvan, C. P.; Seiersen, K.; Andersen, L. H.; Pedersen, H. B.; Heber, O. *Ap. J.* **2000**, *543*, 764–774.

[35] Semaniak, J.; Larson, A.; Le Padellec, A.; Stromholm, C.; Larsson, M.; Rosen, S.; Peverall, R.; Danared, H.; Djuric, N.; Dunn, G. H.; Datz, S. *Ap. J.* **1998**, *498*, 886–95.

[36] Ehlerding, A.; Arnold, S.; Viggiano, A. A.; Kalhori, S.; Semaniak, J.; Derkatch, A.; Rosn, S.; af Ugglas, M.; Larsson, M. *J. Phys. Chem. A* **2003**, *107*(13), 2179–2189.

[37] Geppert, W. D.; Thomas, R. D.; Ehlerding, A.; Hellberg, F.; Osterdahl, F.; Hamberg, M.; Semaniak, J.; Zhaunerchyk, V.; Kaminska, M.; Kallberg, A.; Paal, A.; Larsson, M. In *Dissociative Recombination: Theory, Experiments and Applications*; Wolf, W., Lammich, L., Schmelcher, P., Eds., Vol. 4; Inst. Phys. J. Phys. Conf. Ser. 4: London, 2005; pages 26–31.

[38] Geppert, W.; Thomas, R.; Semaniak, J.; Ehlerding, A.; Millar, T. J.; Osterdahl, F.; Ugglas, M. a.; Djuric, N.; Paal, A.; Larsson, M. *Ap. J.* **2004**, *609*, 459.

[39] Zhaunerchyk, V.; Ehlerding, A.; Viggiano, A. A.; Arnold, S. T.; Geppert, W. D.; Hellberg, F.; Thomas, R.; Osterdahl, F.; Larsson, M. In Wolf, A., Lammich, L., Schmelcher, P., Eds., *Sixth International Conference on Dissociative Recombination: Theory, Experiments and Applications, Mosbach, Germany*, 2004.

[40] Hamberg, M.; Geppert, W. D.; Rosen, S.; Ehlerding, A.; Hellberg, F.; Zhaunerchyk, V.; Kaminska, M.; Thomas, R.; Kallberg, A.; Simonsson, A.; Paal, A.; Larsson, M. In Wolf, A., Ed., *Sixth International Conference on Dissociative Recombination: Theory, Experiments and Applications, Mosbach, Germany*. Inst. Phys. J. Phys.Conf. Ser., 2004.

[41] Hellberg, F.; Zhaunerchyk, V.; Bannister, M. E.; Ehlerding, A.; Geppert, W.; Larsson, M.; Vane, C. R.; Osterdahl, F.; Thomas, R. In Wolf, A., Ed., *Sixth International Conference on Dissociative Recombination: Theory, Experiments and Applications, Mosbach, Germany*. Inst. Phys. J. Phys. Conf. Ser., 2004.

[42] Datz, S.; Larsson, M.; Stromholm, C.; Sundstrom, G.; Zengin, V.; Danared, H.; Kallberg, A.; af Ugglas, M. *Phys. Rev. A* **1995**, *52*, 2901–9.

[43] Datz, S.; Sundstrom, G.; Biedermann, G.; Brostrom, L.; Danared, H.; Mannervik, S.; Mowat, J. R.; Larsson, M. *Phys. Rev. Lett.* **1995**, *74*, 896–9.

[44] Johnsen, R.; Skrzypkowski, M.; Gougousi, T.; Golde, M. F. In *Dissociative Recombination: Theory, Experiment and Applications IV*; Larsson, M., Mitchell, J. B. A., Schneider, I. E., Eds.; World Scientific: Singapore, 2000; page 200.

[45] Adams, N. G.; Babcock, L. M. *J. Phys. Chem.* **1994**, *98*, 4564–4569.

[46] Butler, J. M.; Babcock, L. M.; Adams, N. G. *Mol. Phys.* **1997**, *91*, 81–90.

[47] Bates, D. R. *Adv. Atom. Molec. Opt. Phys.* **1994**, *34*, 427–486.

[48] Bates, D. R. *J. Phys. B.* **1992**, *25*, 5479–5488.

[49] Bates, D. R. *Proc. R. Soc. Lond.* **1993**, *443*, 257–264.

[50] Talbi, D. *Chem. Phys.* **2007**, *332*(2-3), 298–303.

[51] Rosati, R.; Johnsen, R.; Golde, M. F. *J. Chem. Phys.* **2004**, *120*, 8025–30.

[52] Kraemer, W. P.; Hazi, A. U. In *Dissociative Recombination: Theory, Experiment and Applications I.*; Mitchell, J. B. A., Guberman, S. L., Eds.; World Scientific: Singapore, 1989; pages 61–72.

[53] Talbi, D.; Ellinger, Y. In *Dissociative Recombination: Theory, Experiment and Applications II*; Rowe, B. R., Mitchell, J. B. A., Canosa, A., Eds.; Plenum: New York, 1993; pages 59–66.

[54] Tomashevsky, M.; Herbst, E.; Kraemer, W. P. *Ap. J.* **1998**, *498*, 728–734.

[55] Glinski, R. J.; Nuth, J. A.; Reese, M. D.; Sitko, M. *Ap. J.* **1996**, *467*, L109–112.

[56] Yan, M.; Dalgarno, A.; Klemperer, W.; Miller, A. E. S. *Mon. Not. R. Astr. Soc.* **2000**, *313*, L17–18.

[57] Adams, N. G.; Babcock, L. M.; Ray, N. S. In *Atomic Processes in Plasmas*; Schultz, D. R., Meyer, F. W., Ownby, F., Eds.; AIP: Melville, NY, 2002; pages 182–193.

[58] McCarthy, M. C.; Thaddeus, P. *Chem. Soc. Revs.* **2001**, *30*, 177–185.

[59] Thaddeus, P.; McCarthy, M. C. *Spectrochimica Acta* **2001**, *A57*, 757–774.

[60] Jackson, W. M.; Scodinu, A.; Xu, D.; Cochran, A. L. *Ap. J.* **2004**, *607*, L139–L141.

[61] Crovisier, J.; Encrenaz, T. *Comet Science;* Cambridge University Press: Cambridge, 2000.

[62] Gutcheck, R. A.; Zipf, E. C. *J. Geophys. Res.* **1973**, *78*, 5429–36.

[63] Vallee, F.; Rowe, B. R.; Gomet, J. C.; Queffelec, J. L.; Morlais, M. *Chem. Phys. Lett.* **1986**, *124*, 317–20.

[64] Tsuji, M.; Nakamura, M.; Nishimura, Y.; Obase, H. *J. Chem. Phys.* **1995**, *103*, 1413–21.

[65] Adams, N. G. In *Dissociative Recombination: Theory, Experiment and Applications*; Rowe, B. R., Mitchell, J. B. A., Eds.; Plenum Press: New York, 1993; pages 99–111.

[66] Adams, N. G.; Smith, D. *Int. J. Mass Spectrom. Ion Phys.* **1976**, *21*, 349–59.

[67] Adams, N. G. *Int. J. Mass Spectrom. Ion Proc.* **1994**, *132*, 1–27.

[68] Swift, J. D.; Schwar, M. J. R. *Electrical Probes for Plasma Diagnostics.;* Iliffe: London, 1970.

[69] Williams, T. L.; Decker, B. K.; Adams, N. G.; Babcock, L. M.; Harland, P. W. *Rev. Sci. Instrum.* **2000**, *71*, 2169–79.

[70] Mostefaoui, T.; Adams, N. G.; Babcock, L. M. *Rev. Sci. Instrum.* **2002**, *73*, 2044–50.

[71] Schmeltekopf, A. L.; Fehsenfeld, F. C. *J. Chem. Phys.* **1970**, *53*, 3173–3177.

[72] Molek, C. D.; McLain, J. L.; Adams, N. G.; Babcock, L. M.; Gibbs, L. L. *Int. J. Mass Spectrom.* **2004**, *235*, 199–205.

[73] Anicich, V. *An Index of the Literature for Bimolecular Gas Phase Cation-Molecule Reaction Kinetics: JPL Publication 03-19;* Jet Propulsion Laboratory: Pasadena, 2003.

[74] Linstrom, P. J., Mallard, W. G., Eds. *NIST Chemistry WebBook*, NIST Standard Database 69; National Institute of Standards and Technology: Gaithersburg MD, 20899, June 2005.

[75] Fehsenfeld, F. C. *J. Chem. Phys.* **1970**, *53*(5), 2000–2004.

[76] Smith, D.; Adams, N. G.; Alge, E. *J. Phys. B.* **1984**, *17*, 461–472.

[77] Adams, N. G.; Babcock, L. M.; Molek, C. D. In *Encyclopedia of Mass Spectrometry: Theory and Ion Chemistry, Vol.1*; Armentrout, P., Ed., Vol. 1; Elsevier: Amsterdam, 2003; pages 555–561.

[78] Zubek, M.; Gackowska, J.; Snegursky, A. *Rad. Phys. Chem.* **2003**, *68*, 323–328.

[79] Xu, D.; Li, X.; Shen, G.; Wang, L.; Chen, H.; Lou, N. *Chem. Phys. Lett.* **1993**, *210*, 315–321.

[80] Yencha, A. J.; Wu, K. T. *Chem. Phys.* **1980**, *49*, 127–137.

Chapter 4

Development of a Novel Technique for Quantitatively Determining the Products of Electron-Ion Dissociative Recombination[1]

[1]Molek, C. D.; Poterya, V.; Adams, N. G.; McLain, J. L. *Int. J. Mass Spec.*, Submitted. Reprinted here with permission of publisher.

4.1 Introduction

Dissociative electron-ion recombination (DR) is very important, since it is a dominant loss process in many molecular plasma media, e.g. interstellar gas clouds,[1] cometary coma,[2,3] planetary atmospheres,[2,4] combustion flames,[5] etc. One important reason is that DR is generally much more rapid than other recombination processes (radiative, dielectronic, collisional radiative).[6] There has been much experimental data gathered to understand the DR process, such as temperature dependence of the DR process (including rate coefficients), quantitative determination of the products, and determination of states of excitation in the products. Data collected on the DR process has contributed to the understanding of the reaction mechanisms involved. These mechanisms will not be discussed in detail here, but the reader is referred to recent reviews.[7,8]

In spite of the limited data (partly due to the experimental challenge), there has been a considerable effort put into determining the products of DR. Currently, there are two main techniques used to determine the product distributions and these are the Flowing Afterglow (FA) and the Storage Ring (SR). Previously, the FA was used to identify products via vuv absorption spectroscopy and Laser Induced Fluorescence (LIF).[9–11] Although the FA has the strength of chemical versatility, there are difficulties associated with this experimental technique. In particular, the need for multiple quantitative spectroscopic techniques for the different products makes obtaining a full distribution very difficult. The Storage Ring (SR) has its own set of difficulties as well. To get the distribution, a detailed and involved analysis needs to be employed, as well as corrections for collisions with background gases. Also the ability to distinguish between products 1 amu apart in mass for heavier products (e.g. C_nH_m, where n$\geq$2) diminishes. Yet this heavier hydrocarbon chemistry is extremely important, for both the ions and neutrals in Titan's atmosphere and the ISM.[12,13] A few examples of heavy hydrocarbons are presented here ($C_2H_4^+$, $C_3H_4^+$, $C_4H_5^+$, and $C_4H_9^+$); in the case of $C_2H_4^+$ the counts versus energy for the various neutral fragments have not been fully resolved in the SR and peaks need to be fitted using Gaussian profiles.[14] The full resolution for the same number

of carbons was still not possible using deuterated ions (i.e. $C_2D_5^+$).[15] For $C_3H_4^+$, experiments have not resolved the H-atom contribution to the products at all (i.e. only resolves DR products with 1, 2, or 3 carbon atoms).[16] This is also the situation for $C_4H_5^+$ and $C_4H_9^+$, where only the DR products with 1, 2, 3, or 4 carbon atoms have been resolved).[17] In a few instances, where measurements are available, namely for H_2O^+, H_3O^+, and N_2H^+ there are also discrepancies between the FA and SR results. The H_2O^+ literature product distributions are given in Table 4.1, where substantial differences are seen between the two techniques. The

Table 4.1: Products of Dissociative Recombination for H_2O^+

		FA[18,19]		SR[20–22]		
$H_2O^+ + e$	$\rightarrow H + OH + 714$ kJ/mol (7.4 eV)	55%	55%	22%	30%	20%
	$\rightarrow O + H_2 + 733$ kJ/mol (7.4 eV)	<23%	<21%	10%	13%	9%
	$\rightarrow O + 2H + 299$ kJ/mol (3.1 eV)	>22%	>24%	68%	57%	71%

differences between the distributions have been attributed to vibrational excitation in the recombining ion in the FA, which could not be relaxed by resonant charge transfer because it must competed with the reaction channel which forms H_3O^+, see equations (4.1) and (4.2).[18]

$$H_2O^{+*} + H_2O \rightarrow H_2O^* + H_2O^+ \tag{4.1}$$

$$\rightarrow H_3O^+ + OH \tag{4.2}$$

Note that the differences using different Storage Rings are smaller but certainly not negligible. Other FA studies followed with the detection of the H-atom product in the recombinations of N_2H^+, HCO^+, HCO_2^+, N_2OH^+, $OCSH^+$, H_2CN^+, H_3O^+, H_3S^+, NH_4^+, and CH_5^+[11] and the H-atom, O-atom, and OH products of HCO_2^+, N_2OH^+, and H_3O^+ being determined indirectly and directly by laser induced fluorescence.[10,23,24] In these studies, it was ensured that the recombining ions were vibrationally relaxed by resonant proton transfer, e.g.,

$$H_3O^{+*} + H_2O \rightarrow H_2O^* + H_3O^+ \tag{4.3}$$

But even with the H_3O^+ vibrationally relaxed there are still marked differences between the various measured distributions using the two techniques, see Table 4.2. This is also the case

Table 4.2: Products of Dissociative Recombination for H_3O^+

		FA[24]	SR[20,25–27]		
$H_3O^+ + e^-$	$\rightarrow H_2O + H + 617$ kJ/mol (6.4 eV)	5%	33%	18%	25%
	$\rightarrow OH + H_2 + 550$ kJ/mol (5.7 eV)	36%	18%	11%	14%
	$\rightarrow OH + 2H + 125$ kJ/mol (1.3 eV)	29%	48%	67%	60%
	$\rightarrow O + H + H_2 + 135$ kJ/mol (1.4 eV)	30%	1%	4%	1.3%

Table 4.3: Products of Dissociative Recombination for N_2H^+

		FA[11]	SR[15]
$N_2H^+ + e^-$	$\rightarrow N_2 + H + 817$ kJ/mol(8.5 eV)	∼100%	36%
	$\rightarrow NH + N + 217$ kJ/mol(2.3 eV)	∼0%	64%

for N_2H^+ recombination, Table 4.3.

Thus, there is an obvious need for a new and independent technique. This is the subject of the present paper. The technique devised uses the FA for the chemical versatility in conjunction with electron impact ionization and mass spectrometric analysis of the DR products for its selectivity and sensitivity (sensitivity is achieved using pulse counting). Thus, unlike spectroscopy, this enables multiple product channels to be monitored with a single measurement technique. Also, the use of quadrupole mass spectrometry means 1 amu or better resolution can readily be achieved, with the ability to study the individual products from DR of both saturated and unsaturated hydrocarbons. An additional feature of this approach is that it is sensitive to small signals in the presence of a large background. Note that at the electron energy typically used (70 eV), there is some fragmentation of the sample that is being ionized, but there is a wealth of data on the degree of fragmentation at this energy and this affect can be completely accounted for. The distinction between the ionization of products of DR (signal) and residual background gases is realized by pulsed addition of electron attaching gas and other gases.

4.2 Experimental

The generic FA technique has been described in detail previously[28,29] and will only be briefly covered here, whereas the aspects that are different will be emphasized. This technique involves two experimental approaches, which both utilize a FA plasma and these will be described using N_2H^+ and CH_5^+ as examples.

4.2.1 Electron-Attaching Gas Method

For the first method (the electron-attaching gas method), the flow tube pressure is typically 1.4-1.5 Torr with a He flow rate of 16.0 slm, this typical pressure is such that diffusive losses are not very significant and that most of the He^+ has been converted to He_2^+ by the ternary reaction, Equation 4.4, before the other gases are added to the flow tube. Note that both 16.0 slm and 31.4 slm were used for the N_2H^+ DR study, see Section 4.3.2 for details. The He is of 99.997% purity and is further purified with two liquid Nitrogen-cooled sieve traps. Argon gas (99.999%) is added in at ∼22 cm downstream of the microwave discharge through a ring port at a concentration of ∼1.6 x 10^{14} molecules/cm^3, which destroys He^m and increases the ionization number density. Even further downstream (∼70 cm) of the Ar addition, H_2 (99.999% purity further purified by a liquid nitrogen-cooled sieve trap) is added in at a concentration of ∼1 x 10^{13} molecules/cm^3 to quickly create a H_3^+/e^- dominant plasma. Approximately 17 cm downstream of the H_2 addition, the reagent gas of interest is added, in these cases N_2 (99.999% purity) or CH_4 (99.97% purity), at concentrations of ∼5 x 10^{12} molecules/cm^3. This forms the recombining ion of interest, either N_2H^+ or CH_5^+. Equations 4.4 – 4.7 summarize the chemical reactions leading up to H_3^+, which readily proton transfers to N_2 and CH_4, with respective rates of 1.6 x $10^{-9}cm^3s^{-1}$ and 2.4 x $10^{-9}cm^3s^{-1}$, from the

literature compilation.[30]

$$He^+ + He + He \longrightarrow He_2^+ + He \qquad k = 2.0 \times 10^{-31} cm^6 s^{-1} \tag{4.4}$$

$$He_2^+ + Ar \longrightarrow Ar^+ + 2He \qquad k = 2.0 \times 10^{-10} cm^3 s^{-1} \tag{4.5}$$

$$Ar^+ + H_2 \longrightarrow ArH^+ + H \qquad k = 8.6 \times 10^{-10} cm^3 s^{-1} \tag{4.6}$$

$$ArH^+ + H_2 \longrightarrow H_3^+ + H \qquad k = 6.3 \times 10^{-10} cm^3 s^{-1} \tag{4.7}$$

Note that the kinetic data in equations 4.4 and 4.5–4.7 are from the literature.[30,31] A rapidly, electron attaching gas (CCl_4 or sometimes SF_6) is pulsed in ∼10 cm upstream of the reagent gas so that electron attachment, equation (4.8), is 80–90% at the point of introducing the reagent gas and thus with attaching gas added, the DR process is almost completely quenched before the addition of N_2 or CH_4. The amount of attaching gas added does not influence the ion chemistry or change the diffusive loss, which is maintained as electron-ion ambipolar diffusion.

$$CCl_4 + e^- \rightarrow Cl^- + CCl_3 \tag{4.8}$$

Then, the difference between the two pulsed situations is the signal from products of the DR. Note that very pure gases are used to minimize the influence of impurities. Also note that any impurity in the flow tube is a constant value and is subtracted out to get signal, by the difference between the pulsed gas out (A_{n+1}) versus in (B_n) so that,

$$S_{n+1,n} = A_{n+1} - B_n \tag{4.9}$$

A statistically significant S is obtained by integrating S from multiple pulse periods (≥1000),

$$S = \sum_{n=1,3,5,\ldots}^{N} S_{n+1,n} = \sum_{n=1,3,5,\ldots}^{N} (A_{n+1} - B_n) \tag{4.10}$$

Note that the counts in (A_{n+1}) are determined after the counts in (B_n) and thus the system needs to be as stable as possible between these two periods. The concentration of attaching gas is critical, enough is added to maximize signal contribution from DR between the two

channels (A and B), but to keep any ion-ion recombination (iir) between the anion (Cl^-) and recombining ion of interest at a minimum. Note that any products of iir will result in a negative S and if they occur at the same mass as a DR product they will erroneously reduce the DR contributions at these masses. The rate constants of these particular iir are not known and therefore cannot be modeled. However Cl will be contained in the products and this is looked for. In fact, it is shown later that Cl containing products are very minor, thus showing iir is slow. Even so, this small effect is accounted for. However, it is ensured that there is still enough electron density left for ambipolar diffusive ion loss to still be controlled by the electrons.[32] This situation is achieved by monitoring the current profile (proportional to electron density) at a fixed DC voltage (∼3 Volts) applied to the movable Langmuir probe. During this measurement, the probe is set at a fixed position in the flow tube (i.e. the addition point of N_2 or CH_4). Note that, when the pulsed gas is out the ions of interest (N_2H^+ and CH_5^+) will recombine, thus forming DR product neutrals which are thermalized by collisions with the He buffer gas or by radiative relaxation.

The pulse difference technique has been successfully applied with the FA in the past,[33] in which an electron attaching gas is used to quench the DR to monitor excited state emissions resulting from DR. Results from this previous work and present work demonstrate clean pulsing with sticky gases like H_2O. See also the electron current profile, for pulsing CCl_4 in Section 4.3 for further details.

4.2.2 Pulsed Reagent Gas (RG) Method

In the second method (pulsed reagent gas (RG) method), the main difference from the electron-attaching gas method is the flow tube pressure. Also, addition points of gases are changed to ensure that the recombining ion of interest is formed further upstream to maximize signal coming from the products), and the reagent gas is pulsed instead of the attaching gas. The flow tube pressure is 3.0-4.0 Torr with a He flow rate of 31.4 slm; note the higher flow rate is used to maintain the plasma velocity at the higher pressure. Argon and H_2 gas are

added in at ~22 cm downstream of the microwave discharge at concentrations of ~2 x 10^{14} and 5 x 10^{11} molecules/cm^3 respectively. Note, the amount of H_2 added is such that the H_3^+ recombination rate coefficient is ~4 x 10^{-8}molecules/cm^3.[34] The [H_2] is chosen to be small enough to minimize the recombination coefficient of H_3^+ and maintain the ionization density whilst large enough so that H_3^+ is very much the dominant ion at the point of addition of the reagent gases so that rapid proton transfer occurs. Approximately 24 cm downstream of the H_2 addition point, the reagent gas of interest is pulsed, in this case N_2. The concentration of the N_2 is varied over the range from ~8 x 10^9 molecules/cm^3 to ~1 x 10^{14} molecules/cm^3. This concentration range is such that the electron density [e] at the pulse addition point (~3.0 x 10^{10} molecules/cm^3) is within this range, see Section 4.3 for details. To achieve the lowest concentrations of N_2, a 0.2% N_2 in He mix is used. For the higher concentrations the pulsed gas is switched to pure N_2. Again, equations 4.4 – 4.7 summarize the chemical reactions leading up to H_3^+, which readily proton transfers to N_2 forming the recombining ion of interest, N_2H^+. Inherent in this method is that at large N_2 concentrations ([N_2]>[e]) not all of the pulsed gas will be protonated, and the residual gas interferes with the detection of the DR neutral products. Since this interference cannot be removed by difference (unlike the attaching gas method), the flow tube conditions are chosen so that the contribution of DR products to the overall signal is varied. Here, the overall signal is the sum of DR products and fragmentation contribution of the unreacted reagent gas. These contributions are distinguished by monitoring the absolute fraction of products as a function of initial N_2 concentration, $[N_2]_0$. This method requires modeling to extract a product distribution. By using a best fit method, the product distribution percentages used in the model are varied to maximize the agreement between the model and the experimental data. However, the advantage to this method is that ion-ion recombination is not an issue since no attaching gas is added and thus no anions are formed.

4.2.3 Modifications to the Flowing Afterglow

In order to detect the products of DR, an axial electron impact ionizer (Extrel Axial Molecular Beam Ionizer with thoriated iridium filaments) was positioned in front of the quadrupole mass filter to ionize the sampled neutrals (products of DR and background gases). Ions passing through the quadrupole filter are detected by a discrete dynode electron multiplier (ETP model AF553H). This multiplier fits the criteria needed for the experimental situation, where the current output response of the multiplier must increase linearly as the count rate increases up to high count rates. It is difficult to achieve a large dynamic range of counts per second (c/s) with many multipliers. However in the ETP model the deviation from linearity is near zero up to 70 μamps of output current. The output current (I) can be translated into count per second if the gain of the multiplier is known, using equation 4.11:

$$I = qNG \tag{4.11}$$

where q is the charge on an electron, N is the number of counts per second, and G is the gain of the multiplier. For a typical gain of $\sim$1 x 10^7, the maximum count rate is $\sim$5 x 10^7 c/s. In the experiments, count rates are keep below 1 x 10^6 c/s to avoid errors due to multiplier saturation. These counts are collected in two channels of a gated photon counter (Stanford Research Systems model SRS400). The ionizer electron energy is set to 70 eV, which stated previously is used to take advantage of the wealth of experimental data available in the literature.[35] For radical species, fragmentation patterns are obtained from the ratio of the fragment ion to parent ion ionization cross sections, which are readily available in the literature.[36] Data for N_2 and NH are collected in Table 4.4 and in Table 4.5 for CH_4, CH_3, CH_2, and CH. Note that the question marks indicate values that are not known. These values are thought to be small for two reasons. First by the fragmentation of CH_4 to C^+ is only 0.02 and it is not unreasonable to assume that the C^+ fragment from CH_3 and CH_2 will also be small. Secondly, the experimental measurement of the ionization cross section for C^+ channel from CH_2 was not made because it did not have significant signal.[38] The experiment

Table 4.4: Absolute fractions for the fragmentation patterns of N_2 and NH that were used for the N_2H^+ studies. Fragmentation for N_2 is calculated from fragmentation patterns[35] and NH from the ratio of relative ionization cross sections (fragment to parent).[37]

N_2		NH	
Ion	Absolute Fraction	Ion	Absolute Fraction
N_2^+	0.85	NH^+	0.78
N^+	0.15	N^+	0.22

Table 4.5: Absolute fractions for the fragmentation patterns of CH_4, CH_3, CH_2, and CH that are used for the CH_5^+ study. CH_4 is calculated from reference[35] and CH_2 and CH from the ratio of relative ionization cross sections (fragment to parent).[38] CH_3 is calculated from measurements made in our laboratory. The question marks are values that are not available and are expected to be small and also considering that C^+ is only 0.02 from CH_4,see text. Even so, this is taken into account in the error analysis, see Section 4.3.5.

CH_4		CH_3		CH_2		CH	
Ion	Absolute Fraction	Ion	Absolute Fraction	Ion	Absolute Fraction	Ion	Absolute Fraction
CH_4^+	0.44	CH_3^+	0.75	CH_2^+	0.71	CH^+	0.79
CH_3^+	0.40	CH_2^+	0.18	CH^+	0.29	C^+	0.21
CH_2^+	0.09	CH^+	0.7	C^+	?		
CH^+	0.05	C^+	?				
C^+	0.02						

can be set up in two modes, one is sampling plasma ions only to identify the recombining ions and the other is sampling neutral products of recombination plus background neutrals, where the pulse modulation distinguishes the DR neutral products from the background. In the latter case, DR products are sampled with various ions serving as monitors for the various products, N_2^+ for N_2, NH^+ for NH, N^+ for N. Note that the lower mass products have contributions from fragmentation of higher mass products, which have to be accounted for. These modes are selected by application of appropriate potentials to electrostatic lenses (i.e. sampling orifice and subsequent downstream lens) upstream of the axial ionizer and are dependent on the state of the ionizer, i.e., whether in the on or off mode. While monitoring

the plasma ions the potentials on the sample orifice and subsequent lens are near ground or biased negative to allow passage of the ions, see Figure 4.1. In addition the electron impact ionizer is off and an Einzel lens focuses the plasma ions into the mass filter.

In the other mode (mode 2), the plasma ions and electrons need to be diverted, to eliminate possible interference with detection of neutrals within the plasma. To block plasma ions and electrons, potentials($\sim$1–2 Volts) equal in magnitude but opposite in sign are applied to the sample orifice and top hat lens and the ionizer is turned on. It is in this state where only neutrals are being sampled through the sample orifice, thus being ionized. The ion region contains the ionization volume, i.e. where the ions are generated. The potential energy that the ions are born with is dictated by the potential difference between the ion region and pole bias, typically $\leq$10 Volts, where the pole bias is a dc voltage potential on the z-axis of the quadrupole, not shown in Figure 4.1. The extractor lens then pulls these ions from the ionizer region and accelerates them into the focusing region (an Einzel lens), which focuses the ions into the entrance of the quadrupole mass filter. The selected ion is then filtered and detected by the discrete dynode electron multiplier (off-axis). Note that it is the dynodes that are off-axis from the quadrupole exit. This is necessary to prevent interference from radiation coming from the flow tube, specifically from the upstream microwave source. For this reason, the microwave discharge producing the plasma is also off axis from the flow tube. This is the mode that is used to obtain the DR product distributions.

4.3 Results and Discussion

4.3.1 Experimental Checks

In this section, means for minimizing systematic error and increasing the sensitivity of the technique (i.e. signal to background sensitivity) are discussed. There are two important conditions that minimize error if dealt with properly. Firstly, the pulsing needs to be clean and consistent. Secondly, there should be no evidence for signal build up when there is no difference between the two situations (i.e. where there is intentionally no difference between

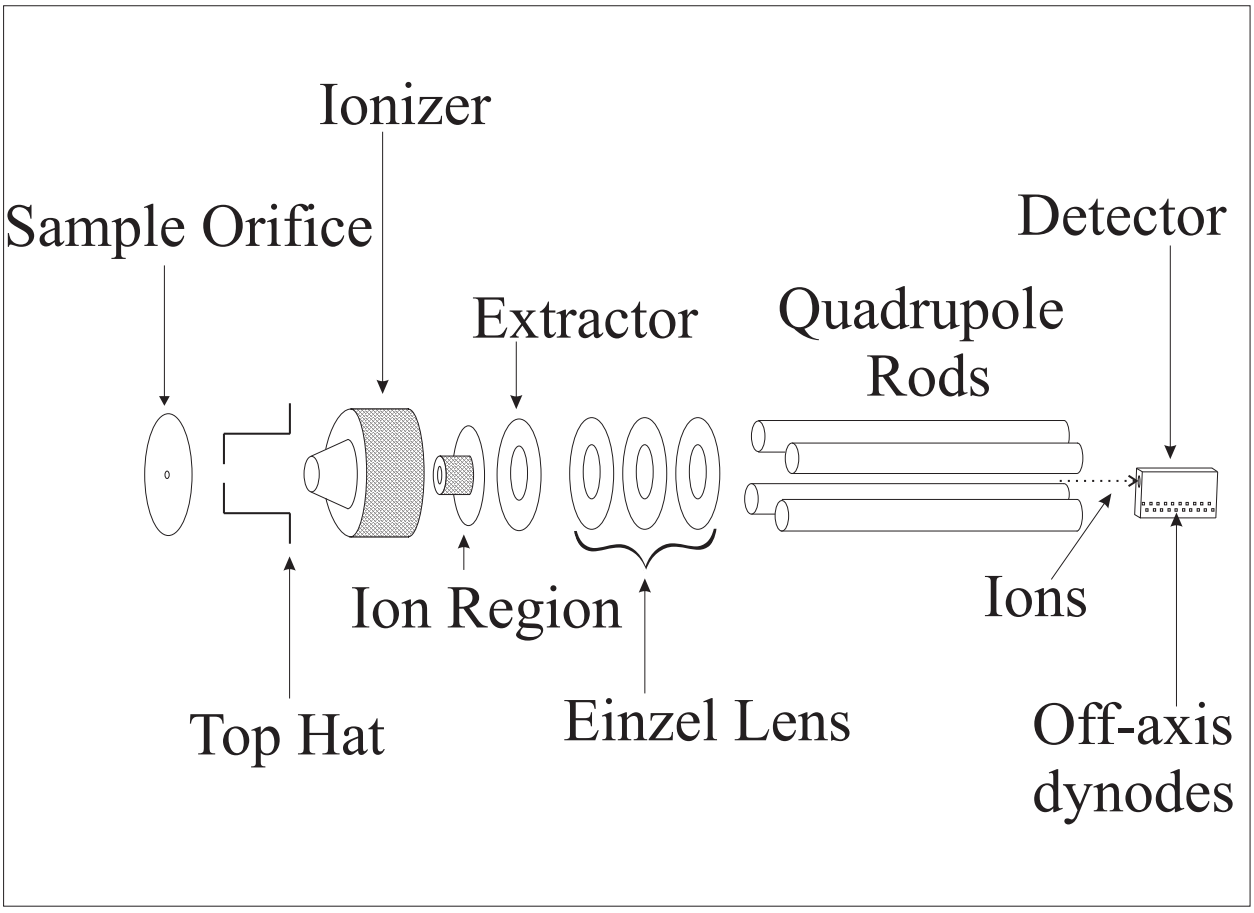

Figure 4.1: Expanded view of the ionization and ion focusing section of the detection system. The sample orifice is a 5.08 x 10^{-2} millimeter hole that allows passage of either ions or neutrals, depending on the mode of operation.

the pulse valve open and closed). This difference can occur if, for example, there is any significant drift in the gas flows. In addition, the sensitivity of the technique was optimized.

Clean pulsing of very sticky gases can be achieved by varying the amount of He in the upstream and downstream flushes of the pulsed gas.[33] The profile of the Langmuir probe current (i.e. [e] variation) as a function of time for pulsing in a 1% mix of CCl_4 in He is illustrated in Figure 4.2.

The optimum profile is a clean reproducible transition (i.e. ∼square wave) between the two pulse valve states (open versus closed), as shown in Figure 4.2. In addition, the optimum concentration of attaching gas is when 80–90% of electron density is destroyed, see Section 4.2.

The second point about minimizing error is to ensure that there is no signal build up when there is no difference between the two pulse valve states. This is achieved by monitoring the masses of the products of the DR of interest while the plasma is off, with no DR occurring. By doing this, it is ensured that there are no impurities in the pulsed electron attaching gas mix, namely the ion that is being used as the monitor and any molecule with an overlapping mass (e.g. O^+ from H_2O overlapping with CH_4^+ from CH_4). This type of error is avoided by using extremely pure gases in the mixes of the pulsed gas. For these conditions, data of the kind illustrated in Figure 4.3 is obtained.

Figure 4.3 is a test for signal build up when the plasma is off. The data collected are the same as the conditions used for the CH_5^+ DR study, but that the plasma is off. Where the red circles (A channel) and black squares (B channel) are plotted as counts per period (0.1 seconds) versus time in seconds. The green triangles (CH_4^+ counts) represent the integration of 400 periods of the CH_4^+ signal. It should be noted that the A and B channels are very stable. The signal from CH_4^+ does not have any significant build up of signal and variations in the integrated signal are due to random errors in the A and B channels, which are associated with counting. Note that this test cannot be performed with method 2 since the reagent gas is being pulsed in, thus even with the plasma off there is a signal difference between the two

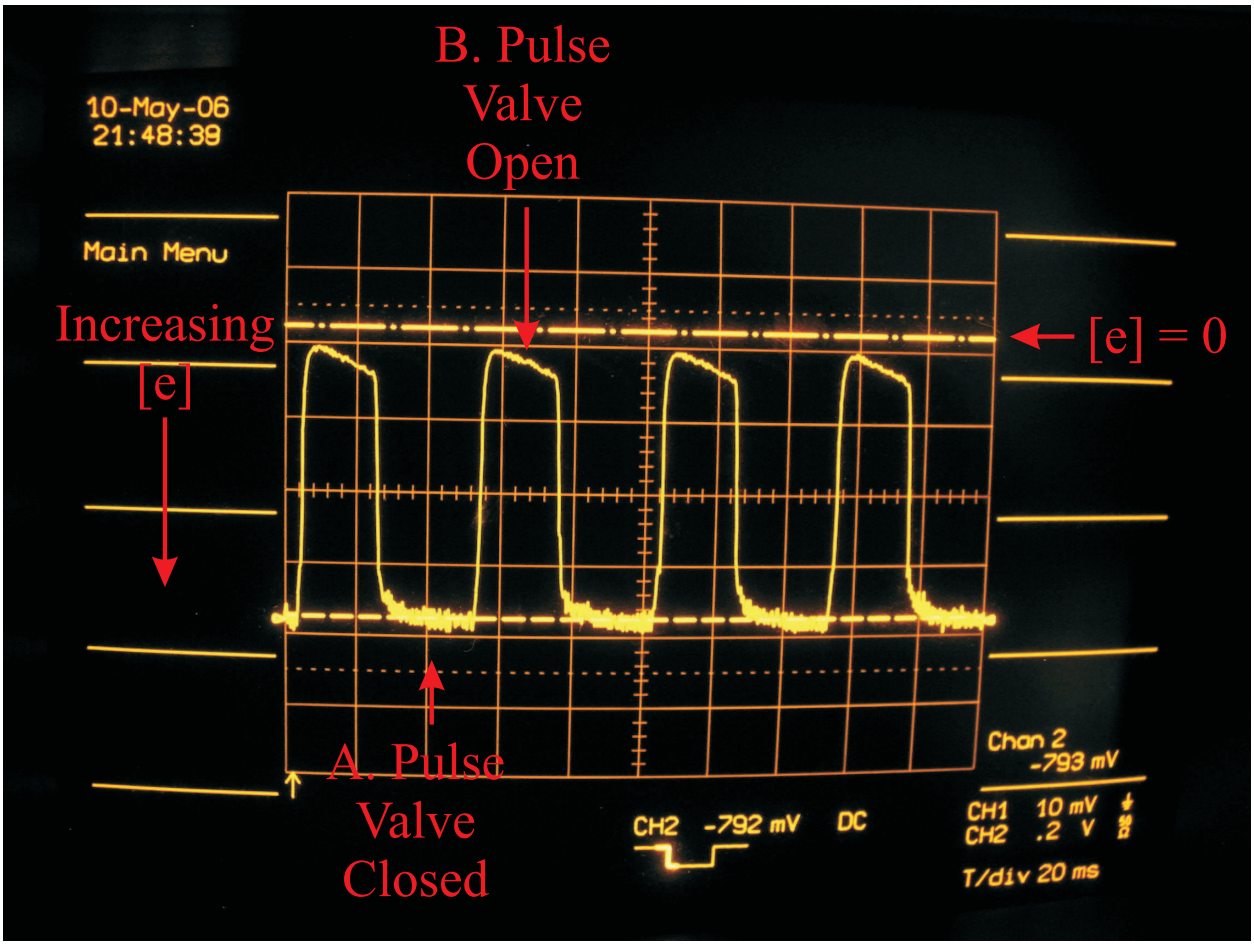

Figure 4.2: The variation, with time, of electron current measured with the Langmuir probe in the plasma. The current is measured by placing a small voltage (+3.0 Volts) on the probe, at position where the reagent gas of interest is added to the flow tube. The difference is created by pulsing in a rapidly electron attaching gas (CCl_4), which quenches DR recombination. This ensures that clean, square modulation of the electron density is occurring where the recombining ion of interest is forming.

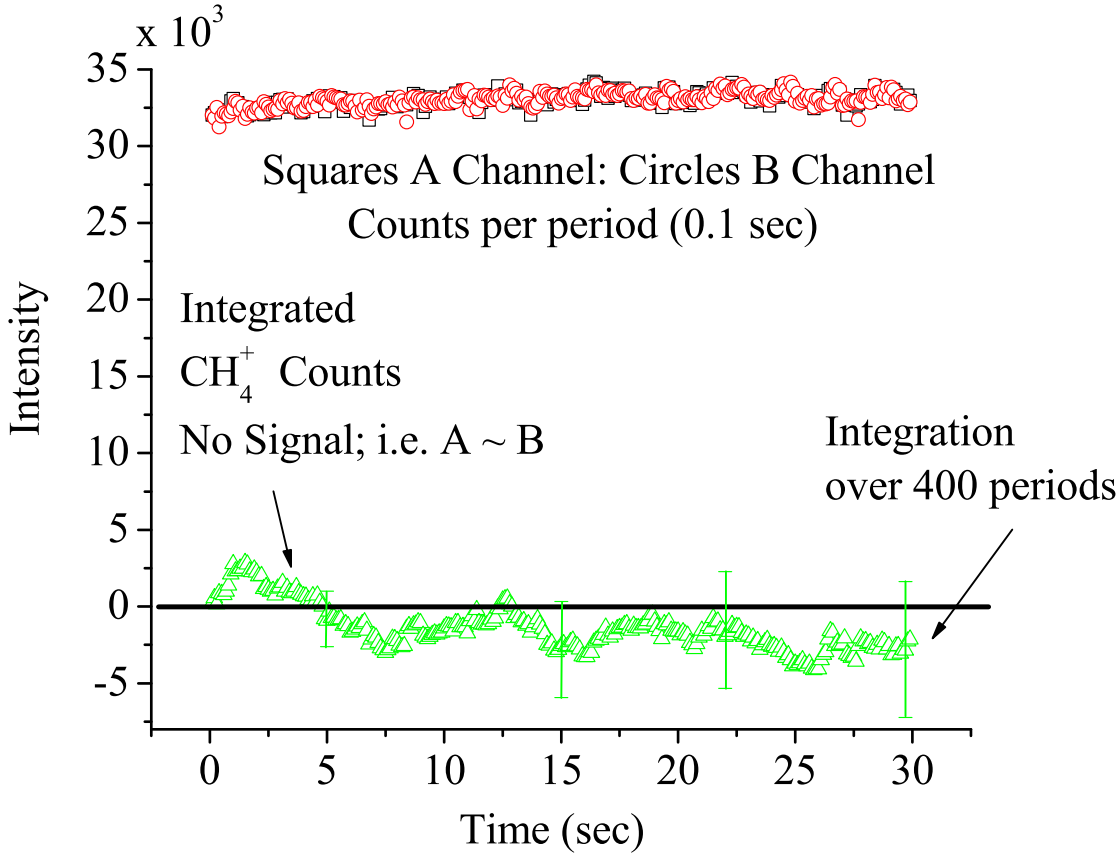

Figure 4.3: The test for erroneous signal build up when no signal is present. The conditions under which this data were collected is the same gas flow conditions as the CH_5^+ DR study, but with the plasma is off. It can be seen that the integrated signal just oscillates close to the zero due this is due to the random errors associated with counting.

channels. Impurities in this case are dealt with by using extremely pure gases, such that any impurity is in the ppm range. With this small concentration any impurity introduced into the flow tube with the reagent gas cannot compete for a proton in the proton transfer reaction, thus will not interfere with the formation of the ion under study. Note that, as the initial reagent gas concentration is changed there are two sources of impurities, the impurities from the reagent gas (N_2) itself and impurities in the He that is used to for the mix; a 0.2% N_2/He mix was used to produce the low concentrations of N_2. The majority of the mix is He and impurities in this could pose a problem. However, this is dealt with by using high purity He and cleaning it with two liquid-nitrogen cooled sieve traps, prior to making the mix. Any impurity of N_2 in the He will of course only act like a slightly enhanced concentration of N_2

In both methods, the pulsing rate is critical to the reduction of error due to any drift in the experiment, since (A) is counted after (B). If the pulse valve operates slowly (i.e. more time spent counting) the drift in the system creates larger errors in the signal (A-B), see Figure 4.4.

Figure 4.4 are the plotted histograms of signal collected which represent two plasma conditions, one that is unstable((a) and (c)) and one that is stable((b) and (d)). Each of the histograms have been fitted by a Gaussian with the respective mean and standard deviation displayed for each plot. Note that the statistics of ion counting is governed by Poisson statistics, yet since the resulting difference in between two channels (i.e. two Poisson distributions) is not necessarily governed by a Poisson distribution. So a Gaussian approximation of each distribution must be made to carry out the difference and calculate the error associated with the difference. This approximation is sufficient if the mean value (μ) of the distribution is $\geq$9 for a given counting period,[39,40] which is the case for typical data obtain in this experiment. For the unstable situation, plot (c) simulates a slower pulse speed (half the rate of (a)). Note that the simulation means that the raw data (which is the fast pulse rate) that is collected in 2000 bins (300 msec for each bin) is added to give 1000 bins (600 msec for each bin), which is essentially the same as slowing the rate of the pulse valve. In the comparison between (a)

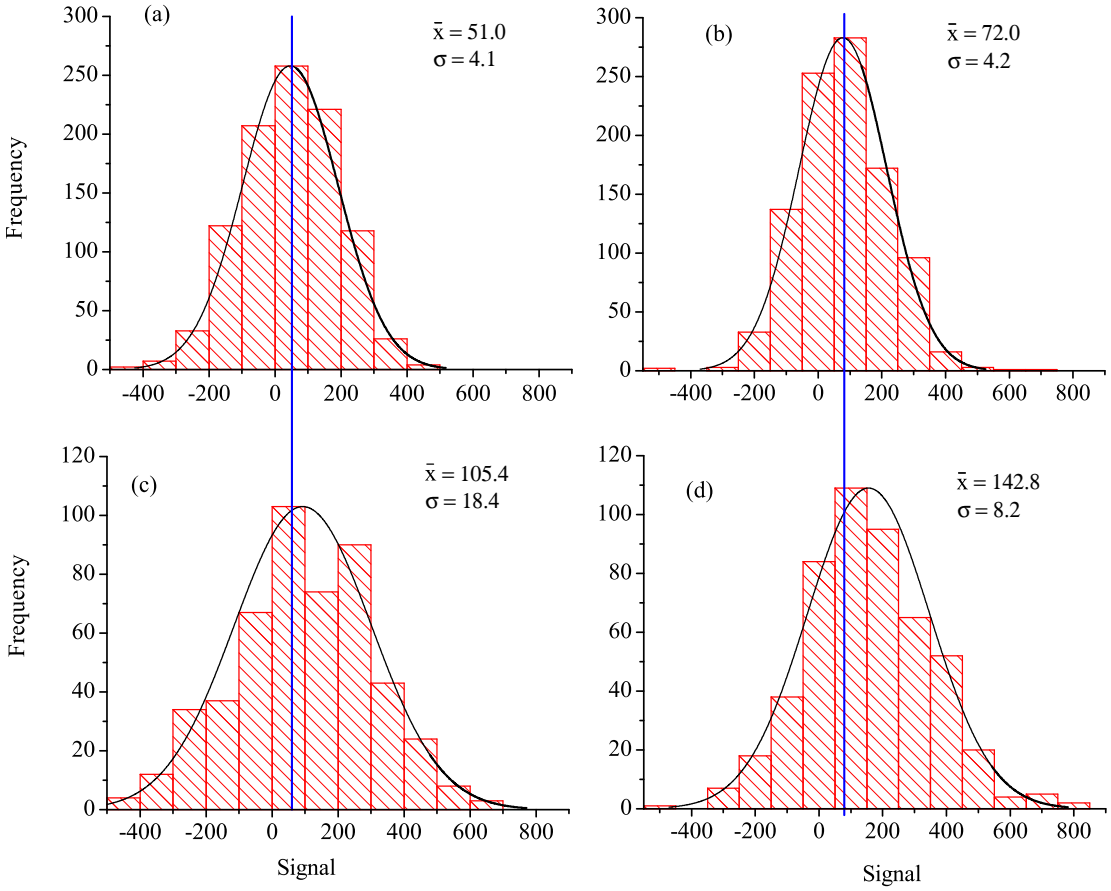

Figure 4.4: A comparisons between two situations: The First condition is unstable conditions with a significant amount of drift in the A and B counts. The second is a stable conditions in the plasma, i.e. all flows are stable and little drift is evident in the A and B counts. The plots (a) and (c) are associated with the unstable conditions and (a) simulates half the time spent counting on A and B (i.e. double the pulse valve rate) compared to (c). The plots (b) and (d) are associated with the stable conditions, where (b) simulates half the time spent counting on A and B compared to that of (d).

and (c) the mean doubles with increased sampling time, but the standard deviation is over 4 times larger. In the stable situation, plot (d) simulates a slower pulsing speed, one that is half the rate of (b). Comparisons between these two show that in addition to the mean, the standard deviation nearly doubles, as expected. This shows that the faster pulse rate eliminates some of the effects of instabilities in the plasma.

Finally, the sensitivity of detection (i.e. detection of a small signal in a large background) was quantified by using a constant large flow of gas, which simulates a large background and in this case CH_4 was used. The small signal was emulated by pulsing in small amount of a $\sim$0.20% CH_4/He mix, which simulates a small signal in a large background. By doing this it was found that the limit of detection is at least $\sim 10^{-3}$ signal to background, see Figure 4.5.

In this experiment, the DR product that typically has the highest background is the one that is the same as the reagent gas that is used, thus detecting the other products should be less of a problem since their associated background is lower. For example, in the case of DR of N_2H^+ the DR product N_2 has the highest background, whereas NH has nearly no background.

4.3.2 N_2H^+ Recombination

The details of the analysis of this recombination case can be found in Molek et al.[41] and only the features that illustrate the technique will be covered here. Note that the He throughput for this study of N_2H^+ was 31.4 slm to decrease the resonant time in the flow tube, thus further reduce any affects due to diffusion of DR products. The experiment was repeated at 16.0 slm for comparison and it was found that no change was observed in the product distribution as expected if diffusive loss is small for both flows. Data presented in this paper for the electron attaching gas method was collect at a 16.0 slm throughput.

Two methods have been applied to this DR case. It should be noted that there are very small N_2 impurities in the He buffer gas but because these are a constant in the flow tube they are subtracted out (see equation 4.9). As mentioned earlier, for each DR product there

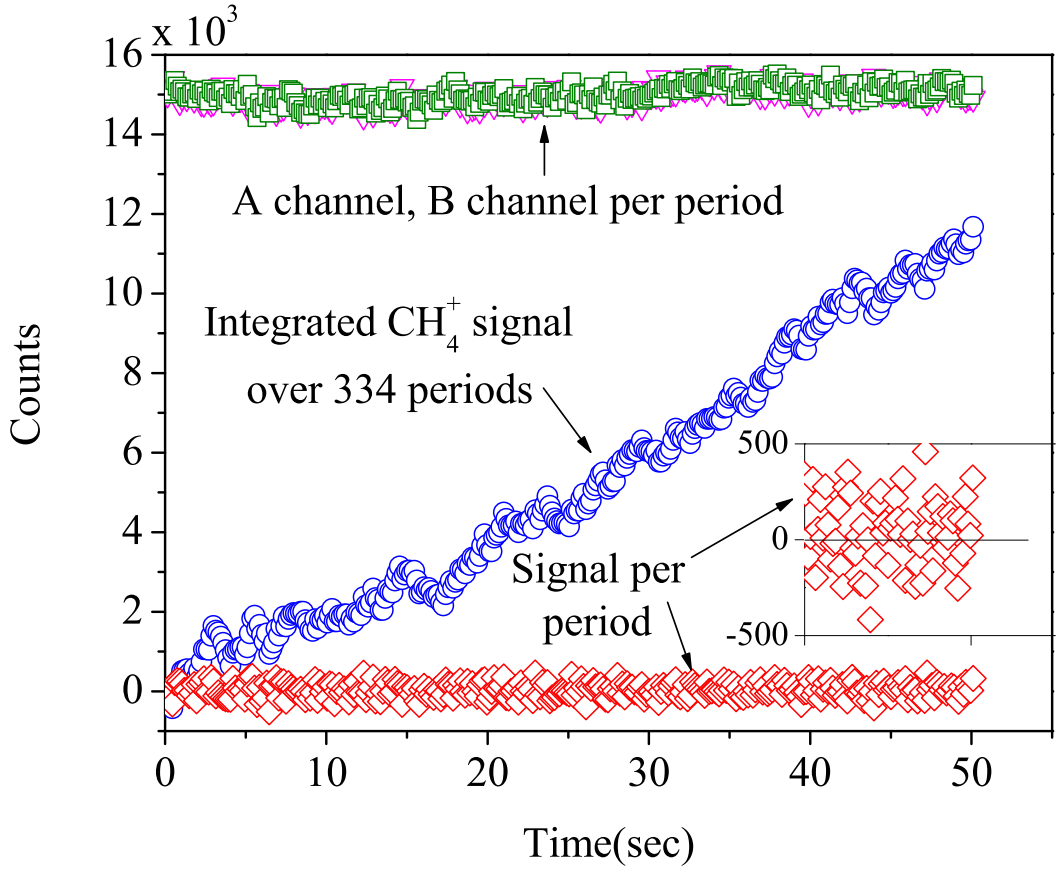

Figure 4.5: A sensitivity test with a small amount of CH_4 pulsed into the flow tube where there is a large constant background of CH_4 (i.e. S/BG $\sim 10^{-3}$. It can be clearly seen that the signal is building up by integrating with time. The magnified inset of the figure shows how close the signal per period is to the zero.

is an associated monitor ion, in other words the following products N_2, NH, and N have the associated monitor ions, N_2^+, NH^+, and N^+, respectively detected after electron impact ionization. Note that when the attaching gas is pulsed in, there is the possibility of some ion-ion recombination (iir) taking place. This is minimized by adjusting the attaching gas concentration to optimize the percent of electrons attached, see Section 4.3.1 and Figure 4.2. Below are the possible products from the iir reaction between N_2H^+ and Cl^-

$$N_2H^+ + Cl^- \rightarrow N_2H + Cl + 5.30eV \tag{4.12}$$

$$\rightarrow N_2 + H + Cl + 4.86eV \tag{4.13}$$

$$\rightarrow N_2 + HCl + 9.34eV \tag{4.14}$$

$$\rightarrow NH + NCl + 2.05eV \tag{4.15}$$

$$\rightarrow NH + N + Cl - 1.41eV \tag{4.16}$$

Yet iir can still pose a small error in the calculation of the DR product, where the products are common between the two processes. Based on the rate difference between these process which is typically about an order of magnitude[42] and assuming a worst case condition that only one product channel of iir is accessed, say channel (4.15), then the maximum error in the NH DR product is ∼8–10%. If the NH product from DR were >10% then it would be detectable and appear to be smaller than it really is, but if it were ∼8–10%, by giving an NH signal in channel B. then the DR signal from this product would appear to be zero. However, here the signal from the NCl product would be negative since it can only result from iir. With this in mind the possible products from iir were monitored (Cl^+, HCl^+, and NCl^+), thus covering all possible channels, see Figure 4.6 below.

It can be seen that products from the iir are almost non-existent, ensuring that the affects of iir are indeed very small, thus implying that this is a slow recombination. Note that any iir recombination product would integrate in the negative direction. This analysis shows that iir is not affecting the DR product distribution. Yet our results for DR of N_2H^+ are

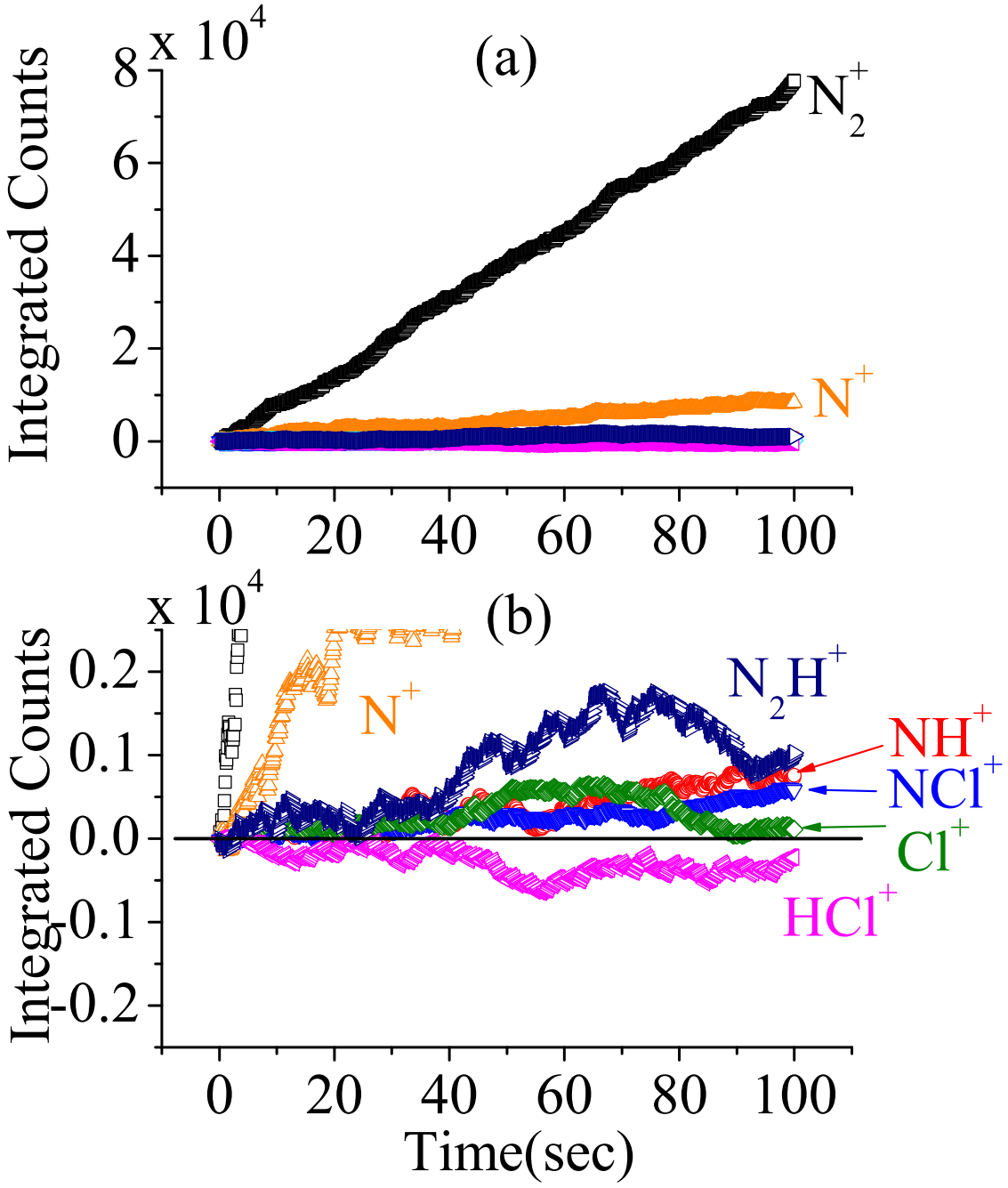

Figure 4.6: Integrated signals for DR of N_2H^+. Shown is the integrated signal from all the monitored species, for both DR and iir products. It can be clearly seen that the biggest signal build up is from N_2^+ monitor ion. The next largest signal is from N^+, which is solely attributed to the electron impact fragmentation of N_2. The (b) plot, is an expanded counts scale, around the zero, of the other products.

in stark contrast with the SR data.[15] To further ensure that iir is not affecting the product distribution and to corroborate the results so far a second methodology was used.

Briefly, the reagent gas, N_2, is pulsed in forming the recombining ion, in this case N_2H^+ where the difference of N_2 out (A) versus N_2 in (B) is the signal, equation 4.9. Note that since N_2 is being pulsed in, the integrated signal is in the negative direction, but in this method the sign of the signal is insignificant because it is the magnitudes that matter for the analysis. There are two contributors to the signal, one is a fraction of unreacted reagent gas (f_1) and the other is the products of DR (f_2). In the experiment, the contribution of f_1 to the total signal needs to be minimized while maximizing f_2 contribution. This is achieved by changing the initial concentration of N_2, $[N_2]_0$, such that the range between the lowest and highest concentrations encompass the electron density ([e] = ∼3.0 x 10^{10} molecules/cm^3) at the pulse addition point. Encompassing the [e] is critical because [e] = [+], where [+] is the total cation density of the plasma. Additionally, the dominant ion (N_2H^+) at this point in the flow tube is ∼ [+], thus ∼ [e] as well. Therefore, $\left[N_2H^+\right]$ must be ≤ [e] and dictates that the DR products are ≤ [e] as well. This concentration is an upper limit for the DR products, and thus constrains the contribution of DR products (f_2) to the total signal. At high $[N_2]_0$ concentrations (∼1 x 10^{14}molecules/cm^3) the fraction of unreacted reagent gas dominates over the DR products by nearly 4 orders of magnitude, therefore a plot of the absolute percent of each ion, in this case N_2^+, NH^+, and N^+(i.e. monitors for N_2, NH, and N), versus $[N_2]_0$ = 1 x 10^{14} molecules/cm^3 results in the absolute fragmentation pattern of N_2, which persists for the higher values of $[N_2]_0$. As the $[N_2]_0$ concentration approaches [e] the fraction of unreacted reagent gas decreases and the fraction of products from DR are not dominated by f_1. This leads to a deviation from the absolute fragmentation pattern of N_2, see Figure 4.7.

Inherent in the pulsing technique is that any impurity in the flow tube is a constant background, which gets subtracted out. This is especially important in the pulsed reagent gas method, where it enables the detection of N_2 products at the low $[N_2]_0$ concentrations

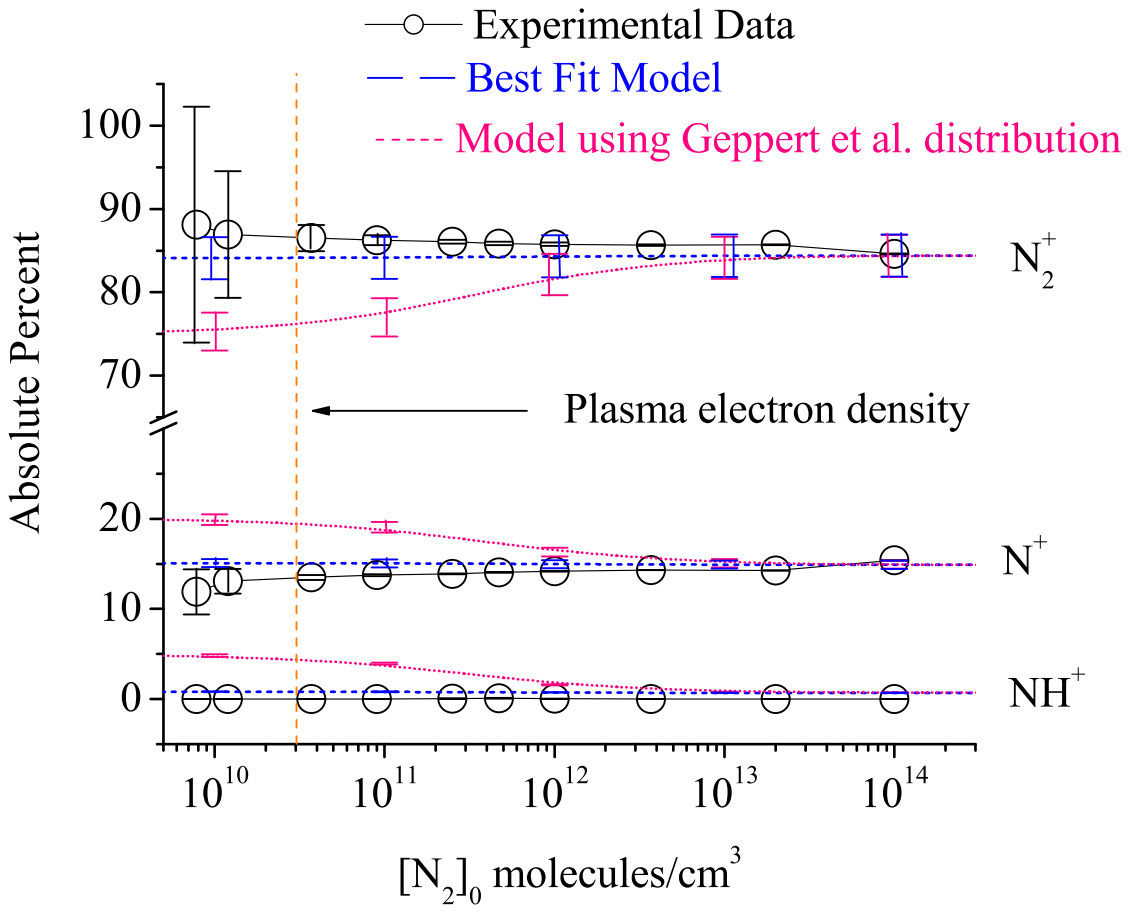

Figure 4.7: Absolute ion percentages of the monitor ions, model and experiment, as a function of initial N_2 concentration. The solid lines with open circles represent the experimental data. The blue dashed and pink dotted lines represent the kinetic model results using two different values for the absolute DR product percentages. The pink dotted line uses Geppert et al. results,[15] N_2 (36%) and NH (64%), and the blue dashed lines are the models best fit which uses N_2 (98%) and NH (2%). The best fit model from agrees with the experimental data far better than the model of Geppert et al. results. In addition, error bars are include on the experimental data and estimations of error on the model, see Section 4.3.4 for details.

needed to observe the deviation from the fragmentation pattern. It should be noted that the data point at the lowest $[N_2]_0$ concentration is difficult to obtain with an error of <10% in the final product distribution a reasonable amount of time. The final DR distributions from these two methods are shown in Table 4.6

Table 4.6: Remeasured values of the Products of Dissociative Recombination for N_2H^+

			FA[41]		SR[15]
			Method 1	Method 2	
$N_2H^+ + e^-$	$\rightarrow$	$N_2 + H$	95-100%	95-100%	36%
	$\rightarrow$	NH + N	0-5%	0-5%	64%

An exhaustive effort has been made during these experiments to reconcile the difference between the current FA measurements and SR measurements of Geppert et al. In particular, possible errors in the FA study have been analyzed in great detail. For the SR it is known that there are contamination issues due to $^{14}N^{15}N^+$ in the ring; this would DR into ^{14}N + ^{15}N, where the ^{15}N would appear to be ^{14}NH product. The ion source in the SR study is a hot filament ion source that operates at temperatures over 1000K.[43] N_2 ionizes 3 times more efficiently for the experimental conditions; thus to get N_2H^+ into the ring it relies on the reaction,

$$N_2^+ + H_2 \rightarrow N_2H^+ + H \tag{4.17}$$

yet it is not known what the N_2H^+ to N_2^+ ratio is when ions are extracted from the ion source and injected into the ring. It is a concern that Geppert et al. quote a room temperature rate coefficient for reaction (4.17), since there is experimental evidence for similar reactions showing that the rate constants tend to decrease as the temperature increases.[41] It should be noted that due to our measurements the SR is devoting time to repeating the original SR measurements and preliminary measurements are suggesting problems with the original experiment and that the NH channel is now much lower than originally thought.[44] This illustrates the importance of measuring DR product distributions with more than one technique.

4.3.3 CH_5^+ Recombination

This recombination is particularly relevant to the interstellar medium since it was thought to be a source of CH_4,[45] until storage ring measurements showed CH_3 (∼75%) as a dominant product from this recombination.[46] This removed the CH_5^+ DR as a source of methane out of the models of the interstellar clouds.[45] In the recombination of CH_5^+ the following energetic pathways were considered,

$$CH_5^+ + e^- \rightarrow CH_4 + H + 769kJ/mol(8.0eV) \tag{4.18}$$

$$\rightarrow CH_3 + H_2 + 766kJ/mol(7.9eV) \tag{4.19}$$

$$\rightarrow CH_3 + 2H + 330kJ/mol(3.4eV) \tag{4.20}$$

$$\rightarrow CH_2 + H_2 + H + 307kJ/mol(3.2eV) \tag{4.21}$$

$$\rightarrow CH + 2H_2 + 317kJ/mol(3.3eV) \tag{4.22}$$

Since method 1 is an extremely effective way to determine the products of DR and enables a search for ion-ion recombination products, efforts have been concentrated on this approach. The experiments show a large build up of the CH_4^+ signal, a monitor ion for CH_4. This signal is due to the DR product of CH_4 and not the unreacted CH_4 in the flow tube. This is reinforced by two experimental examples. The first was shown in Figure 4.3 and discussed in detail in the text, see Section 4.3.1. It demonstrates the ability to integrate to ∼0 signal even when there is a large background (3 x 10^5 counts/sec) of CH_4, thus unreacted background is not contributing to signal build up. The second example is discussed in detail in Molek et al.[41] Briefly, Two DR systems were studied, HCO^+ and CO^+, while one monitor ion (CO^+ for CO DR product) is the focus. Since CO^+ can only dissociate upon recombination (i.e. no product CO), the CO^+ monitor should integrate around the zero for this recombination. However, in the case of HCO^+, CO is a major product (92%)[47] of DR and therefore an integrated signal of the CO^+ monitor should be very evident. What is seen in the Figure 5 in Molek et al.[41] is for the HCO^+ DR, the CO^+ monitor ion builds up over time corresponding to CO product. However in the CO^+ DR case, the CO^+ monitor ion is oscillating around

the zero over time, which is expected since CO is not a product from the recombination. Therefore, there is no erroneous build up of signal.

The experimental conditions for DR study of CH_5^+ are the same as listed in Section 4.2.1. The build up of CH_4^+ and CH_3^+ monitor ions can be seen in Figure (4.8a) below. Note that CH_3^+ is a major ion fragment of electron impact ionization of CH_4,[35] thus the CH_3^+ integrated ion signal is nearly all attributable to the fragmentation contribution of electron impact ionization of the DR product CH_4.

The (b) plot shows the monitor ions for some of the energetically possible iir products as well as the CH_2^+ and CH^+ monitor ions, where the energetically accessible channels are given below.

$$CH_5^+ + Cl^- \rightarrow CH_4 + HCl + 856kJ/mol(8.9eV) \tag{4.23}$$

$$\rightarrow CH_4 + H + Cl + 424kJ/mol(4.4eV) \tag{4.24}$$

$$\rightarrow CH_3 + H_2 + Cl + 424kJ/mol(4.4eV) \tag{4.25}$$

$$\rightarrow CH_3Cl + H_2 + 773kJ/mol(8.01eV) \tag{4.26}$$

$$\rightarrow CH_3 + H + HCl + 424kJ/mol(4.4eV) \tag{4.27}$$

$$\rightarrow CH_3Cl + 2H + 341kJ/mol(3.5eV) \tag{4.28}$$

$$\rightarrow CH_2 + H_2 + HCl + 390kJ/mol(4.0eV) \tag{4.29}$$

$$\rightarrow CH_2Cl + H_2 + H + 354kJ/mol(3.7eV) \tag{4.30}$$

$$\rightarrow CHCl + 2H_2 + *eV \tag{4.31}$$

It should be noted that it is very difficult to monitor the H_2^+ and H^+ ions since that are at a very low mass in the mass range of the quadrupole mass filter. This results in difficulties getting quantitative values for these products. It is noticed that there is a small negative build up of the Cl^+. This product is small (<2%) but still indicates that some iir is taken place. In the case of Cl^+, the presence of CCl_3 may contribute to some of the negative build up. As far as the authors are aware the fragmentation pattern of CCl_3 is not available in the literature, thus the Cl^+ contribution from this source cannot be assessed. However, in looking at the

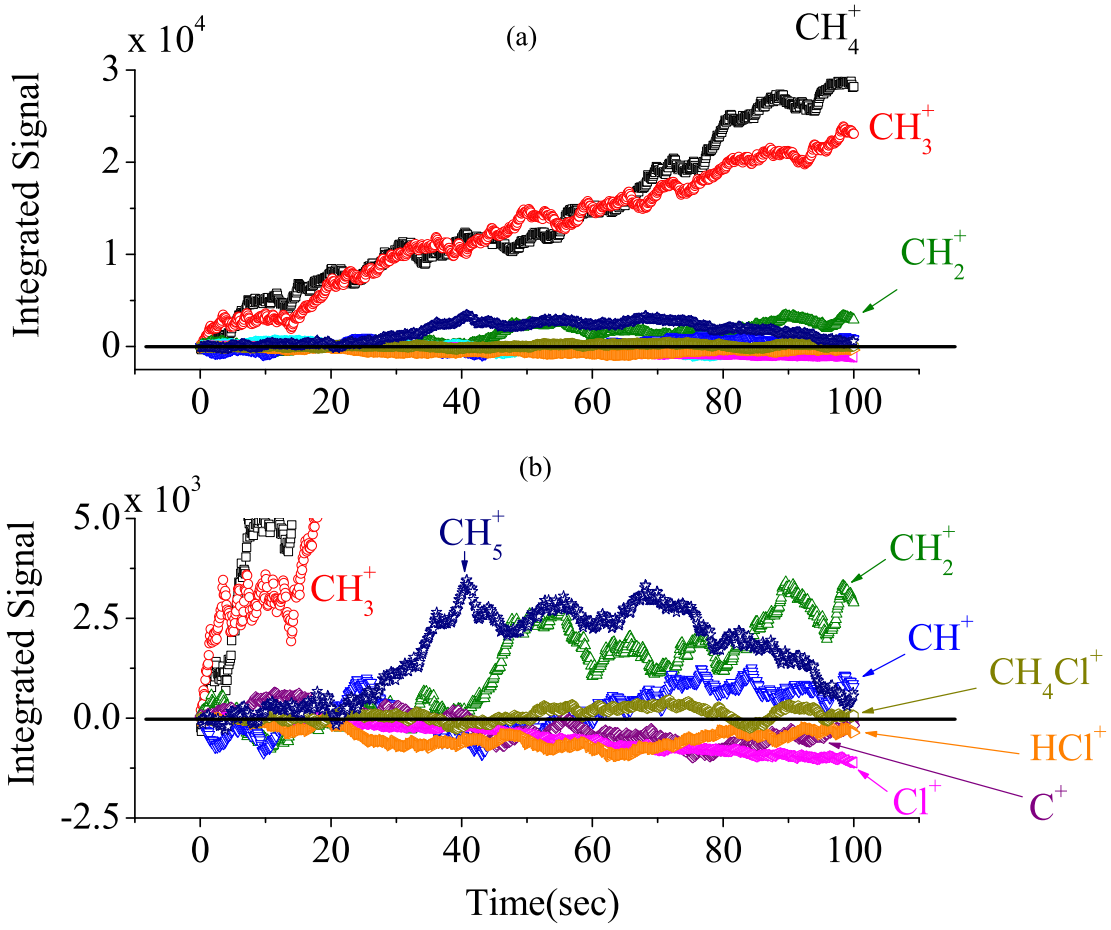

Figure 4.8: The integrated signal build up of all the monitored species, for both DR and iir products of CH_5^+, is shown in (a). It can be clearly seen that the biggest signals are from CH_4^+ and CH_3^+ monitor ions. The majority of the CH_3^+ signal is from the fragmentation of CH_4. In the (b) plot, is an enlarged scale, around the zero, of the other products. There is a small negative build up of Cl^+ and possibly HCl^+, products of iir, however, these are very small signals see text below for further analysis.

N_2H^+ recombination Cl^+ is not seen at all and this is for similar experimental conditions, thus implying that CCl_3 does not fragment significantly to Cl^+. This is an indicator that Cl is a product of iir, which suggests a general way of determining the products of iir. More experimentation with the recombination optimized for this iir process would have to be performed to confirm this. Note that electron impact ionization of CCl_4 cannot be a source of Cl^+ since all of this is destroyed in the electron attachment process. To the authors knowledge this is the first data obtained for the products of iir for $CH_5^+ + Cl^-$. The CH_5^+ DR product distribution determined for the present study is shown below in Table 4.7 together with the SR data from Semaniak et al.[46] The dominant product in the FA measurement,

Table 4.7: Product distributions for CH_5^+ recombination. Results of the current work and comparison to SR data.

			FA (this work)	SR[46]
$CH_5^+ + e^-$	$\rightarrow$	$CH_4 + H$	95% ±5%	4.9%±1.3%
	$\rightarrow$	$CH_3 + H_2$	≤8%	4.8%±0.2%
	$\rightarrow$	$CH_3 + 2H$		69.8%±0.8%
	$\rightarrow$	$CH_2 + H + H_2$	≤1%	17.2%±1.6%
	$\rightarrow$	$CH + H_2 + H_2$	≤1%	3.3%±1.1%

CH_4, is stark contrast to the SR data where the dominant product is CH_3. The reasons for this difference are not understood.

4.3.4 Sources of Error

The possible sources of error in our measurements that need to be explored are (i) ion-ion recombination, (ii) DR product loss due to neutral-neutral reactions, and (iii) neutral diffusive loss. These sources of error have been discussed for the N_2H^+ recombination by Molek et al.[41] For the CH_5^+ recombination, the iir product channels that would take away from the CH_3 DR product are channels (4.25) and (4.27). In the worst case situation that the observed Cl^+ and HCl^+ products are only coming from channels (4.25) and (4.27) and not the others (i.e. (4.23), (4.24), and (4.29)) then the CH_3 product would only increase

$\leq$2%, which does not explain the large difference with the SR. The next two loss processes are neutral-neutral reactive loss and diffusive loss of the radical neutrals. These losses are considered by a kinetic model of the flow tube chemistry. Note it is assumed in the model that the radical species will diffuse to the walls of the flow tube and then be lost at the walls by reactions with other available neutrals. Of all the possible neutral-neutral reactions that would deplete the DR products, only four have an effect on the distribution. These four reactions are listed below:

$$CH_3 + CH_3 \rightarrow C_2H_6 + H \quad k = 4.6 \times 10^{-11} cm^3 s^{-1(48)} \tag{4.32}$$

$$CH_3 + CH_2 \rightarrow C_2H_4 + H \quad k = 2.1 \times 10^{-10} cm^3 s^{-1(48)} \tag{4.33}$$

and

$$CH + H_2 \rightarrow CH_2 + H \quad k = 2.34 \times 10^{-12} cm^3 s^{-1(49)} \tag{4.34}$$

$$CH + CH_4 \rightarrow Products \quad k = 5.4 \times 10^{-11} cm^3 s^{-1(50)} \tag{4.35}$$

Starting with the Semaniak et al.[46] distribution, which is used to gauge how these losses ((ii) and (iii)) in the FA experiment are affecting the distribution. It can be seen in Table 4.8 that the effects of these losses are only a few percent. This is no where near enough to explain

Table 4.8: Results from modeled losses in the FA starting with the Semaniak et al.[46] product distribution. Listed are the products and the distribution from the model with considerations for diffusion of radicals (CH_3, CH_2, and CH) and neutral-neutral reactions (4.32–4.35). Then for comparison, the distribution obtained by Semaniak et al.[46]

	Model results using Semaniak et al.[46] data	
	Distribution (Semaniak)	Distribution (Model)
CH_4	4.9%	7.1%
CH_3	74.6%	73.3%
CH_2	17.2%	18.6%
CH	3.3%	0.95%

the reasons for discrepancy between the current FA measurements and the SR measurements. Every effort has been made to account for any losses in any of the product channels.

The values quoted for our distribution take into consideration the three possible losses (iir, neutral-neutral reactions, and neutral diffusive loss) in all channels and the errors associated with calculating the distribution.

4.3.5 Errors in the Product Distributions

To evaluate the error on the FA product distributions, detailed error analysis is done on each DR system. The majority of the error in the distribution is associated with the random error inherent in counting statistics, where the error (σ_S) is,

$$\sigma_S = \sqrt{A + B} \tag{4.36}$$

see reference[39] for details. In addition and with less significance, is the error associated with the fragmentation patterns and ionization cross sections. Again these are evaluated for each DR study. All of these errors were considered for both the N_2H^+ and CH_5^+ DR systems, thus giving the error or upper limit for the respective products, see Tables 4.6 and 4.7

The calculations for the product distribution from the measured counts are complex but relatively straightforward. For example, the DR of an ion, with the general formula H_nX^+, is given three possible DR products: H_2X, HX, and X.

$$H_3X^+ + e^- \rightarrow x_1H_2X + H \tag{4.37}$$

$$\rightarrow x_2HX + H_2(2H) \tag{4.38}$$

$$\rightarrow x_3X + H_2(2H) + H \tag{4.39}$$

Each of these product channels contribute some fraction (x_1, x_2, and x_3) to the total number of neutral DR products (N). Each of the neutral products, when ionized by 70 eV electrons, may non-dissociatively ionize or dissociatively ionize where the amount of each ion produced is dictated by the product of the total cross section (σ_{Tn}, n is denotes the number of H-atoms

in a neutral product) and absolute fraction (d_{mn}) for that ionization pathway, see below.

$$H_2X(x_1N) \xrightarrow{e^-} H_2X^+\,(\sigma_{T2}d_{22}) \tag{4.40}$$

$$\longrightarrow HX^+\,(\sigma_{T2}d_{21}) \tag{4.41}$$

$$\longrightarrow X^+\,(\sigma_{T2}d_{20}) \tag{4.42}$$

The notation for the absolute fraction is represented as, m being the number of H's in the neutral and n the number of H's in the ion produced by electron impact. For example, d_{21} is the fraction of HX^+ coming from H_2X product neutral. The rest of the DR products follow the same logic.

$$HX(x_2N) \xrightarrow{e^-} HX^+\,(\sigma_{T1}d_{11}) \tag{4.43}$$

$$\longrightarrow X^+\,(\sigma_{T1}d_{10}) \tag{4.44}$$

$$X(x_3N) \xrightarrow{e^-} X^+\,(\sigma_{T0}d_{00}) \tag{4.45}$$

Note that the total cross sections, σ_{Tn}, correct for the difference in ionization sensitivity for each of the DR products. To calculate the monitor ions that should be detected, the different contributors to each ion must be summed together. Starting with H_2X^+ (this is the largest mass so there is only one contributing term)

$$\left\{H_2X^+\right\}_{detected} = x_1N\sigma_{T2}d_{22} \tag{4.46}$$

where N is the total number of recombinations, such that x_1N is the fractional contribution of H_2X to the DR product distribution and $\{H_2X^+\}_{detected}$ represents the total number of H_2X^+ monitor ions detected. The signal from the smaller ions also have the additional contribution from the larger ions represented below, viz

$$\left\{HX^+\right\}_{detected} = x_2N\sigma_{T1}d_{11} + \overbrace{x_1N\sigma_{T2}d_{21}}^{\frac{d_{21}}{d_{22}}\left\{H_2X^+\right\}_{detected}} \tag{4.47}$$

$$\left\{X^+\right\}_{detected} = x_3 N\sigma_{T0}d_{00} + \overbrace{x_2 N\sigma_{T1}d_{10}}^{\frac{d_{10}}{d_{11}}\left(\left\{HX^+\right\}_{detected} - \frac{d_{21}}{d_{22}}\left\{H_2X^+\right\}_{detected}\right)} + \overbrace{x_1 N\sigma_{T2}d_{20}}^{\frac{d_{20}}{d_{22}}\left\{H_2X^+\right\}_{detected}} \tag{4.48}$$

The only unknown values in equations (4.46–4.48) are the fraction contributions of each product to the DR distribution (x_1, x_2, and x_3). The equations can be rearranged to solve for these values giving,

$$x_1 N = \frac{\left\{H_2X^+\right\}_{detected}}{\sigma_{T2}d_{22}} \tag{4.49}$$

$$x_2 N = \frac{\left(\left\{HX^+\right\}_{detected} - \frac{d_{21}}{d_{22}}\left\{H_2X^+\right\}_{detected}\right)}{\sigma_{T1}d_{11}} \tag{4.50}$$

$$x_3 N = \frac{\left(\left\{X^+\right\}_{detected} - \frac{d_{20}}{d_{22}}\left\{H_2X^+\right\}_{detected} - \frac{d_{10}}{d_{11}}\left(\left\{HX^+\right\}_{detected} - \frac{d_{21}}{d_{22}}\left\{H_2X^+\right\}_{detected}\right)\right)}{\sigma_{T0}d_{00}} \tag{4.51}$$

Note that N is an absolute number of recombinations which we do not know, but only relative values of the fractions are needed so this is of no consequence.

4.4 Conclusions

A new technique has been developed to quantitatively determine the products of DR. It has been shown that this technique is immensely valuable for this purpose. As it stands there are multiple discrepancies in the literature between the SR and previous spectroscopic measurements. This technique may bring a better understanding as to the reasons for the differences. As a case in point, for the N_2H^+ recombination the SR results are being re-measured and preliminary findings are showing the NH product is not as important as originally thought.[44] As for the CH_5^+ recombination, all possible sources of error have been evaluated for the new FA technique, yet the discrepancies have not been reconciled. It is interesting to note that

the CH_4 + H channel is supported by Bates' theory for this recombination.[51] It is critical to resolve the difference since DR of CH_5^+ forming CH_4 is likely to be a very important source of methane in the ISM.[45]

In the SR, the possibility of vibrational excitation in the recombining CH_5^+ ion has been suggest by Sheehan et al.[52] In a merged beam, the recombination rate constant was measure as a function of temperature (k = 2.9 x 10^{-7} cm^3s^{-1} with a temperature dependence of -0.46) and is very consistent with the SR results (k = 2.8 x 10^{-7} cm^3s^{-1} with a temperature dependence of -0.52).[46] Note that the room temperature value is a factor of 2.5 - 5.0 below the FA values.[53–56] In the Sheehan study, it was known that there was vibrational excitation in the ion and thus it was suggested, on the basis of agreement, that the SR results may have vibrational excitation in the ion. This is consistent with reports from the SR that the ion source used in the experiment produces vibrationally excited molecular ions[43] may be an indication that there might be some residual excitation in the recombining ions.

H_3O^+ DR, in which disagreement still exists is an important case which requires further study. Due to their relevance to the ISM and Titan's atmosphere other ions of particular interest are NH_4^+, $CH_3OH_2^+$, and $CH_3OCH_4^+$. In addition to these room temperature studies, there is the possibility of investigating the temperature dependence of the product distribution. Lastly, experimental conditions can easily be changed to enhance ion-ion recombination and enabling the study of products for this process. The products formed can give insight into the mechanism that is occurring, be it a long range charge transfer or an intimate encounter pathway. This will give the first experimental insight into the mechanism of this process, which has been long considered as a long range electron transfer.

4.5 References

[1] Herbst, E. In *Rate Coefficients in Astrochemistry*; Millar, T. J., Williams, D. A., Eds., Vol. 146; Kluwer: Dordrecht, 1988; pages 239–262.

[2] Cravens, T. E. In *Dissociative Recombination of Molecular Ions with Electrons*; Guberman, S. L., Ed.; Kluwer: New York, 2003; pages 385–400.

[3] Eberhardt, P.; Reber, M.; Krankowsky, D.; Hodges, R. R. *Astronomy & Astrophysics* **1995**, *302*(1), 301–316.

[4] Fox, J. L. In *Dissociative Recombination Theory, Experiment and Applications II*; Rowe, B. R., Mitchell, J. B. A., Canosa, A., Eds.; Plenum: New York, 1993; page 219.

[5] Goodings, J. M.; Karellas, N. S.; Hasanali, C. S. *Int. J. Mass Spectrom. Ion Proc.* **1989**, *89*, 205–226.

[6] Adams, N. G.; Babcock, L. M.; McLain, J. L. In *Encyclopedia of Mass Spectrometry: Theory and Ion Chemistry, Vol.1*; Armentrout, P., Ed., Vol. 1; Elsevier: Amsterdam, 2003; pages 542–555.

[7] Adams, N. G.; Poterya, V.; Babcock, L. M. *Mass Spectrom. Revs.* **2006**, *25*, 798–828.

[8] Florescu-Mitchell, A. I.; Mitchell, J. B. A. *Physics Reports-Review Section of Physics Letters* **2006**, *430*(5-6), 277–374.

[9] Rowe, B. R.; Queffelec, J. L. In *Dissociative Recombination: Theory, Experiment and Applications*; Mitchell, J. B. A., Guberman, S. L., Eds.; World Scientific: Singapore, 1989; pages 151–61.

[10] Herd, C. R.; Adams, N. G.; Smith, D. *Ap. J.* **1990**, *349*, 388–392.

[11] Adams, N. G.; Herd, C. R.; Geoghegan, M.; Smith, D.; Canosa, A.; Gomet, J. C.; Rowe, B. R.; Queffelec, J. L.; Morlais, M. *J. Chem. Phys.* **1991**, *94*, 4852–4857.

[12] Waite, J. H.; Nieman, H.; Yelle, R. V.; Kasprzak, W. T.; Cravens, T. E.; Luhmann, J. G.; McNutt, R. L.; Ip, W.-H.; Gell, D.; de la Haye, V.; Muller-Wordag, I.; Magee, B.; Borggren, N.; Ledvina, S.; Fletcher, G.; Walter, E.; Miller, R.; Scherer, S.; Thorpe, R.; Xu, J.; Block, B.; Arnett, K. *Science* **2005**, *308*, 982–986.

[13] Cravens, T. E.; Robertson, I. P.; Waite, J. H.; Yelle, R. V.; Kasprzak, W. T.; Keller, C. N.; Ledvina, S. A.; Nieman, H. B.; Luhmann, J. G.; McNutt, R. L.; Ip, W.-H.; de la Haye, V.; Mueller-Wodarg, I.; Wahlund, J.-E.; Anicich, V.; Vuitton, V. *Geophys. Res. Letts.* **2006**, *33*, L07105.

[14] Ehlerding, A.; Hellberg, F.; Thomas, R.; Kalhori, S.; Viggiano, A. A.; Arnold, S. T.; Larsson, M.; Ugglas, M. a. *Phys. Chem. Chem. Phys.* **2004**, *6*, 949–954.

[15] Geppert, W.; Thomas, R.; Semaniak, J.; Ehlerding, A.; Millar, T. J.; Osterdahl, F.; Ugglas, M. a.; Djuric, N.; Paal, A.; Larsson, M. *Ap. J.* **2004**, *609*, 459.

[16] Geppert, W.; Thomas, R.; Ehlerding, A.; Hellberg, F.; Osterdahl, F.; Ugglas, M. a.; Larsson, M. *Int J. Mass Spectrom.* **2004**, *237*, 25–32.

[17] Mitchell, J. B. A.; Rebrion-Rowe, C.; Le Garrec, J. L.; Angelova, G.; Bluhme, H.; Seiersen, K.; Andersen, L. H. *Int. J. Mass Spectrom.* **2003**, *227*, 273–279.

[18] Vallee, F.; Gomet, J. C.; Rowe, B. R.; Queffelec, J. L.; Morlais, M. In *Astrochemistry*; Varda, M. S., Tarafdar, S., Eds.; Kluwer: Dordrecht, 1987; pages 29–30.

[19] Rowe, B. R.; Vallee, F.; Queffelec, J. L.; Gomet, J. C.; Morlais, M. *J. Chem. Phys.* **1988**, *88*, 845–850.

[20] Vejby-Christensen, L.; Andersen, L. H.; Heber, O.; Kella, D.; Pedersen, H. B.; Schmidt, H. T.; Zajfman, D. *Ap. J.* **1997**, *483*, 531–540.

[21] Jensen, M. J.; Bilodeau, R. C.; Heber, O.; Pedersen, H. B.; Safvan, C. P.; Urbain, X.; Zaijman, D.; Andersen, L. H. *Phys Rev. A* **1999**, *60*, 2970–6.

[22] Rosen, S.; Derkatch, A. M.; Semaniak, J.; Neau, A.; Al-Khalili, A.; Le Padellec, A.; Vikor, W. S. L.; Thomas, R.; Danared, H.; af Ugglas, M.; Larsson, M. *Farad. Discuss.* **2000**, *115*, 295–302.

[23] Adams, N. G.; Herd, C. R.; Smith, D. *J. Chem. Phys.* **1989**, *91*, 963–973.

[24] Williams, T. L.; Adams, N. G.; Babcock, L. M.; Herd, C. R.; Geoghegan, M. *Mon. Not. Roy. Astr. Soc.* **1996**, *282*, 413–420.

[25] Andersen, L. H.; Heber, O.; Kella, D.; Pedersen, H. B.; Vejby-Christensen, L.; Zajfman, D. *Phys. Rev. Letts.* **1996**, *77*, 4891–4.

[26] Neau, A.; Khalili, A. A.; Rosen, S.; Le Padellec, A.; Derkatch, A. M.; Vikor, W. S. L.; Semaniak, J.; Thomas, R.; Nagard, M. B.; Anderson, K.; Danared, H.; af Ugglas, M. *J. Chem. Phys.* **2000**, *113*, 1762–1770.

[27] Jensen, M. J.; Bilodeau, R. C.; Safvan, C. P.; Seiersen, K.; Andersen, L. H.; Pedersen, H. B.; Heber, O. *Ap. J.* **2000**, *543*, 764–774.

[28] Alge, E.; Adams, N. G.; Smith, D. *J.Phys.B.* **1983**, *16*, 1433–1444.

[29] Smith, D.; Adams, N. G. In *Physics of Ion-Ion and Ion-Electron Collisions*; Brouillard, F., McGowan, J. W., Eds.; Plenum Press: New York, 1983; pages 501–31.

[30] Anicich, V. *An Index of the Literature for Bimolecular Gas Phase Cation-Molecule Reaction Kinetics: JPL Publication 03-19;* Jet Propulsion Laboratory: Pasadena, 2003.

[31] Ikezoe, Y.; Matsuoka, S.; Takebe, M.; Viggiano, A. A. *Gas Phase Ion-Molecule Reaction Rate Constants through 1986;* Ion Reaction Research Group of the Mass Spectroscopy Society of Japan: Tokyo, 1987.

[32] Smith, D.; Dean, A. G.; Adams, N. G. *J.Phys.D.* **1974**, *7*, 1944–62.

[33] Mostefaoui, T.; Adams, N. G.; Babcock, L. M. *Rev. Sci. Instrum.* **2002**, *73*, 2044–50.

[34] Plasil, R.; Glosik, J.; Poterya, V.; Kudrna, P.; Vicher, M.; Pysanenko, A. In *Dissociative Recombination of Molecular Ions with Electrons*; Guberman, S. L., Ed.; Kluwer: New York, 2003; pages 249–63.

[35] Linstrom, P. J., Mallard, W. G., Eds. *NIST Chemistry WebBook*, NIST Standard Database 69; National Institute of Standards and Technology: Gaithersburg MD, 20899, June 2005.

[36] Baiocchi, F. A.; Wetzel, R. C.; Freund, R. S. *Phys. Rev. Lett.* **1984**, *53*(8), 771–774.

[37] Tarnovsky, V.; Deutsch, H.; Becker, K. *Int. J. Mass Spec.* **1997**, *167*, 69–78.

[38] Tarnovsky, V.; Levin, A.; Deutsch, H.; Becker, K. *J. of Phys. B-At. Mol. Opt. Phys.* **1996**, *29*, 139–152.

[39] Jenkins, R.; Gould, R. W.; Gedcke, D. *Quantitative X-ray Spectrometry*, Vol. 20; Marcel Dekker, Inc., 2nd ed., 1995.

[40] Beers, Y. *Introduction to the Theory of Error;* Addison-Wesley, 1953.

[41] Molek, C. D.; McLain, J. L.; Poterya, V.; Adams, N. G. *J. Phys. Chem. A* **2007**, *111*, 6760–6765.

[42] Adams, N. G.; Babcock, L. M.; Molek, C. D. In *Encyclopedia of Mass Spectrometry: Theory and Ion Chemistry, Vol.1*; Armentrout, P., Ed., Vol. 1; Elsevier: Amsterdam, 2003; pages 555–561.

[43] Kallberg, A. In *Manne Siegbahn Laboratory Annual Report 1999*; Kallberg, A., Oppenheimer, E., Eds.; Manne Siegbahn Laboratory, 2000; pages 1–115.

[44] Larsson, M. Department of Physics, Stockholm University, Sweden, private communication, 2007.

[45] Herbst, E. *Journal of Physics: Conference Series* **2005**, *4*, 17–25.

[46] Semaniak, J.; Larson, A.; Le Padellec, A.; Stromholm, C.; Larsson, M.; Rosen, S.; Peverall, R.; Danared, H.; Djuric, N.; Dunn, G. H.; Datz, S. *Ap. J.* **1998**, *498*, 886–895.

[47] Geppert, W. D.; Thomas, R. D.; Ehlerding, A.; Hellberg, F.; Osterdahl, F.; Hamberg, M.; Semaniak, J.; Zhaunerchyk, V.; Kaminska, M.; Kallberg, A.; Paal, A.; Larsson, M. In *Dissociative Recombination: Theory, Experiments and Applications*; Wolf, W., Lammich, L., Schmelcher, P., Eds., Vol. 4; Inst. Phys. J. Phys. Conf. Ser. 4: London, 2005; pages 26–31.

[48] Wang, B.; Fockenberg, C. *J. Phys. Chem. A* **2001**, *105*, 8449–8455.

[49] Becker, K. H.; Kurtenback, R.; Wiesen, P. *J. Phys. Chem.* **1991**, *95*, 2390–2394.

[50] Anderson, S. M.; Freeman, A.; Kolb, C. E. *J. Phys. Chem.* **1987**, *91*, 6272–6277.

[51] Bates, D. R. *Adv. Atom. Molec. Opt. Phys.* **1994**, *34*, 427–486.

[52] Sheehan, C. H.; St.-Maurice, J.-P. *Adv. Sp. Res.* **2004**, *33*, 216–220.

[53] Lehfaoui, L.; Rebrion-Rowe, C.; Laube, S.; Mitchell, B. A.; Rowe, B. R. *J. Chem. Phys.* **1997**, *106*(13), 5406–5412.

[54] Gougousi, T.; Golde, M. F.; Johnsen, R. *Chem. Phys. Lett.* **1997**, *265*, 399–403.

[55] Adams, N. G.; Smith, D.; Alge, E. *J. Chem. Phys.* **1984**, *81*, 1778–1784.

[56] Smith, D.; Spanel, P. *Int J. Mass Spectrom. Ion Proc.* **1993**, *129*, 163–182.

Chapter 5

A Remeasurement of the Products for Electron Recombination of N_2H^+ using a New Technique: No Significant NH + N Production[1]

[1]Molek, C. D.; McLain, J. L.; Poterya, V. and Adams, N. G. *J. Phys. Chem. A* **2007**, *111*, 6760–6765. Reprinted here with permission of publisher.

5.1 Introduction

Dissociative electron-ion recombination (DR) is very important, since it is a dominant loss process in many plasma media, e.g. interstellar gas clouds,[1] cometary coma,[2,3] planetary atmospheres,[2,4] combustion flames,[5] and others. In particular, the recombination of N_2H^+ is important,

$$N_2H^+ \longrightarrow N_2 + H + 8.47eV \tag{5.1}$$

$$\longrightarrow NH + N + 2.25eV \tag{5.2}$$

since N_2H^+ has been detected in multiple places in the ISM, (e.g. dark clouds that are precursor sites to high mass star formation[6] and in areas of pre-protostellar collapse[7]) and rotational emission lines from both N_2H^+, (1-0) and (3-2), and N_2D^+, (2-1) and (3-2), have been used to search for massive pre-stellar cores.[8] DR of N_2H^+ is perhaps the most studied of all recombinations[9–17] in both the flowing afterglow (FA) and the storage ring (SR) and has been reviewed recently.[18,19] Studies have been made to determine the rate coefficient, α_e, of this DR as a function of temperature and quantitatively determine the products (both ground and excited state). The former FA study determined that α_e was essentially independent of temperature.[17] In the latter, FA experiments involving optical emission from this DR have yielded electronically excited N_2 as a product by identification of various vibrational bands of the $N_2(B^3\Pi_g) \rightarrow N_2(A^3\Sigma_u^+)$ transition.[13] Emissions from excited state NH were also searched for. Vibrational bands, (0,0) and (1,1), of the spin forbidden $NH(a^1\Delta) \rightarrow NH(X^3\Sigma^-)$ transition are in the experimental accessible wavelength range and have appreciable Franck-Condon factors, yet these were not observed.[13] Other earlier FA studies using vuv absorption of L_α to detect H-atoms, implied that the product channel to N_2 + H was very dominant.[9] However, recent studies in a SR by Geppert et al. gave product channels of 36% (N_2 + H) and 64% (NH + H); these include both ground and excited states.[16] This is a surprising result given that breaking the N≡N triple bond is the dominant pathway.[9,13,20] Additional spectroscopic data were published the same year as the SR results and determined the total

emission intensity from the excited state product $N_2(B, \nu' \geq 1)$, which was translated to a quantitative product yield of 18% ± 9% for N_2 from this DR. However, this does not resolve the conflict between the earlier measurements.[15] The use of an independent technique to directly measure the products of this recombination is desperately needed to resolve the discrepancy; such a technique is presented here.

5.2 Experimental

A brief overview of this new technique is presented here; a detailed explanation will be given elsewhere.[21] The technique involves two basic experimental approaches, both of which utilize a flowing afterglow (FA) plasma. These differ in the means of determining the products, with the method of production of the recombining ions being common. The plasma source is a microwave discharge He plasma operating at 1.4 Torr (4.0 Torr for the second method), thus creating a He_2^+/e^- dominant plasma, see Figure 5.1.

The He is of 99.997% purity and is further purified with two liquid nitrogen cooled sieve traps. Downstream from the cavity, about 2mTorr of Ar (99.999% purity) is added to the flow, which destroys He^m and increases the ionization number density (i.e. electron density, [e], increases). Further downstream from the introduction of Ar, sufficient H_2 (99.999% purity further purified by a liquid nitrogen cooled sieve trap) is added to rapidly generate a H_3^+/e^- dominate plasma and this readily proton transfers to N_2 (99.999% purity) added just downstream of H_2 forming the recombining ion of interest, N_2H^+. A summary of the chemical reactions leading to N_2H^+ production are presented below:

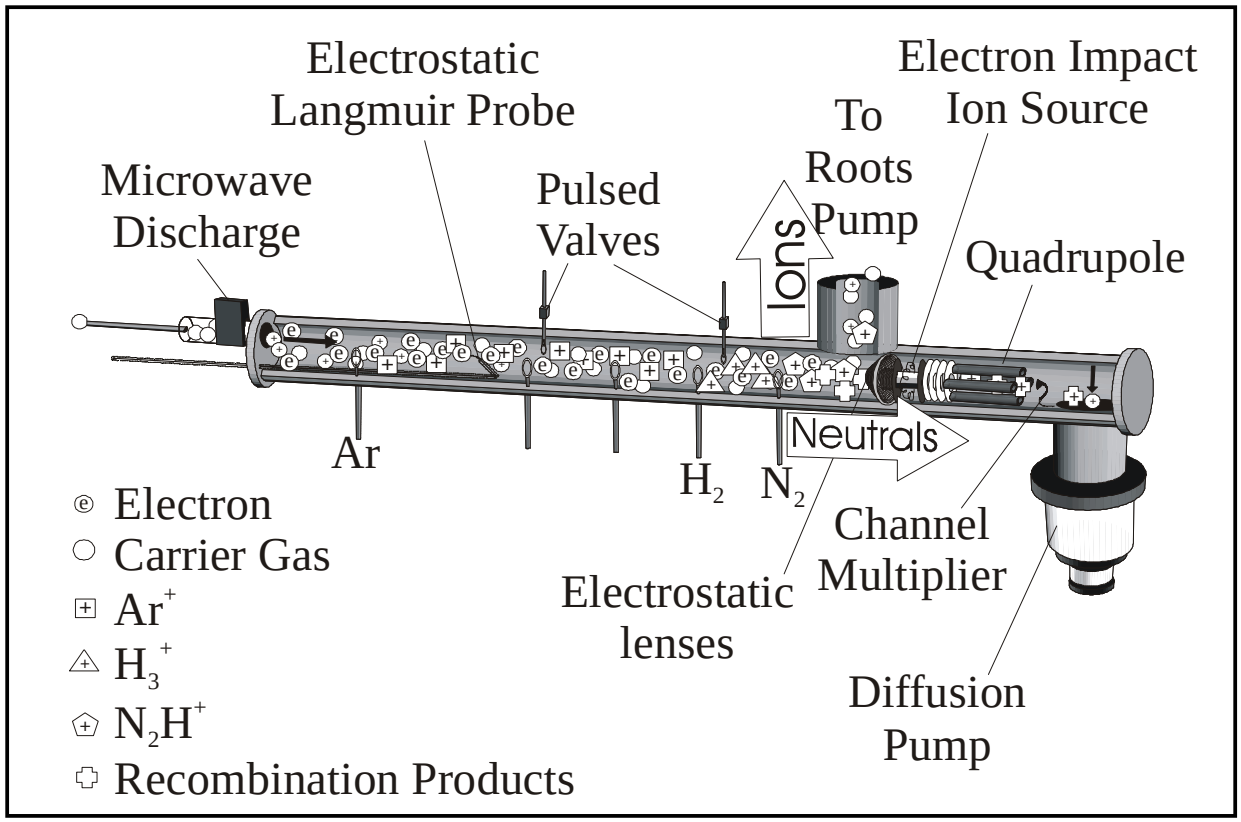

Figure 5.1: Diagram of FA modified to quantitatively determine the products of DR. This shows the various reagent gas inlet ports, pulsed valves (attaching gas or reagent gas added), electrostatic lenses that block ions from entering the detection system, electron impact ion source, and the quadrupole mass filter.

$$He^+ + He + He \longrightarrow He_2^+ + He \qquad k = 2.0 \times 10^{-31} cm^6 s^{-1}\ ^{(22)} \qquad (5.3)$$

$$He_2^+ + Ar \longrightarrow Ar^+ + 2He \qquad k = 2.0 \times 10^{-10} cm^3 s^{-1}\ ^{(23)} \qquad (5.4)$$

$$Ar^+ + H_2 \longrightarrow ArH^+ + H \qquad k = 8.6 \times 10^{-10} cm^3 s^{-1}\ ^{(23)} \qquad (5.5)$$

$$ArH^+ + H_2 \longrightarrow H_3^+ + H \qquad k = 6.3 \times 10^{-10} cm^3 s^{-1}\ ^{(23)} \qquad (5.6)$$

$$H_3^+ + N_2 \longrightarrow N_2H^+ + H_2 \qquad k = 1.6 \times 10^{-9} cm^3 s^{-1}\ ^{(23)} \qquad (5.7)$$

It should be noted that a small amount of He^+ still exists at the point of N_2 addition, 9% of the H_3^+, which reacts readily with N_2 to form $N^+(60\%)$ and $N_2^+(40\%)$,[24] in which N^+ does not recombine with electrons and reacts slowly with H_2 (1.5 x 10^{-10} cm^3s^{-1}); this N^+ obviously will not effect the measurements. The N_2^+ that is formed reacts rapidly with H_2 to yield N_2H^+. Also, note that the reagent gases flow rates are measure by a capillary system, thus accurate number densities of each gas can be introduced in the FA. In the case of the very small N_2 additions, a 0.2% mix of N_2 in He was used. Note that in these studies, very pure gases were used to minimize N_2 impurities. In any case, impurities in the flow tube would not be pulsed and would not be detected as recombination products. The N_2H^+ thus produced, then recombines forming neutral products, which are either thermalized via collisions with the He carrier gas or by radiative relaxation. The ions and neutrals in the flow tube can be detected by a downstream quadrupole mass filter/ion detection system, which can separately monitor either ions or neutrals from the plasma as dictated by the operating mode of the experiment. Plasma ions are detected in the conventional way. Neutrals that exist in the plasma can be monitored by ionizing them with an electron impact (EI) ionization source just upstream of the quadrupole mass filter (see Figure 5.1). In this case, application of appropriate potentials to the electrostatic lenses just upstream of the EI ionization source prevents plasma ions and electrons from entering the detection system, eliminating interference from plasma ions while monitoring neutrals. These neutrals have multiple sources being a combination of

un-reacted reagent gases, products of upstream ion-molecule reactions, and products of e-i recombination. The central part of the technique is to distinguish the recombination products from these other sources and this has been done in two ways.

5.2.1 Electron Attaching Gas Method

In this approach, a rapidly electron attaching gas (e.g., CCl_4)

$$e + CCl_4 \longrightarrow Cl^- + CCl_3 \tag{5.8}$$

is pulsed into the flow tube. When the attaching gas is present, the electrons are scavenged generating anions (Cl^-) and e-i recombination is quenched. Thus, the difference between ion counts from ionized neutrals with the pulsed gas being out (A) versus in (B) is a positive signal (S = A - B) from the products of DR. The use of an electron attaching gas to identify signal originating from DR has been very successfully used previously to identify spectroscopic emissions from excited state products of DR.[25] In the present use of this technique, the concentration of attaching gas and flow conditions are optimized so that quenching of DR is maximized with the effect of ion-ion recombination between N_2H^+ and the anion (Cl^-) being minimized. This is achieved by monitoring the modulated electron density with a Langmuir probe at the point of introduction of the attaching gas. For an optimum situation, 80-90% of the electron density is destroyed, which ensures that the signal from DR products is large enough to give a good statistical representation of the product distribution in a reasonable time (< 250 seconds). Since typical room temperature reaction rate coefficients, α_i, for ion-ion recombination, iir, are an order of magnitude (or more)[26] smaller than the room temperature DR rate coefficient for N_2H^+, the effects of ion-ion recombination can be kept to $\leq$ 8-9% relative to the DR products. Even so, there is a potential for some overlap between products of ion-ion recombination and products of DR. Note that the products of iir would appear as a negative signal (i.e., S negative), since for this A will be smaller than B. No such negative signal has been observed in any of our

experiments and this is unlikely to be a significant source of error. Even so, to eliminate this possibility, the second experimental approach was applied.

5.2.2 Pulsed Reagent Gas (RG) Method

In this experimental technique, the RG (N_2), a N_2 mix (0.2% N_2 in He) was pulsed into the flow, generating a N_2H^+/e^- plasma. Note, the reaction sequence is the same as the previous method. The difference between N_2 out (A) versus in (B) creates a signal (S = A - B) that is a fraction of unreacted N_2 (f_1) plus a fraction of products of DR (f_2). If only N_2H^+ exists, there is no residual N_2, then all of the signal would be from DR products. At a higher N_2 concentration, there will be some fraction (f_1) of signal from unreacted N_2 with the remaining fraction (f_2) of signal being due to products from DR of N_2H^+. To identify the contribution of each fraction and to maximize f_2 and minimize f_1, the initial concentration of N_2, $[N_2]_0$, was varied around the magnitude of [e] (3.0 x 10^{10} molec/cm^3) at the position where N_2 is injected whilst monitoring energetically allowed products of the DR. This should yield a transition from the electron impact (EI) pattern of N_2 which occurs at high concentrations of N_2 ($[N_2]_0 >> [e]$ and $f_1 >> f_2$) to some fractional mixture of the EI pattern of unreacted N_2 and products of DR ($[N_2]0 < [e]$ and f_2 is optimized so its contribution can be observed as a deviation from the EI pattern. To model the fractional contributions of f_1 and f_2 over the concentration range of N_2, a model of the reactive system was constructed, which calculated the absolute percent monitor ion signals versus $[N_2]_0$ (the values of $[N_2]_0$ used in the model encompass the experimental range of concentrations). A series of possible product distributions were used and the model results compared to the experimental data to determine the agreement. The product distribution in the model was then varied to maximize the agreement.

5.3 Results

5.3.1 Electron Attaching Gas Method

In the electron impact ionization and quadrupole mass analysis, N_2^+, NH^+ and N^+ serve as monitors of the N_2, NH, and N DR products respectively. The signals of these ions were integrated over time to build up statistically significant signals, whether it be from direct ionization of the DR products or from dissociative EI ionization of a larger molecule (i.e. N_2 fragments to 14% N^+ signal). For this study, a very significant N_2^+ signal was observed, with no NH^+ signal, but with some N^+ signal (not shown), see Figure 5.2.

Figure 5.2 shows the integrated signal of monitor ion N_2^+ building up over time from EI ionization of recombination product N_2, while the signal from NH^+ remains at zero. Not shown in Figure 5.2 is the N^+ signal; this signal is attributed only to the dissociative ionization of N_2 that occurs with 70 eV electrons in the EI source and thus mirrors the N_2^+ signal. Signals from the EI dissociative ionization process and parent ionization process give information on the fragmentation pattern (cracking pattern) of the N_2 molecule. Detailed knowledge of such fragmentation is essential so that the observed ion signal can be corrected for the effect of fragmentation, yielding the true DR product distribution. Fortunately, this information is readily available for many stable molecules like N_2 in the NIST database.[27] However, data for unstable molecules such as radicals is generally not available. Fragmentation patterns of some radical species can be obtained if the relative ionization cross sections of fragment ions to parent ions are available in the literature.[28] This information is available for the NH radical,[29] giving the fragmentation pattern as 78% NH^+ and 22% N^+. Thus, if NH is a product from the DR of N_2H^+, NH^+ signal should be observed. The fact that it is not seen is in stark contrast to SR results where NH is reported as the major product channel (64%).[16] To ensure that our experimental data was properly interpreted, a model of the chemistry in the flow tube was also constructed. This replicates the experimental conditions

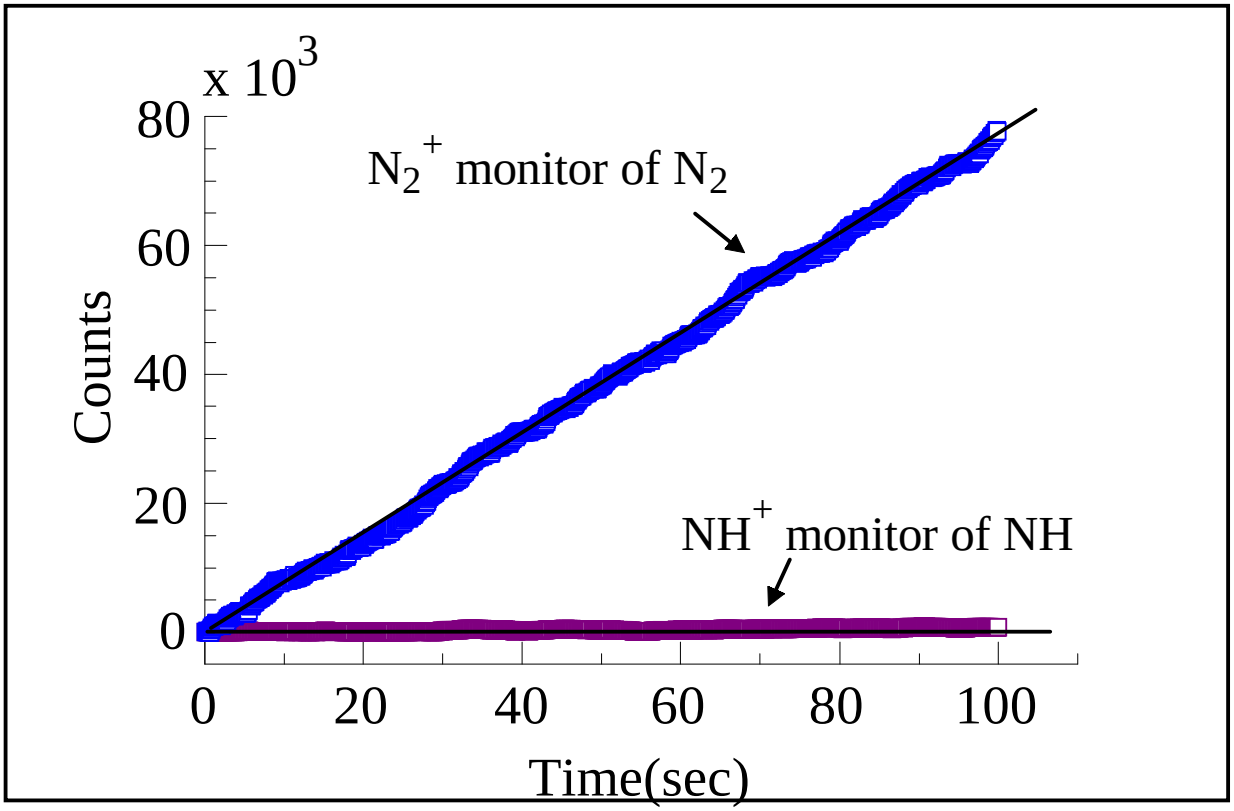

Figure 5.2: Integrated signals of the ion monitors N_2^+ and NH^+ for the possible products, N_2 and NH, from DR of N_2H^+. Signals were obtained from the difference between the two channels, A and B. The difference was created by pulsing in a rapidly electron attaching gas(CCl_4), which quenches DR recombination.

described in the experimental section for the electron attaching gas method and is shown in Figure 5.3.

In Figure 5.3, the results from Geppert et al.[16] are used to show the expected formation of products of DR. It is clearly seen that the NH^+ monitor dominates over the N_2^+ monitor by 1.52 times, and that if NH is a 64% channel then it would have readily been detected.

5.3.2 Pulsed Reagent Gas (RG) Method

To confirm the absence of an NH channel and corroborate the results of the electron attaching gas method, this additional experiment technique was used. Note that in this technique, there are two extreme situations with a crossover between them. In the limit $[N_2]_0 >> [e]$, the ion signals observed should be the EI fragmentation pattern of N_2. In the opposite limit, $[N_2]_0 < [e]$, the ion signals should be a mix of the EI ionized products of DR and some N_2 fragmentation pattern. The N_2 fragmentation pattern contributes because as less N_2 is introduced into the FA this increases the reaction time for the proton transfer between H_3^+ and N_2. Thus, the time for this reaction to go to completion becomes longer than the resonance time in the flow tube and this leaves some unreacted reagent gas that gets sampled. The cross over between these limits occurs when $[N_2]_0$ is somewhere close to [e], 3.0 x 10^{10} molecules/cm^3, in the flow tube at the point of introduction of the N_2 reagent gas. The model for this, using the results of Geppert et al. is given together with our experimental results, see Figure 5.4a.

The dashed lines represent the modeled results and the solid lines with the symbols are the experimental results and the dashed vertical line, 3.0 x 10^{10} molecules/cm^3, is the electron number density in the FA at the N_2 introduction point, measured with a movable Langmuir probe. Note that, the experimental data at the lowest concentration has a much larger amount of error (~14%) than any of the other points. This is because as $[N_2]_0$ is reduced, so is the detected signal, which makes it difficult to obtain data that has error <10% in the final product distribution within any reasonable amount of time when $[N_2]_0$

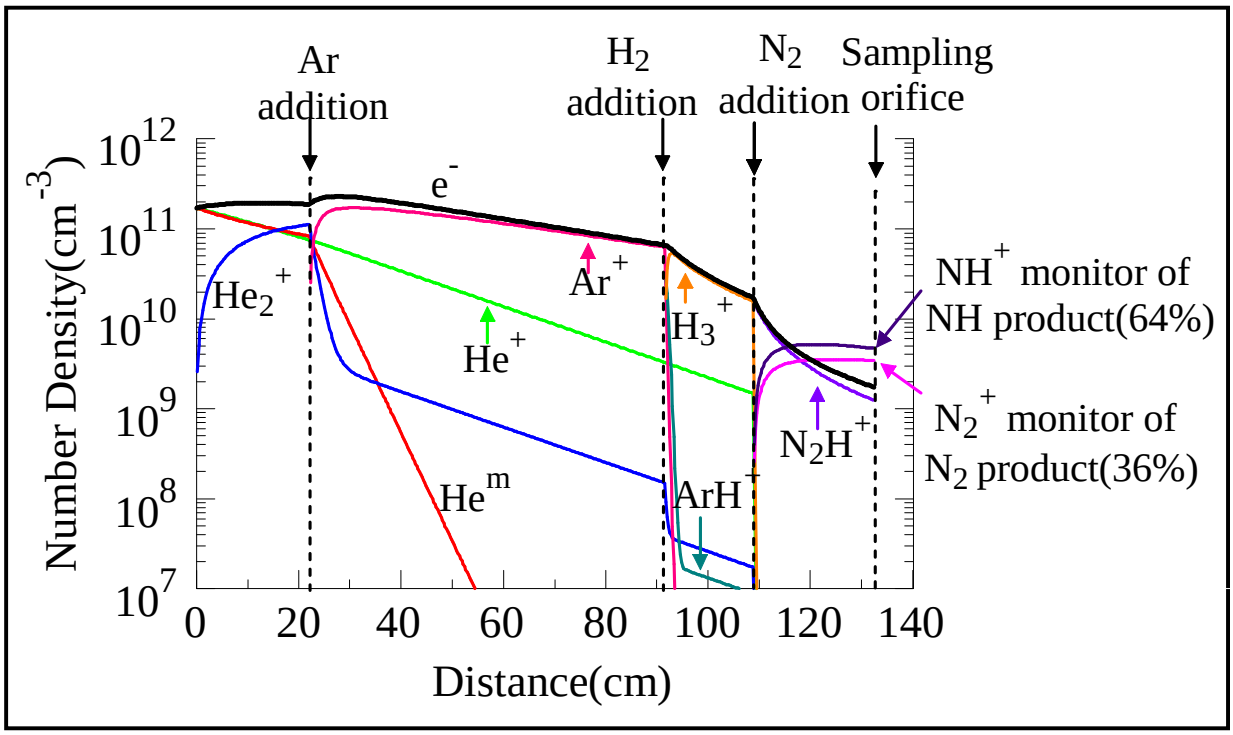

Figure 5.3: Kinetic model of the plasma dynamics as a function of distance down the flow tube from the microwave discharge source, represented as at 0 cm. There are three gas additions points for argon, hydrogen, and nitrogen to generate the ion of interest, N_2H^+. The product channel percentages used in this model are taken from Geppert el al.[16] Therefore, the appearance of the N_2^+ and NH^+ ions, which are monitor ions for the N_2 and NH products of DR, can be seen as N_2H^+ recombines with electrons. If this product distribution were valid, then the NH^+ monitor ion would be very evident.

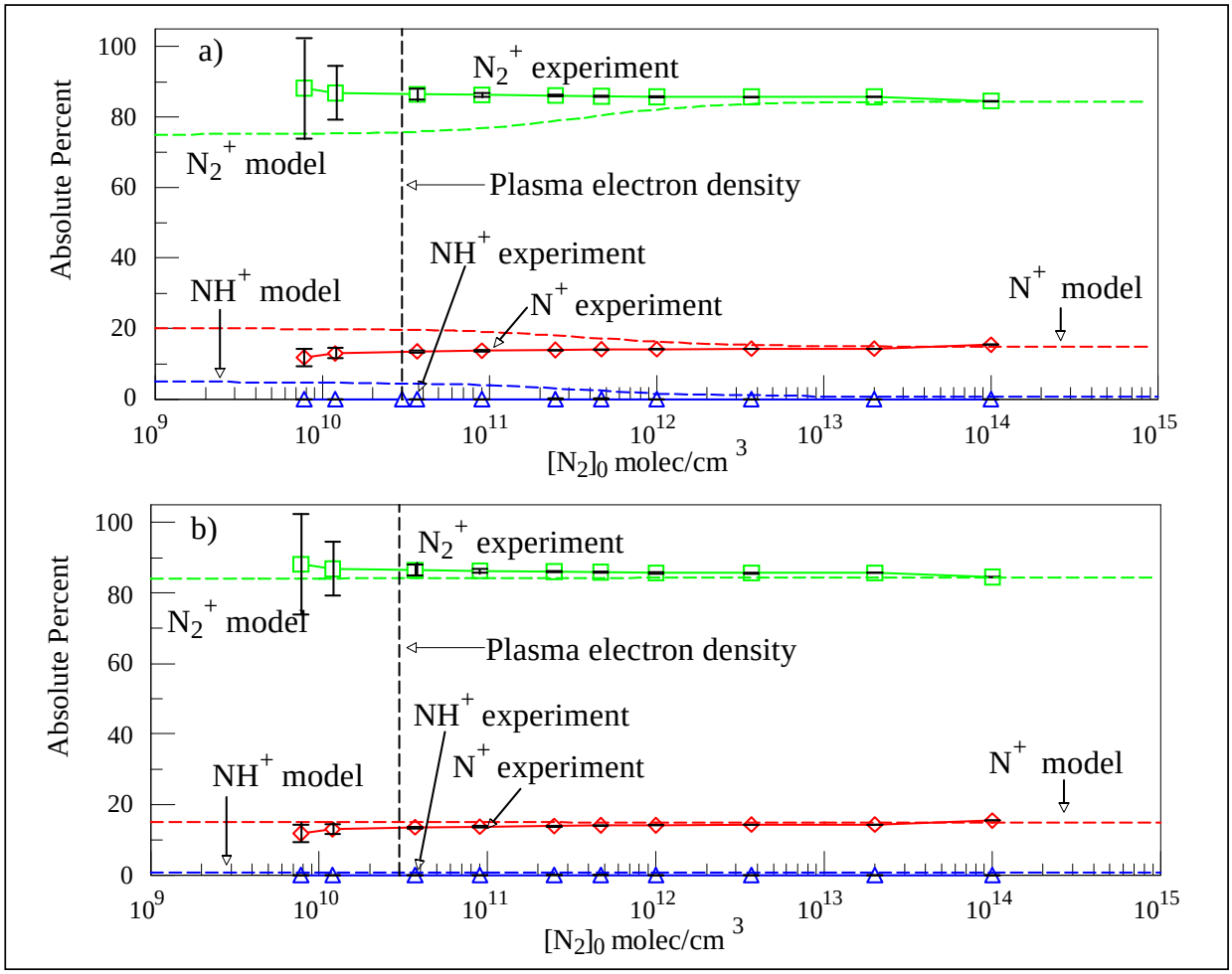

Figure 5.4: Absolute ion percentages of the monitor ions, model and experiment, as a function of initial N_2 concentration. The solid lines with open symbols represent the same experimental data in both (a) and (b). The dashed lines represent the kinetic model results using two different values for the absolute DR product percentages, (a) using N_2(36%) and NH(64%) and (b) using N_2(98%) and NH(2%). The model from (b) agrees with the experimental data far better than the model from (a).

below 8.0 x 10^9 molecules/cm^3. The ability to detect $[N_2]_0$ at lower concentrations is possible by the pulsing technique, where any impurities in the FA are constant, thus subtracted by S = A - B. The detection limit is the ratio of signal to background, in this case 10^{-3}.[21] Concerning the other data points, the error decreases dramatically (<1%) at highest $[N_2]_0$ concentrations such that error bars are less than the symbol size. The experimental data in 5.4a is the same as 5.4b, but the model shown uses a 98% N_2 + H product and a 2% NH + N product.

5.4 Discussion

5.4.1 Electron Attaching Gas Method

The experimental results from the electron attaching gas method show a large build up of the N_2^+ signal. This signal is due to the DR product N_2 and cannot be from the unreacted N_2 neutrals in the flow tube since these are not modulated. This was confirmed by experiments[21] with the DR of CO^+ and HCO^+. From previous work, the major HCO^+ DR product channel is known to be CO + H,[13,30] but for CO^+ the only possible channel is the dissociation to C + O.[31–33] With these results in mind, there should not be a CO^+ signal, the monitor ion for CO, in the CO^+ DR but it should be very substantial in the HCO^+ DR. This is exactly what is seen in the data presented in Figure 5.5.

In the case of DR for HCO^+, the build up of CO^+ monitor ion is not due to unreacted CO in the flow tube, since there is no such build-up of the CO^+ monitor in the DR of CO^+. Thus, all this build up is due to the product CO in the DR of HCO^+. This confirms that any signal from the unreacted reagent gas is completely subtracted out. This is also be true for the N_2H^+ recombination, and the signal thus originates from the N_2 product of the DR. From the lack of any NH^+ there cannot be any NH in the DR. However, it must be established that there are no loss processes for NH or reverse mass discrimination, which would prevent its observation. First, there are several reactive possible loss processes of NH

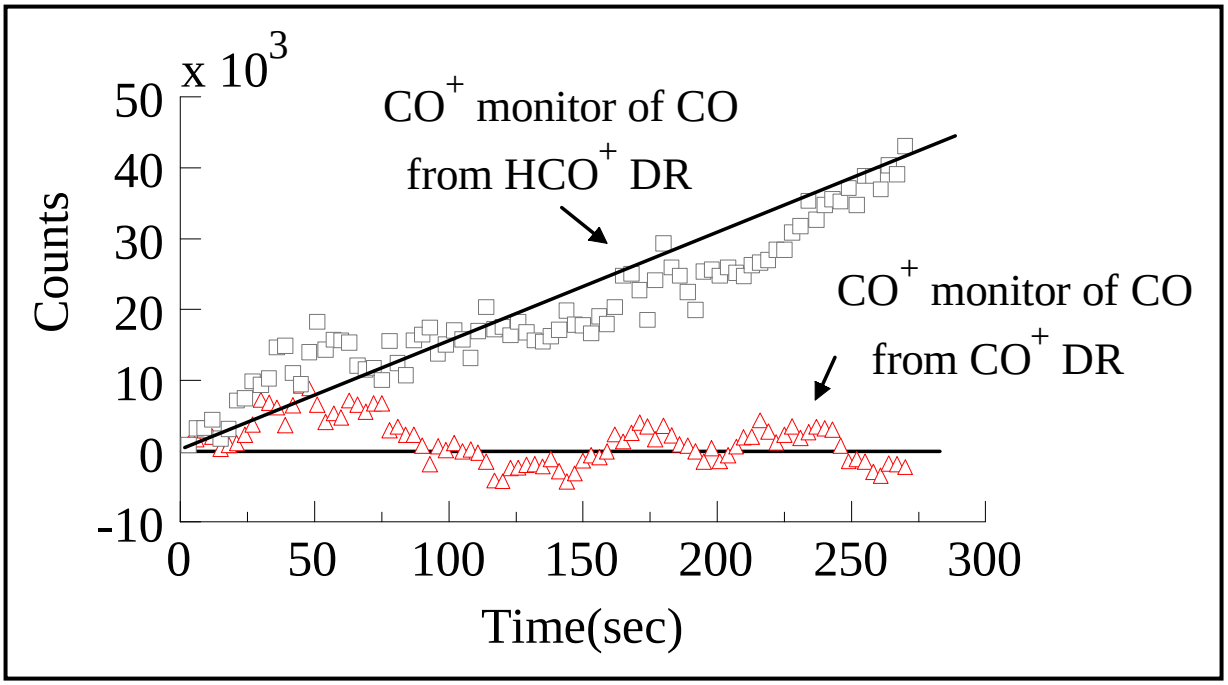

Figure 5.5: Integrated signal of monitor CO^+ for CO originating from the DR of HCO^+ and DR of CO^+. The squares are the CO^+ monitor for DR of HCO^+, which previous experimental FA and SR results have shown CO as a major product. The triangles are the CO^+ monitor for DR of CO^+, which cannot yield CO as a product since the recombination is dissociative. It is clear that there is signal build up in the DR of HCO^+ and not in the DR of CO^+, which indicates that no background CO reagent gas is being counted as signal for the products of recombination. This is showing that the technique is performing exactly as expected.

by radical-radical reactions:

$$NH + NH \longrightarrow N_2 + H_2 \qquad 1.6 \times 10^{-9} cm^3 s^{-1} \ ^{(34)} \tag{5.9}$$

$$NH + H \longrightarrow N + H_2 \qquad 7.6 \times 10^{-11} cm^3 s^{-1} \ ^{(35)} \ ^{theoretical\ value\ at\ 400\ K} \tag{5.10}$$

$$NH + N \longrightarrow N_2 + H \qquad 2.5 \times 10^{-11} cm^3 s^{-1} \ ^{(36)} \tag{5.11}$$

Also diffusive loss of NH (reactive loss on the walls of the flow tube) is a possibility, this is treated as 100% loss in the model described below. In addition to these losses, products from ion-ion recombination need to be considered because signal from this process in one of the possible products will reduce the observed signal attributed to that product in DR. All of these situations except for the loss of NH on the walls and effects from ion-ion recombination (iir) have been consider in the model shown in Figure 5.3 and yet the model, with 64% NH + N channel assumed, shows a dominance of NH product, not seen in our experiment. In the model, the predicted loss of NH is less than 1/3, but NH is still 1.4 times larger than N_2 so there would be no problem detecting NH if it were present. The affects of iir need special attention. The reaction sequence below is considered:

$$N_2H^+ + Cl^- \longrightarrow N_2H + Cl + 5.30eV \tag{5.12}$$

$$\longrightarrow N_2 + H + Cl + 4.86eV \tag{5.13}$$

$$\longrightarrow N_2 + HCl + 9.34eV \tag{5.14}$$

$$\longrightarrow NH + NCl + 2.05eV \tag{5.15}$$

$$\longrightarrow NH + N + Cl - 1.41eV \tag{5.16}$$

The production of channel 5.15 or 5.16 would take away from the NH product in the e-i process; channel 5.16 is endothermic and is not considered further. This leaves channel 5.15 as the only channel which could take signal away from the DR NH product channel, but for channel 5.15 to occur there must be an intimate interaction between N_2H^+ and Cl^-, specifically a bond between the Cl and one of the nitrogen atoms must form for this channel to be exothermic. This is contrary to the mechanism usually assumed for iir, which is electron

transfer at long range when there is a curve crossing.[37] In addition, the point at which the neutral product curve, NH + NCl, crosses the ion-ion attractive Coulombic potential is around 5.2Å, which is well away from the equilibrium bond length of NCl(1.61Å) and seems unlikely that this channel will occur, see Figure 5.6 below:

This will bring the relative percent of 5.15 to DR below the previously mentioned 8-9% (iir percentage relative to DR). In addition, there was no signal from possible neutral products Cl, HCl, or NCl coming from iir and, since the neutrals HCl and NCl have zero background, they would easily have been detected.

The last effect that needs to be addressed is the possibility of mass discrimination against NH; this can be taken into account by comparing at the relative amount of N_2^+ signal to that of N^+ and comparing the results to the NIST electron impact fragmentation pattern. Then since there is little difference in mass discrimination of masses differing by only 1 amu (N^+ and NH^+), the effects of mass discrimination on NH product can easily be taken into account. For this experiment, there was not any mass discrimination against N^+. After evaluating the experimental data in this method and modeling the experimental conditions, it is concluded that there is not a significant NH depletion due to any of the possible loss processes for NH discussed above. Thus, there is no experimental evidence for NH production with the DR channel to N_2 + H being 95-100% and the NH + N channel 0-5%. To further access the influence of iir and also validate the DR channel magnitudes, the second experimental approach will be discussed.

5.4.2 Pulsed Reagent Gas (RG) Method

Since iir does not occur it will not affect the chemistry in this experimental approach; the signal is due to either excess neutral N_2 from unreacted reagent gas or products of DR of N_2H^+. To ascertain the amount of signal originating from DR, a model was employed in which the magnitudes of the products from DR were varied until the model output matched the experimental data. Note, all of the NH loss processes considered in the model for electron

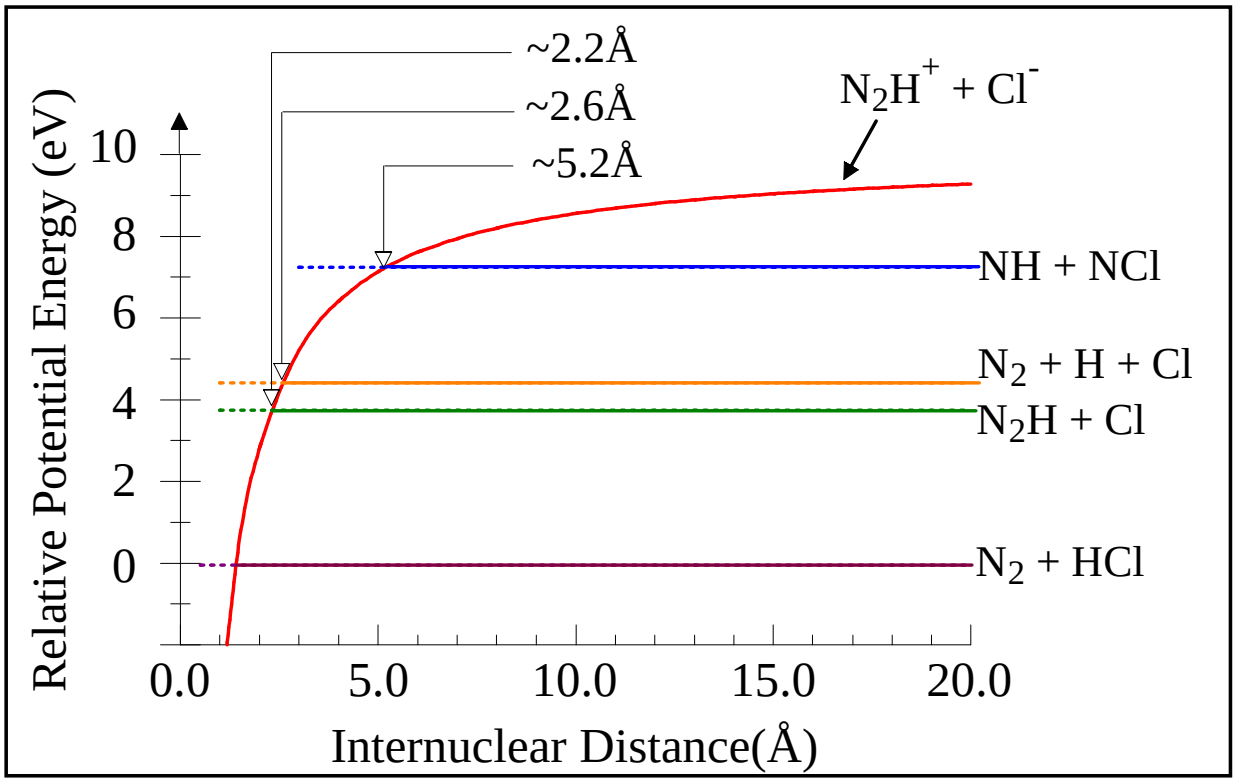

Figure 5.6: Ion-ion attractive Coulombic potential, $N_2H^+ + Cl^-$ crosses the neutral product curve, $N_2 + H + Cl$ near 2.6Å. The NH + NCl product curve crosses near 5.2Å. This is well away from the equilibrium bond length of NCl(1.61Å) and seems unlikely that this channel will occur.

attaching gas technique were included. In addition, contributions of ^{15}N to the ^{14}NH channel are incorporated. Two possible variants shown in Figure 5.4. In (a), the values obtained by Geppert et al. are used. Here, the model predicts a clear change over from high $[N_2]_0$ 1 x 10^{15} molecules/cm^3 to low $[N_2]_0$ 1 x 10^9 molecules/cm^3, as the N_2^+ ion signal decreases and the NH^+ signal increases. Note that these results for the model disagree with the experimental results. It is also noticed that the absolute percentage for N_2^+ at low initial $[N_2]_0$ concentration never reaches the 36% that is given by Geppert et al. This is due to two factors, the first is caused by remaining N_2 still contributing to the signal and thus bringing the percent of N_2^+ signal up. This results in the absolute percentage of the monitors (NH^+ and N^+ for NH and N respectively) being lower, since the absolute percent of products is the amount of signal for each channel normalized to the total signal from all channels. The second factor is that the modeled results are intended to replicate the results coming directly from the experiment, before corrections for fragmentation effects have been made. Figure 5.4b is the magnitude of products that best matched the experimental data with N_2 + H being 98% and NH + N being 2%. Excellent agreement can be seen between the model and the experimental data and in both the experimental data and the model it is noticed that the change in products is small between the two extreme concentrations. This is expected since the major product from DR of N_2H^+ is N_2, giving the same absolute product percentage as electron impact fragmentation. Comparing these experimental data to the modeled result, it is concluded that the DR product channel going to N_2 + H is 95-100% and the NH + N channel is limited to 0-5%. Another product that has not been addressed thus far is the H-atom. This product is difficult to quantitatively measure due to a large mass discrimination relative to other products; such a measurement was not necessary since both channels were already monitored.

5.5 Conclusions

Based on our two experimental techniques and the modeling of each technique, all of the possible concerns have been considered, yet these results are still in sharp contradiction to the results published by Geppert et al. It is not known why there should be such a drastic difference between these FA and SR experimental data. An exhaustive effort has been made to consider all possible sources of error in the present FA experiments and it is believed that all of these have been taken into account. Considering the results from Geppert et al., there is some concern about the operation of the hot filament ion source with the N_2/H_2 mixtures. It is known from their work that there is contamination of N_2H^+ due to the $^{14}N^{15}N$ isotope, but this is assessed as only 8% as measured by a mass spectrometer. It may be possible, that with large extraction voltages there is a short residence time in the ion source, and that $^{14}N^{15}N^+$ is preferentially extracted before the N_2^+ reaction with H_2 takes place;

$$N_2^+ + H_2 \longrightarrow N_2H^+ + H \tag{5.17}$$

It is of great concern that a large room temperature rate coefficient is used for reaction 5.17 with a source operating at high temperatures (1000-2000K),[38] especially since there is evidence for a decrease in rate coefficient as temperature increases for ion-molecule reactions of similar type (i.e., hydrogen abstraction). For example the reaction,

$$CH_4^+ + H_2 \longrightarrow CH_5^+ + H \tag{5.18}$$

has been reported to have negative temperature dependence with a rate coefficient approaching 1 x 10^{-11} cm^3s^{-1} at 1000K.[39] To our knowledge, there has been no study of the rate for the N_2^+ + H_2 reaction above room temperature. It is thus unclear how much of the N_2^+ is reacting with the H_2 before mass 29 is injected in the ring and if any modeling of the chemistry in the ion source was undertaken. It is interesting to note that in the case of HCO^+, even where enough energy is available to break the CO partial triple bond, there is a large CO + H channel (88%) and small C + OH and CH + O channels

(6% for both)[30] as detected in Storage Ring measurements. Note, that although the CH + O channel is observed it is endothermic by ∼0.2 eV. In this experiment, the isotopic forms ^{13}CO and D are used to allow the $D^{13}C^{16}O^+$ ion to be preferentially selected. This eliminates the possibility of injecting a different isotopic species of the same mass as the ion of interest. In summary, in the present study, there is no experimental evidence for a significant NH product from direct measurements of the ground state neutral DR products. The two experiments techniques adopted in this study are consistent, with N_2 as the major product having conservative limits of 95-100% for the electron attaching gas method and 95-100% for the pulsed reagent gas method.

5.6 References

[1] Herbst, E. In *Rate Coefficients in Astrochemistry*; Millar, T. J., Williams, D. A., Eds., Vol. 146; Kluwer: Dordrecht, 1988; pages 239–262.

[2] Cravens, T. E. In *Dissociative Recombination of Molecular Ions with Electrons*; Guberman, S. L., Ed.; Kluwer: New York, 2003; pages 385–400.

[3] Eberhardt, P.; Reber, M.; Krankowsky, D.; Hodges, R. R. *Astronomy & Astrophysics* **1995**, *302*(1), 301–316.

[4] Fox, J. L. In *Dissociative Recombination Theory, Experiment and Applications II*; Rowe, B. R., Mitchell, J. B. A., Canosa, A., Eds.; Plenum: New York, 1993; page 219.

[5] Goodings, J. M.; Karellas, N. S.; Hasanali, C. S. *Int. J. Mass Spectrom. Ion Proc.* **1989**, *89*, 205–226.

[6] Ragan, S. E.; Bergin, E. A.; Plume, R.; Gibson, D. L.; Wilner, D. J.; O'Brien, S.; Hails, E. *Ap. J. Supp. Series* **2006**, *166*(2), 567–584.

[7] Flower, D. R.; des Forets, G. P.; Walmsley, C. M. *Astronomy & Astrophysics* **2006**, *456*(1), 215–223.

[8] Fontani, F.; Caselli, P.; Crapsi, A.; Cesaroni, R.; Molinari, S.; Testi, L.; Brand, J. *Astronomy & Astrophysics* **2006**, *460*(3), 709–720.

[9] Adams, N. G.; Herd, C. R.; Geoghegan, M.; Smith, D.; Canosa, A.; Gomet, J. C.; Rowe, B. R.; Queffelec, J. L.; Morlais, M. *J. Chem. Phys.* **1991**, *94*, 4852–4857.

[10] Adams, N. G.; Smith, D.; Alge, E. *J. Chem. Phys.* **1984**, *81*, 1778–1784.

[11] Smith, D.; Adams, N. G. *Ap. J. Lett.* **1984**, *284*, L13–16.

[12] Adams, N. G.; Smith, D. In *Molecular Astrophysics - State of the Art and Future Directions*; Diercksen, G. e. a., Ed.; Reidel: Dordrecht, 1985; pages 657–659.

[13] Adams, N. G.; Babcock, L. M. *J. Phys. Chem.* **1994**, *98*, 4564–4569.

[14] Butler, J. M.; Babcock, L. M.; Adams, N. G. *Mol. Phys.* **1997**, *91*, 81–90.

[15] Rosati, R.; Johnsen, R.; Golde, M. F. *J. Chem. Phys.* **2004**, *120*, 8025–30.

[16] Geppert, W.; Thomas, R.; Semaniak, J.; Ehlerding, A.; Millar, T. J.; Osterdahl, F.; Ugglas, M. a.; Djuric, N.; Paal, A.; Larsson, M. *Ap. J.* **2004**, *609*, 459.

[17] Poterya, V.; McLain, J. L.; Adams, N. G.; Babcock, L. M. *J. Chem. Phys. A* **2005**, *109*, 7181–7186.

[18] Adams, N. G.; Poterya, V.; Babcock, L. M. *Mass Spectrom. Revs.* **2006**, *25*, 798–828.

[19] Florescu-Mitchell, A. I.; Mitchell, J. B. A. *Physics Reports-Review Section of Physics Letters* **2006**, *430*(5-6), 277–374.

[20] Adams, N. G.; Herd, C. R.; Smith, D. In *Proc. XVI ICEAC*, pages 90–95, 1989.

[21] Molek, C. D.; Poterya, V.; Adams, N.; McLain, J. L. *In Preparation* **2007**.

[22] Ikezoe, Y.; Matsuoka, S.; Takebe, M.; Viggiano, A. A. *Gas Phase Ion-Molecule Reaction Rate Constants through 1986;* Ion Reaction Research Group of the Mass Spectroscopy Society of Japan: Tokyo, 1987.

[23] Anicich, V. *An Index of the Literature for Bimolecular Gas Phase Cation-Molecule Reaction Kinetics: JPL Publication 03-19;* Jet Propulsion Laboratory: Pasadena, 2003.

[24] Anicich, V.; Wilson, P.; McEwan, M. J. *Amer. Soc. Mass Spectrom.* **2003**, *14*, 900–915.

[25] Mostefaoui, T.; Adams, N. G.; Babcock, L. M. *Rev. Sci. Instrum.* **2002**, *73*, 2044–50.

[26] Adams, N. G.; Babcock, L. M.; Molek, C. D. In *Encyclopedia of Mass Spectrometry: Theory and Ion Chemistry, Vol.1*; Armentrout, P., Ed., Vol. 1; Elsevier: Amsterdam, 2003; pages 555–561.

[27] Linstrom, P. J., Mallard, W. G., Eds. *NIST Chemistry WebBook*, NIST Standard Database 69; National Institute of Standards and Technology: Gaithersburg MD, 20899, June 2005.

[28] Baiocchi, F. A.; Wetzel, R. C.; Freund, R. S. *Phys. Rev. Lett.* **1984**, *53*(8), 771–774.

[29] Tarnovsky, V.; Deutsch, H.; Becker, K. *Int. J. Mass Spec.* **1997**, *167*, 69–78.

[30] Geppert, W. D.; Thomas, R.; Ehlerding, A.; Semaniak, J.; Osterdahl, F.; af Ugglas, M.; Djuric, N.; Paal, A.; Larsson, M. *Faraday Discussions* **2004**, *127*, 425–437.

[31] Feldman, P. D. *Astronomy & Astrophysics* **1978**, *70*(4), 547–53.

[32] Laube, S.; Lehfaoui, L.; Rowe, B. R.; Mitchell, J. B. A. *J. Phys. B* **1998**, *31*, 4181–9.

[33] Rosen, S.; Peverall, R.; Larsson, M.; Le Padellec, A.; Semaniak, J.; Larson, A.; Stromholm, C.; van der Zande, W. J.; Danared, H.; Dunn, G. H. *Phys. Rev. A* **1998**, *57*(6), 4462–4471.

[34] Meaburn, G. M.; Gordon, S. *J. Phys. Chem.* **1968**, *72*(5), 1592–&.

[35] Pascual, R. Z.; Schatz, G. C.; Lendvay, G.; Troya, D. *J. Phys. Chem. A* **2002**, *106*(16), 4125–4136.

[36] Hack, W.; Wagner, H. G. *Berichte Der Bunsen-Gesellschaft-Phys. Chem. Chem. Phys.* **1994**, *98*(2), 156–164.

[37] Olson, R. E. *J. Chem. Phys.* **1972**, *56*, 2979–2984.

[38] Kallberg, A. In *Manne Siegbahn Laboratory Annual Report 1999*; Kallberg, A., Oppenheimer, E., Eds.; Manne Siegbahn Laboratory, 2000; pages 1–115.

[39] Asvany, O.; Savic, I.; Schlemmer, S.; Gerlich, D. *Chem. Phys.* **2004**, *298*(1-3), 97–105.

Chapter 6

Conclusions and Future Work

DR product distributions are very important data for the models predicting the observed abundances of molecules in the ISM. Yet where comparisons are available with different techniques (FA and SR) there are discrepancies. In addition, SR studies of heavy hydrocarbons are only able to resolve splitting of carbon-carbon bonds, giving no information on the number of H-atoms attached to the products. The studies of hydrocarbon reactions, both ions and neutrals, are very important to the chemistry taking place in the atmosphere of Titan.[1,2] It has been shown that our recently developed technique is valuable for the study of products of DR. For the first time, products of DR can be detected with very good mass separation, which is especially important for the heavy hydrocarbon species. This, in combination with the chemical versatility of the FA, has made this new technique a valuable resource for DR product distribution studies. The N_2H^+ recombination is a good example of why other techniques in addition to the SR are needed. To elaborate, the data obtained by SR where NH + N is the dominant pathway is counter intuitive in that the breaking of a N≡N triple bond would occur rather than the breaking of the single bond in NN–H. Yet these data were influential enough that chemical models of the ISM were recalculated and republished. Due to the recent work using our new technique on this recombination it was established that N_2 + H dominates by at least 95%. Following suggestions made in the publication of our work, the SR measurement was repeated and very little NH + N channel was detected. It was discovered that the ion source from which N_2H^+ was being generated, via $N_2^+ + H_2$ reaction, ran out of H_2 during the experiment and the net result was a study

of $^{15}N^{14}N^+$ recombination, which generates the product channel ^{15}N + ^{14}N; ^{15}N was thought to be the ^{14}NH channel.[3]

For the case of the CH_5^+ recombination, there are also very large discrepancies in the dominant product channel between the present work and the SR measurements. It is not entirely clear as to why these distributions differ, but with the FA a very careful evaluation of the data has been made of the possible sources of error in the product distribution. Yet the distributions cannot be reconciled. It is important to note that in the cases of N_2H^+ and CH_5^+ the possible influences on the DR product distribution has been considered and these effects are minimal. The three most important processes are diffusional loss of the reactive radical species, ion-ion recombination products which are the same as the DR products, and neutral-neutral reactive loss of the DR products.

With the validation of the technique, many future studies are possible. These studies include DR of H_3O^+, NH_4^+, $CH_3OH_2^+$, and $CH_3OCH_4^+$, due to the relevance to the ISM and Titan's atmosphere. Work on H_3O^+ especially needs to be performed to try to resolve the current discrepancy in the literature. The products of this DR effect the ISM modeling immensely; the production of H_2O is an important source of coolant in star formation,[4] where as the production of OH leads to molecular oxygen by the reaction with atomic oxygen. NH_4^+ is important in the atmosphere of Titan, which can be used to compute the abundance of NH_3 in the atmosphere.[2] DR of has been thought to be the dominant route to the abundances of methanol in the ISM, however a recent SR measurements suggests that the dominant channels are CH_3 + OH + H (51%) and CH_2 + H_2O + H (21%), whereas the methanol channel is only 3%.[5] As for dimethyl ether, it is known to be important due to its large abundance in star forming regions.[6,7]

This technique can also be used to study the iir process, for which there has never been a complete product distribution studied. These studies could be done by simply optimizing the conditions in the FA for iir to occur. This could be achieved by increasing the the negative ion concentration in the flow tube or increasing the amount of time for reaction between the

positive and negative ions. In addition, information on the products would give insight into the mechanism of iir. It has always been thought to occur by a long range charge transfer type mechanism, which would be evident based on the products of iir. For example, if $N_2H^+ + Cl^-$ iir is studied, then a long range charge transfer mechanism would lead to the appearance of Cl^+ in the detected monitor ions. If an intimate encounter were occurring, then HCl^+ or NCl^+ may form.

Lastly, the FA at the University of Georgia is set up for variable temperature measurements. It would be interesting to perform some temperature dependent studies on the DR products, especially those that fragment more at room temperature. Preliminary studies, using the new technique, for the $C_2H_3^+$ recombination has shown that C_2H is a significant product. What happens to the product distribution when the temperature is lowered; this is not known. If there is change this would be evidence of a relative energy difference between where the neutral dissociative potential energy curves cross the bound ion potential energy surface, which would be extremely interesting. These type of effects can be studied as the temperature is increased as well.

In conclusion it is an exciting time for the new technique. There are vasts amounts of studies that can be done on the products of both DR and iir as functions of temperature. Data of this type has never before been collect! In addition, this new data would provide significant insight into the mechanisms of DR and iir.

6.1 References

[1] Waite, J. H.; Nieman, H.; Yelle, R. V.; Kasprzak, W. T.; Cravens, T. E.; Luhmann, J. G.; McNutt, R. L.; Ip, W.-H.; Gell, D.; de la Haye, V.; Muller-Wordag, I.; Magee, B.; Borggren, N.; Ledvina, S.; Fletcher, G.; Walter, E.; Miller, R.; Scherer, S.; Thorpe, R.; Xu, J.; Block, B.; Arnett, K. *Science* **2005**, *308*, 982–986.

[2] Cravens, T. E.; Robertson, I. P.; Waite, J. H.; Yelle, R. V.; Kasprzak, W. T.; Keller, C. N.; Ledvina, S. A.; Nieman, H. B.; Luhmann, J. G.; McNutt, R. L.; Ip, W.-H.; de la

Haye, V.; Mueller-Wodarg, I.; Wahlund, J.-E.; Anicich, V.; Vuitton, V. *Geophys. Res. Letts.* **2006**, *33*, L07105.

[3] Larsson, M. Department of Physics, Stockholm University, Sweden, private communication, 2007.

[4] Neufeld, D. A.; Lepp, S.; Melnick, G. J. *Ap. J. Suppl.* **1995**, *100*, 132–147.

[5] Geppert, W. D.; Hamberg, M.; Thomas, R. D.; Osterdahl, F.; Hellberg, F.; Zhaunerchyk, V.; Ehlerding, A.; Millar, T. J.; Roberts, H.; Semaniak, J.; af Ugglas, M.; Kallberg, A.; Simonsson, A.; Kaminska, M.; Larsson, M. *Far. Diss.* **2006**, *133*, 177–190.

[6] Mehringer, D. M.; Snyder, L. E. *A & A* **1996**, *471*, 897–902.

[7] Albert, S.; Herbst, E.; De Lucia, F. C. *Ap. J.* **1998**, *500*, 1059–1063.

Appendix A

Pulsing Circuitry

This section describes the pulsing circuitry that coordinates the Gated Photon Counter (GPC) data acquisition to the pulse valve (PV) opening and closing. This was developed because it was noticed during preliminary experiments, that when no signal should have been present, there was a build up of the integrated signal. In these preliminary experiments the GPC was used in its "dual counting mode" in which the GPC is set with the appropriate gate delays and gate widths, thus data is put into the correct bins for when the pulse valve was opening, Figure A.1. The problem of signal build up using this method was discovered to be in the circuitry of the GPC itself. It routed the A Channel and B channel through separate circuitry, including separate voltage discriminators. These discriminators were the culprit because they were not matched well enough such that it caused signal to a build up. Thus to avoid this, the signal input was sent through one channel of the GPC and the pulsing circuitry was build to get the data in the correct bins. The basic idea is that the GPC must be triggered to collect data at twice the rate of the pulse valve operation, but the trick is to get the counter in sink with the pulse valve. The reasons for this is that the counter is stopped when the computer is collecting the data from bins A_n and bins B_m, where $n = 1, 3, 5..., 1999$ and $m = 2, 4, 6..., 2000$. The computer always takes the signal (S_{nm}) to be A_n - B_m, thus the A_n must always be tied to one of the pulse valve states, in this case A_n is pulse valve closed. To do this, a TTL circuit was build with the overall outcome of this: a 2 Hz TTL signal is fed into the circuit. There are two outputs, one goes to the pulse valve driver (output 1) and the other to the GPC (output 2), see Figure A.3. The one that goes to the pulse valve driver is half the frequency of the input, thus the PV operates at 1 Hz.

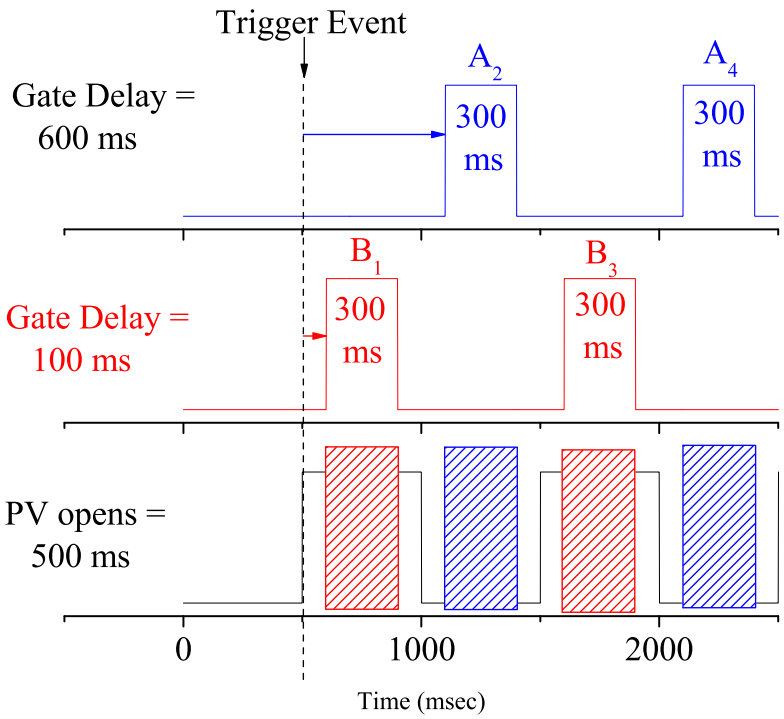

Figure A.1: Old way of collecting data using the GPC in the "dual counting mode".

The output to the GPC is dictated by the on/off switch, see Figure A.3. This output is at ground when the switch is in the off state. When the switch is turned on, the output is at ground until the next rising edge of the PV output, which triggers output 2 to start and the result from output 2 is a 2 Hz TTL signal that continues until its switch is turned back to the off state, see Figure A.2. In this figure the top plot is the input signal of 2 Hz. In this

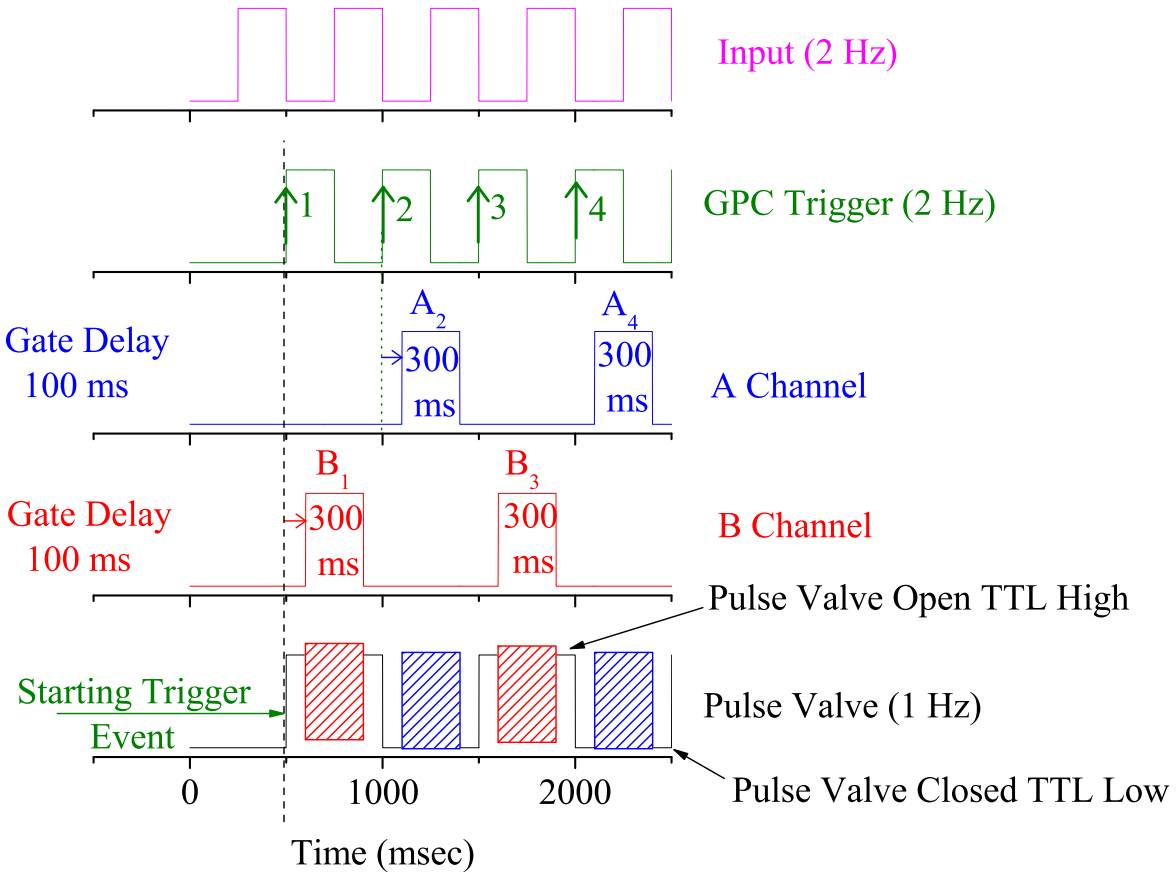

Figure A.2: Pulse valve timing diagram using the pulse valve circuitry. The red rectangles on the pulse valve TTL represent the counting for the B-gates of the GPC and the blue rectangles are counting for the A-gates.

figure the switch is turned on at time equals zero. The GPC trigger frequency is at TTL low until the first rising edge of the pulse valve TTL, then it becomes a TTL of signal at 2 Hz. Each rising edge (symbolized with a upward arrow and a number beside it) of the GPC TTL is a trigger to tell the GPC to start the gate delay, which is fixed at 100 ms. The gate

width is set for 300 ms and the GPC has a value that tells it when to stop, called the TSet. The TSet value is the gate delay plus the gate width and this must be <(pulse valve rate/2). The only time the GPC is actually collecting data is during the gate width. Thus the gate delay of 100 msec keeps the start of the counting away from the pulse valve transition and the TSet of 400 msec causes the counting to stop 100 ms before the pulse valve transition. In this way the counting is done in the most stable regions of the PV being opened and closed.

The circuit that allow all of this to take place is shown below in Figure A.3. The 2 Hz

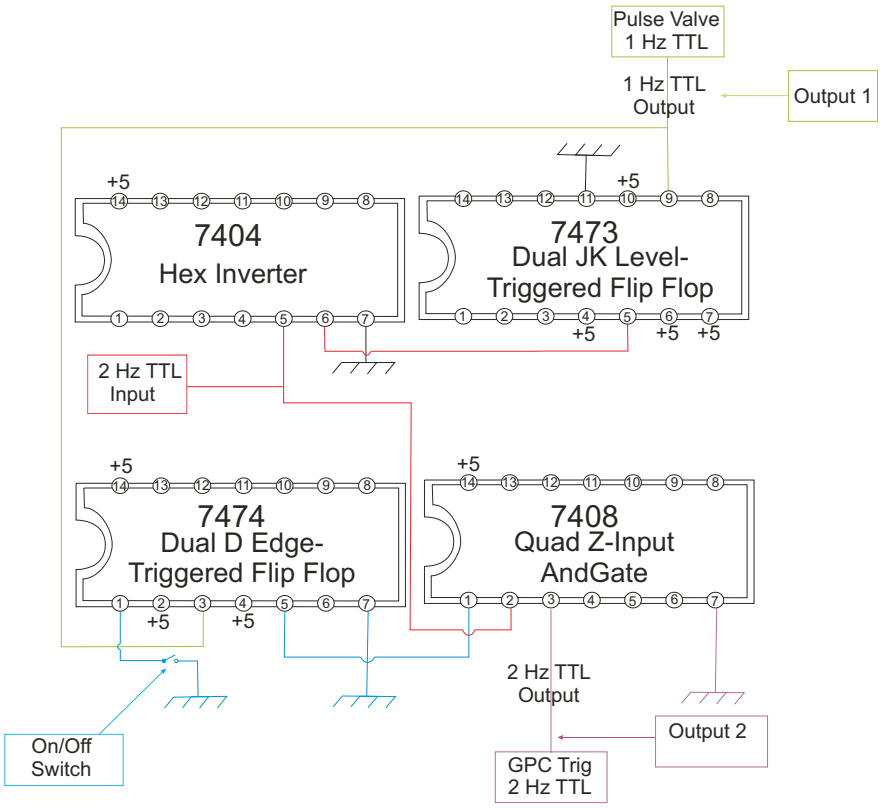

Figure A.3: TTL circuit that coordinates all of the timing between the GPC and the pulse valve.

input frequency goes into the input pin (5) of the 7404 Hex inverter (which just inverts the signal of the TTL) and to one of the input pins (2) on the 7408 AndGate. The output TTL from the 7404 (pin 6) ties into the clock pin (5) of the 7473 JK Flip Flop and the J and K pins (pins 7 and 10 respectively) are tied to +5, thus in this state the output (Q, pin 9) will toggle on every HIGH to LOW transition of the clock. This cuts the TTL frequency in

half. Now since the JK Flip Flop toggles on the HIGH to LOW transition of the clock, the original TTL input (2Hz) must be inverted so that each rising edge of the 1 Hz corresponds to a rising edge of the GPC trigger. Thus far the 1 Hz signal goes to the PV and also gets routed to the clocking pin (3) of the 7474 Dual D Edge-Triggered Flip Flop. In the set up here, when the set and reset pins (pins 4 and 1 respectively) are in the high state the voltage state on the data pin (in this case +5, pin 2) gets transferred to the output (Q, pin 5) on the LOW to HIGH transition of the clock (1 Hz TTL, pin 3). Now the set input (pin 4) is tied to +5 but the reset (pin 1) is tied to ground through a switch. Therefore when the switch is closed, this pin is at ground and the state of the data pin does not get transferred to the output pin, thus the output is at ground. When the switch is opened the reset pin goes to a high state and at the next rising edge of the 1 Hz TTL the output pin will go to high. At this point the output pin of the 7474 is tied to one of the two inputs of the 7408 AndGate. This means that when ever the switch is closed, the one input pin of the 7408 is always at ground and therefore so is the output of the 7408. When the switch is opened the next rising edge of the PV TTL sends the 7408 pin to a high state and the 2 Hz TTL can get through to the output of the 7408. Since every rising edge of the PV corresponds to a rising edge of the 2 Hz the start of the GPC will correspond to the opening of the PV.

Appendix B

Annotated Mathematica Modeling Code

Below is an example of the mathematic calculations for the kinetics of Reagent gas method. The code is split into sections and each section pertains to the gases that are in the FA at the time then these sections are split into parts so that each part of the code can be described. This section clears all of the variables.

B.1 Variable Definitions and Assignments

```
Clear[A, k1, k2, k3, k4, k5, k6, k7, k8, k9, k10, k11, k12, k13, k14, k15,
k16, k17, k18, k19, k20, k21, k22, k23, k24, k25, k26, k27, k28, k29, k30,
k31, k32, k33, k34, k35, k36, k37, k38, k39, k40, p0, ne, He, H2]
```

This section assigns the variables for flow tube pressure (p0), initial plasma electron density (ne), initial Helium density (He), and initial reagent gas density (H_2).

```
p0=4.000;
ne=1.7*^11;
He=p0*3.3*^16;
H2 = 3.69*^11;
Ar = 1.6*^14;
```

The following is assigning all the rate constants (kn, where n = 1–38 in this example). Note for clarification there are a few extra rates assigned beyond `k38`.

```
A = (1.5*^-31)*(He)^2;
k1 = 2.9*^-9;
k2 = 1*^-13;
k3 = 4*^-10;
k4 = 3.18*^-11;
```

```
k5 = 1.3*^-16;
k6 = 2*^-9;
k7 = 2*^-8;
k8 = 4*^-8;
k10 = 7.04*^-11;
k11 = 3*^-9;
k12 = 1*^-9;
k13 = 3.8*^-11;
k14 = 2*^-10;
k15 = 1.1*^-8;
k16 = 5.1*^-18;
k17 = 4.1*^10;
k18 = 2.6*^-9;
k19 = 8.8*^-10;
k20 = 1.07*^-9;
k21 = 2.4*^-7;
k22 = 1.5*^-9;
k23 = 1.2*^-9;
k24 = 2.0*^-9;
k25 = 1.86*^-9;
k26 = 0;
k27 = 5.8*^-10;
k28 = 5.0*^-10;
k29 = 2.7*^-9;
k30 = 2.0*^-9;
k31 = 1.5*^-9;
k32 = 3.0*^-10;
k33 = 1.2*^-9;
k34 = 1.7*^-9;
k35 = 5.0*^-10;
k36 = 1.23*^-9;
k37 = 6.5*^-10;
k38 = 6.96*^-11;
k311 = 7.04*^-11;
k411 = 1.0*^-13;
k511 = 2.0*^-10;
k1111 = 8.9*^-10;
k1211 = 6.3*^-10;
k1611 = 2.1*^-9;
k3211 = 1.0*^-11;
k3311 = 4.2*^-10;
k3411 = 2.0*^-13;
```

The variables are cleared and the residence times are calculated based on the velocity (v). Where md, p2, p3, p4, p5, p6 are for microwave discharge, ring port 2a, ring port 3, ring port 4, ring port 5, and ring port 6 respectively. For example, the variable mdp2 is assigned the residence time of the plasma traveling from the microwave discharge to port 2, which is calculated by the distance 22 cm divide by the velocity.

```
Clear[v, velocity, mdp2, mdp3, mdp4, mdp5, mdp6, mdqp, p2p3, p2p4, p2p5,
p2p6, p2qp, p3p4, p3p5, p3p6, p3qp, p4p5, p4p6, p4qp, p5p6, p5qp, p6qp,
p1, p2, p3, p4]

v = 4100;
velocity = v;
mdp2 = N[((22)/v)];
mdp3 = N[((22 + 24.135)/v)];
mdp4 = N[((22 + 24.135 + 17.52)/v)];
mdp5 = N[((22 + 24.135 + 17.52 + 27.88)/v)];
mdp6 = N[((22 + 24.135 + 17.52 + 27.88 + 17.28)/v)];
mdqp = N[((22 + 24.135 + 17.52 + 27.88 + 17.28 + 23.85)/v)];
p2p3 = N[((24.135)/v)];
p2p4 = N[((24.135 + 17.52)/v)];
p2p5 = N[((24.135 + 17.52 + 27.88)/v)];
p2p6 = N[((24.135 + 17.52 + 27.88 + 17.28)/v)];
p2qp = N[((24.134 + 17.52 + 27.88 + 17.28 + 23.85)/v)];
p3p4 = N[((17.52)/v)];
p3p5 = N[((17.52 + 27.88)/v)];
p3p6 = N[((17.52 + 27.88 + 17.28)/v)];
p3qp = N[((17.52 + 27.88 + 17.28 + 23.85)/v)];
p4p5 = N[((27.88)/v)];
p4p6 = N[((27.88 + 17.28)/v)];
p4qp = N[((27.88 + 17.28 + 23.85)/v)];
p5p6 = N[((17.28)/v)];
p5qp = N[((17.28 + 23.85)/v)];
p6qp = N[((23.85)/v)];
p1 = mdp2;
p2 = p2p3;
p4 = p3qp;
```

This part calculates the ambipolar diffusion coefficients (niX, where X indicates the atom or molecule) for the model using the reduced zero-field mobilities (KX, where X indicates the atom or molecule) for the various ions in a He buffer. The treatment of diffusion of radicals is

done by assuming the radicals cannot diffuse faster than the free diffusion coefficient for any of the ions, thus they are assigned a "mobility" of half that of an ion of respective atomic or molecular size, i.e. N^+ has μ_0 of 20.0 $cm^2/V{\cdot}sec$ and the assigned "mobility" for N radical is 10.0, which calculates to half the diffusion coefficient. The variable r is the radius of the flow tube in centimeters.

```
Clear[ T1, r, lambda, KHep, KHe2p, KHp, KH2p, KH3p, KN2Hp,
KNHp, KNH2p, KN2p, KNp, KNit2, KNit, KNH, KHydro, niHep, niHe2p, niHp,
niH2p, niH3p, niN2Hp, niNHp, niNH2p, niN2p, niNp, niNH,
niNit2, niNit, niHydrogen];

T1 = 300;
r = 3.65;
KHep = 10.3; KHe2p = 16.7; KHp = 30; KH2p = 30; KH3p = 30.5; KN2Hp = 19.5;
KNHp = 20; KNH2p = 20; KN2p = 19.5; KNp = 20;
KNit = 15; KNH = 15; KHydro = 15;

lamda = r^2/(2.405^2);

Da[K_, T_, p_] := Module[{P}, P = 2*(1.38*^-23*T/1.602*^-19*
(K*(760/p)*(T/273.16)))];

ni[D_, lambda_] := Module[{N}, N = D/lambda];

niHep = ni[Da[KHep, T1, p0], lambda];
niHe2p = ni[Da[KHe2p, T1, p0], lambda];
niHp = ni[Da[KHp, T1, p0], lambda];
niH2p = ni[Da[KH2p, T1, p0], lambda];
niH3p = ni[Da[KH3p, T1, p0], lambda];
niN2Hp = ni[Da[KN2Hp, T1, p0], lambda];
niNHp = ni[Da[KNHp, T1, p0], lambda];
niNH2p = ni[Da[KNH2p, T1, p0], lambda];
niN2p = ni[Da[KN2p, T1, p0], lambda];
niNp = ni[Da[KNp, T1, p0], lambda];
niNit2 = ni[Da[KNit2, T1, p0], lambda];
niNit = ni[Da[KNit, T1, p0], lambda];
niNH = ni[Da[KNH, T1, p0], lambda];
niHydrogen = ni[Da[KHydro, T1, p0], lambda];
```

B.2 Microwave Discharge to Ring Port 2, Just He

This solves the differential equations for the reactions that are taking place with He present. `He+`, `He2+`, and `Hem` represent He^+, He_2^+, and He^m respectively. The `{t,0,1}` is for the start time to maximum time in seconds, which needs to be larger than the residence time from the start point to the end point. `He2+[0] == 0` is the initial conditions for the differential equation. The `MaxSteps` value is the maximum number of steps or iterations the NDSolve function can take, typically this is set to a value higher than what it takes to get through the start time to maximum time. The step size is dynamic in that if the solution appears to be changing rapidly it reduces the step size it takes to track the solution better, i.e. it solves stiff differential equation where there are several concentrations that are changing at different rates, some very fast and some slowly.

```
sol = NDSolve[{
He+'[t] == -(A) He+[t] - niHep He+[t],
He2+'[t] == (A) He+[t] - niHe2p He2+[t],
Hem'[t] == -k1 (Hem[t])^2,
e'[t] == k1 (Hem[t])^2 - niHep He+[t] - niHe2p He2+[t],

He+[0] == e[0] == ne,
Hem[0] == 5*^10,
He2+[0] == 0},

{He+, He2+, Hem, e},{t,0,1}, MaxSteps -> 3000];
```

This code puts the number density of each of the ions at the addition point of the next gas into a table form.

```
TableForm[{{
{``He+ = `` , He+[p1]},
{``He+ = `` , He+[p1]},
{``He+ = `` , He+[p1]},
{``He+ = `` , He+[p1]}
}/.sol}, TableAlignments -> Center]
```

The next variable adds all the ions together and it should equal the electron number density [e].

```
etest = {He+[p1] + He2[p1]} /. sol
```

This part clears the variables, `Hep, Hem, He2p, ele`, and assigns each one the number density at the addition point of the next gas. These are going to be used as initial conditions in the next section of differential equations.

```
Clear[Hep, Hem, He2p, ele]
Hep = Part[He+[p1] /. sol, 1];
Hem = Part[Hem[p1] /. sol, 1];
He2p = Part[He2+[p1] /. sol, 1];
ele = Part[e[p1] /. sol, 1];
```

B.3 Ring Port 2 to Ring Port 3, Ar and H_2 added in

The next set of differential equations

```
sol = NDSolve[{
He+'[t] == (A)He+[t] - niHep He+[t] - k2 He+[t]H2 - k411 He+[t]Ar,
He2+'[t] ==(A)He+[t] -niHe2p He2[t] - k3 He2+[t]H2 - k511 He2+[t]Ar,
Hem'[t] == -k1(Hem[t])^2 - k4 Hem[t]H2 - k311Hem[t]Ar,
Ar+'[t] == k311 Hem[t]Ar + k411 He+[t]Ar + k511 He2+[t]Ar - k1111 Ar+[t]H2 -
           niArpAr+[t],
ArH+'[t] ==(0.98) k1111 Ar+[t]H2 + k1611 H2+[t]Ar - k1211 ArH+[t]H2 -
                  niArHp ArH+[t],
Hydrogen'[t] == (0.83)k2 He+[t]H2 + k6 H2+[t]H2 - niHydrogenHydrogen[t] -
                1.0*^-9  Hydrogen[t]Hydrogen[t],
H+'[t] == (0.83)k2 He+[t]H2 - k5 H+[t] H2 - niHp H+[t],
H2+'[t] == (0.17)k2 He+[t]H2 + (0.37)k3 He2+[t]H2 - k6 H2+[t]H2 +
           k4 Hem[t]H2 - k7 H2+[t]e[t] - niH2p H2+[t] -
           k1611 H2+[t]Ar + (0.02) k1111Ar+[t]H2,
HeHy+'[t] == (0.26)k3 He2+[t]H2 - k31 HeHy+[t]H2 - niHep He+[t],
He2Hyd+'[t] == (0.37)k3 He2+[t]H2 - k32 He2Hyd+[t]H2 - niHe2p He2+[t],
H3+'[t] == k5 H+[t]H2 + k6 H2+[t]H2 + k31 HeHy+[t]H2 + k32 He2Hyd+[t]H2 -
           k8 H3+[t]e[t] - niH3p H3+[t] + k1211 ArH+[t] H2,
e'[t] ==  k1 (Hem[t])^2 - niHep He+[t] - niHp H+[t] - niHe2p He2+[t] -
          k7 H2+[t]e[t] - niH2p H2+[t] -k8 H3+[t]e[t] - niH3p H3+[t] +
          k4 Hem[t] H2 - niHe2p He2+[t] - niHep He+[t] + k311 Hem[t]Ar -
          niArp Ar+[t] - niArHp ArH+[t],

He+[0] == Hep,
Hem[0] == Hem,
```

```
He2+[0] == He2p,
Ar+[0] == 0,
ArH+[0] == 0,
e[0] == ele,
H+[0] == 0,
Hydrogen[0] == 0,
H2+[0] == 0,
HeHy+[0] == 0,
He2Hyd+[0] == 0,
H3+[0] == 0}], "}"}],

{He+, He2+, Hem, Ar+, ArH+, H+, Hydrogen, H2+, HeHy+, He2Hyd+, H3+, e},
{t, 0, p2}, MaxSteps -> 3000];
```

The rest of the code just builds upon itself and only additional commentary will be added where needed.

```
TableForm[{{
{"He+ = ", He+[p2]},
{"He2+ = ", He2+[p2]},
{"Hem = ", Hem[p2]},
{" Ar+ = ", Ar+[p2]},
{"ArH+ = ", ArH+[p2]},
{"H+ = ", H+[p2]},
{"Hydrogen = ",Hydrogen[p2]},
{"H2+ = ", H2+[p2]},
{"HeHy+ = ", HeHy+[p2]},
{"He2Hyd+ = ", He2Hyd+[p2]},
{"H3+ = ", H3+[p2]},
{"e = ", e[p2]}
} /.sol}, TableAlignments -> Center]

etest = {He+[p2] + He2+[p2] + Ar+[p2] + ArH+[p2] + H+[p2] + H2+[p2] +
HeHy+[p2] + He2Hyd+[p2] + H3+[p2]}/.sol

Clear[Hep, Hem, He2p, Hp, HydrN, H2p, HeHyp, He2Hydp, H3p, ele]
Hep = Part[He+[p2]/. sol, 1];
Hem = Part[Hem[p2]/. sol, 1];
He2p = Part[He2+[p2]/. sol, 1];
Hp = Part[H+[p2]/. sol, 1];
HydrN = Part[Hydrogen[p2]/. sol, 1];
H2p = Part[H2+[p2]/. sol, 1];
HeHyp = Part[HeHy+[p2]/. sol, 1];
He2Hydp = Part[He2Hy]+[p2]/. sol, 1];
```

```
H3p = Part[H3+[p2]/. sol, 1];
ele = Part[e[p2]/. sol, 1];
```

B.4 Pulse Valve Port 3 (Near RP3) to Sample orifice, N_2 is pulsed in

This section has a few new variables (`fracN2, fracNH`) are the variables DR product distribution. The variables (`EIN2toN2p, EINHtoNHp, EIN2toNitp, EINHtoNitp, EIN2toN15p, EINtoNitp`) are for the EI fragmentation pattern, these are the absolute values.

```
Clear[fracN2, fracNH, EIN2toN2p, EINHtoNHp, EIN2toNitp, EINHtoNitp,
EIN2toN15p, EINtoNitp]

fracN2 = 1 - fracNH;
fracNH = 0.02;
EIN2toN2p = 0.85;
EIN2toN15p = 0.007;
EINHtoNHp = 0.78;
EIN2toNitp = 0.15;
EINHtoNitp = 0.22;
EINtoNitp = 1.0;

sol = NDSolve[{
He+'[t] == -(A)He+[t] - niHep He+[t] - k2 He+[t]H2 - k22 He+[t]Nit2[t]
- k411 He+[t]Ar,
He2+'[t] == (A)He+[t] - niHe2p He2+[t] - k3 He2+[t]H2 - k23 He2+[t]Nit2[t]
      - k511 He2+[t]Ar,
Hem'[t] == -k1 (Hem[t])^2 - k4 Hem[t]H2 - k38 Hem[t]Nit2[t]
- k311 Hem[t]Ar, Ar+'[t] == k311 Hem[t]Ar + k411 He+[t]Ar +
k511 He2+[t]Ar - k1111 Ar+[t]H2 - k3211 Ar+[t]Nit2[t] +
      k3411 N2+[t]Ar - niArp Ar+[t],
ArH+'[t] == (0.98) k1111 Ar+[t]H2 + k1611 H2+[t]Ar - k1211 ArH+[t]H2
      - k3311 ArH+[t]Nit2[t] - niArHp ArH+[t],
H+'[t] == (0.83) k2 He+[t]H2 - k5 H+[t]H2 - niHp (H+[t],
H2+'[t] == (0.17) k2 He+[t]H2 + (0.37) k3 He2+[t]H2 - k6 (H2+[t]H2
+ k4 Hem[t]H2 - k7 H2+[t]e[t] - niH2p H2+[t] -
      k24 H2+[t]Nit2[t] - k1611 H2+[t]Ar + (0.02) k1111 Ar+[t]H2,
HeHy+'[t] == (0.26) k3 He2+[t]H2 - k31 HeHy+[t]H2
      - k34 HeHy+[t]Nit2[t] - niHep He+[t],
He2Hyd+'[t] == (0.37) k3 He2+[t]H2 - k32 He2Hyd+[t]H2 - niHe2p He2+[t],
H3+'[t] == k5 H+[t]H2 + k6 H2+[t]H2 + k31 HeHy+[t]H2 + k32 He2Hyd+[t]H2
- k8 H3+[t]e[t] - niH3p H3+[t] - k25 H3+[t]Nit2[t]
+ (0.15) k36 NH+[t]H2 + k1211 ArH+[t]H2,
```

```
Nit2'[t] == -k22 He+[t]Nit2[t] - k23 He2+[t]Nit2[t] - k24 H2+[t]Nit2[t] -
      k25 H3+[t]Nit2[t] - niNit2 Nit2[t] - k38 Hem[t]Nit2[t] -
      k3311 ArH+[t]Nit2[t] - k3211 Ar+[t]Nit2[t],
N2H+'[t] == k24 H2+[t]Nit2[t] + k25 H3+[t]Nit2[t] +
      k34 HeHy+[t]Nit2[t] - k16 N2H+[t]H2 - k21 N2H+[t]e[t]
      - niN2Hp N2H+[t] + k3311 ArH+[t]Nit2[t] + k30 N2+[t]H2
      + k37 NH+[t]Nit2[t],
N2+'[t] == (0.44) k22 He+[t]Nit2[t] + k23 He2+[t]Nit2[t] - niN2p N2+[t] -
      k21  N2+[t]e[t] + k3211 Ar+[t]Nit2[t] - k3411 N2+[t]Ar
      - k30 N2+[t]H2 + k38 Hem[t]Nit2[t],
NH+'[t] == k35 N+[t]H2 - niNHp NH+[t] - k36 NH+[t]H2 -
      k37 NH+[t]Nit2[t],
NH2+'[t] == (0.85) k36 NH+[t]H2 - niNH2p NH2+[t],
N+'[t] == 0.56) k22 He+[t]Nit2[t] - niNp N+[t] - k35 N+[t]H2,
e'[t] == k1 (Hem[t])^2 - niHep He+[t] - niHe2p He2+[t] -
      niHp H+[t] - k7 H2+[t]e[t] - niH2p H2+[t] -
      k8 H3+[t]e[t] - niH3p H3+[t] + k4 Hem[t]H2 - k21 N2+[t]e[t] +
      k38 Hem[t]Nit2[t] - k21  N2H+[t]e[t] - niN2Hp N2H+[t] -
      niN2p N2+[t] - niNp N+[t] - niHe2p He2+[t] -
      niHep He+[t] - niNHp NH+[t] - niNH2p NH2+[t] +
      k311 Hem[t]Ar - niArHp ArH+[t] - niArp Ar+[t],
Hydrogen'[t] == (0.83) k2 He+[t]H2 + k6 H2+[t]H2 +
      k24 H2+[t]Nit2[t] + (0.60) 6.5*^-10  H3+[t]
      Nitrogen[t] + (2.49*^-11) ElectronIonPNH[t]Nitrogen[t] -
      - niHydrogen Hydrogen[t] - 1.0*^-9  Hydrogen[t]Hydrogen[t] +
      k35 N+[t]H2 + (0.85) k36 NH+[t]H2,
Nitrogen'[t] == -(1) 6.5*^-10  H3+[t]Nitrogen[t] + (0.60)k22 He+[t]Nit2[t] -
      niNit Nitrogen[t] + (0.15) k36 NH+[t]H2 + k37 NH+[t]Nit2[t],
ProductsN2Hp'[t] == k21  N2H+[t]e[t],
ElectronIonPN2'[t] == (fracN2) k21  N2H+[t]e[t] + (1.6*^-9)
        ElectronIonPNH[t]ElectronIonPNH[t] + (2.49*^-11)
        ElectronIonPNH[t]Nitrogen[t] - niNit2 ElectronIonPN2[t],
ElectronIonPNH'[t] == (fracNH) k21  N2H+[t]e[t] - (1) (1.6*^-9)
        ElectronIonPNH[t]ElectronIonPNH[t] - (1) (1.0*^-10)
        ElectronIonPNH[t]Hydrogen[t] - (1) (2.49*^-11)
        ElectronIonPNH[t]Nitrogen[t] - niNH ElectronIonPNH[t],
ElectronIonPNit'[t] == (fracNH) k21  N2H+[t]e[t] + (2)
        k21  N2+[t]e[t] + (1) (1.0*^-10) ElectronIonPNH[t]
        Hydrogen[t] - (1) (2.49*^-11) ElectronIonPNH[t]Nitrogen[t]
        - niNit ElectronIonPNit[t],

He+[0] == Hep,
Hem[0] == Hem,
He2+[0] == He2p,
e[0] == ele,
```

```
Hydrogen[0] == HydrN,
Nitrogen[0] == 0,
Ar+[0] == Arp,
ArH+[0] == ArHp,
H+[0] == Hp,
H2+[0] == H2p,
HeHy+[0] == HeHyp,
He2Hyd+[0] == He2Hydp,
H3+[0] == H3p,
ProductsN2Hp[0] == 0,
ElectronIonPN2[0] == 0,
ElectronIonPNH[0] == 0,
ElectronIonPNit[0] == 0,
Nit2[0] == 1*^15,
N2H+[0] == 0,
NH+[0] == 0,
NH2+[0] == 0,
N2+[0] == 0,
N+[0] == 0},


{He+, He2+, Hem, Ar+, ArH+, H+, H2+, HeHy+,
He2Hyd+, H3+, ProductsN2Hp,
Hydrogen, Nitrogen, ElectronIonPN2, ElectronIonPNH,
ElectronIonPNit, Nit2, VEINit2, N2H+, NH+, NH2+, N2+,
N+, e}, {t, 0, p4}, MaxSteps -> 3000];

TableForm[{{
{"He+ = ", He+[p4]},
{"He2+ = ", He2+[p4]},
{"Hem = ", Hem[p4]},
{"Hydrogen = ", Hydrogen[p4]},
{"Nitrogen = ", Nitrogen[p4]},
{"Ar+ = ", Ar+[p4]},
{"ArH+ = ", ArH+[p4]},
{"H+ = ", H+[p4]},
{"H2+ = ", H2+[p4]},
{"HeHy+ = ", HeHy+[p4]},
{"He2Hyd+ = ", He2Hyd+[p4]},
{"H3+ = ", H3+[p4]},
{"Nit2 = ", Nit2[p4]},
{"N2H+ = ", N2H+[p4]},
{"NH+ = ", NH+[p4]},
{"NH2+ = ", NH2+[p4]},
{"N2+ = ", N2+[p4]},
```

```
{"N+ = ", N+[p4]},
{"ProductsN2H+ = ", ProductsN2Hp[p4]},
{"ElectronIonPN2 = ", ElectronIonPN2[p4]},
{"ElectronIonPNH = ", ElectronIonPNH[p4]},
{"ElectronIonPNit = ", ElectronIonPNit[p4]},
{"e = ", e[p4]}
} /. sol}, TableAlignments -> Center]

etest = {He+[p4] + He2+[p4] + Ar+[p4] + ArH+[
        p4] + H+[p4] + H2+[p4] + HeHy+[p4] + He2Hyd+[p4]
        + H3+[p4] + N2H+[p4] + NH+[p4] + NH2+[p4] + N2+[p4]
        + N+[p4]} /. sol
```

This section accounts for the fragmentation patters of both the DR products and the background of unreacted reagent gases. These are the values that get outputted into a "*.dat" file. This program is run 1 iteration for each value of $[N_2]_0$. The results from this can then be manipulated in Excel to get the Absolute value of each monitor ion versus $[N_2]_0$. The DR products are represented by `EIN2Pro, EINHPro, EINPro` and the background is represented by `EIN2BG, EIN15BG, EINBG`.

```
Clear[EIN2Pro, EINHPro, EINPro, EIN2BG, EIN15BG, EINBG, TotalN2, TotalNH,
TotalN]

EIN2Pro = {EIN2toN2p*ElectronIonPN2[p4]} /. sol;
EINHPro = {EIN2toN15p*ElectronIonPN2[p4] + EINHtoNHp*ElectronIonPNH[p4]}
/.sol
EINPro = {EIN2toNitp*ElectronIonPN2[p4] + EINtoNitp*ElectronIonPNit[p4] +
          EINHtoNitp*ElectronIonPNH[p4]} /. sol;
EIN2BG = {EIN2toN2p*Nit2[p4]} /. sol;
EIN15BG = {EIN2toN15p*Nit2[p4]} /. sol;
EINBG = {EIN2toNitp*Nit2[p4]} /. sol;
TotalN2 = EIN2Pro + EIN2BG;
TotalNH = EINHPro + EIN15BG;
TotalN = EINPro + EINBG;
```

This section of code outputs the following values to a "*.dat" file, `EIN2Pro, EINHPro, EINPro, EIN2BG, EIN15BG, EINBG, TotalN2, TotalNH, TotalN` and `{Part[Nit2[0] /. sol, 1]` is the initial number density of the N_2.

```
Export["HeH2PN21.dat", TableForm[{Part[Nit2[0] /. sol, 1], EIN2Pro, EINHPro,
EINPro, EIN2BG, EIN15BG, EINBG, TotalN2, TotalNH, TotalN},
TableDirections -> Row]]
```